# Molecular Mechanisms of E1A Splicing and Innate Immune Suppression by Human Adenovirus

By: Drayson Graves

A thesis submitted to the Faculty of Graduate Studies of The University of Manitoba in partial fulfillment of the requirements of the degree of

Doctor of Philosophy

Department of Microbiology

University of Manitoba

*To my parents, Darren and Kenzie-Lee Graves, and to my beautiful wife, Samantha. You all put up with me for so long, and provided nothing but love and support in return. We finally made it.*

# Table of Contents

## Acknowledgements

The following work was supported by grants from the Natural Sciences and Engineering Research Council (grant RGPIN/05366-2019) and the Canadian Institutes of Health Research (grants PJT-173376 and PJT-166198).

I thank Frank Graham for provision of low-passage HEK 293 cells, and Joe Mymryk for virus stocks, 11S E1A cDNA, and for critical feedback on aspects of this thesis.

I extend my personal thanks to my supervisor Peter Pelka, and to the members of his lab (with special mention to my fellow graduate students Leandro Crisostomo, Nikolas Akkerman, Lauren Fulham, and Rafe Helwer), for their help with the experiments that produced this thesis (specified in sections 3.1 and 4.1), and for the warm, fun atmosphere they provided throughout my studies.

# List of Tables

# List of Figures

# List of Abbreviations

| | |
|---|---|
| 2D-LC-MS-MS | Two-Dimensional Liquid Chromatography Tandem Mass Spectrometry |
| ALCAM | Activated Leukocyte Cell Adhesion Molecule |
| CBP | CREB-Binding Protein |
| ChIP | Chromatin Immunoprecipitation |
| CPE | Cytopathic Effect |
| CR1 through CR4 | Conserved Region 1 through Conserved Region 4 |
| CtBP | C-Terminal Binding Protein |
| DCAF7 | DDB1 and CUL4 Associated Factor 7 |
| E1 through E4 | Adenovirus Early Protein 1 through Early Protein 4 |
| EPHA2 | Ephrin Receptor A2 |
| FoxK1/2 | Forkhead Box K1/K2 |
| GAPDH | Glyceraldehyde-3-Phosphate Dehydrogenase |
| HAdV | Human Adenovirus |
| HMW | High Molecular Weight |
| IFN | Interferon |
| IP | Immunoprecipitation |
| IRF9 | Interferon Regulatory Factor 9 |
| ISG | IFN-Stimulated Gene |
| ISGF3 | IFN-Stimulated Gene Factor 3 Complex |
| MLP | Adenovirus Major Late Promoter |
| MOI | Multiplicity of Infection |
| Mre11 | Mre11 Homolog, Double Strand Break Repair |
| Nbs1 | Nibrin |
| Nek9 | Never in Mitosis Gene A (NIMA) Related Kinase 9 |
| ORF/Orf | Open Reading Frame |
| p53 | Tumor Protein p53 |
| p107 | Rb-Like 1 |
| p130 | Rb-Like 2 |
| p300 | Histone Acetyltransferase E1A-Associated Protein 300 |
| PML | Promyelocytic Leukemia Protein |
| pRb/Rb | Retinoblastoma Protein |
| PTPRF | Receptor-type tyrosine-protein phosphatase F |
| Rad50 | DNA Repair Protein RAD50 |
| RCV | Replication-Competent Virus |
| RNAi | RNA Interference |
| RPII | RNA Polymerase II |
| RuvBL1/2 | RuvB-Like Protein 1/2 |
| SAHUE | Severe Acute Hepatitis of Unknown Etiology |
| siRNA | Short Interfering RNA |
| SMARCAL1 | SWI/SNF Related, Matrix Associated, Actin Dependent |
| snRNP | Small Nuclear Ribonucleoprotein |
| STAT1/2 | Signal Transducer and Activator of Transcription 1/2 |
| VA-RNA | Virus-Associated RNA |

**Abstract**

Human adenovirus (HAdV) is a collection of viral species (A through G) within the family *adenoviridae* that are associated with a wide variety of diseases including respiratory and gastrointestinal infections, as well as keratoconjunctivitis. Most infections tend to be mild and self-clearing, but certain species (HAdVs B and E especially) are much more dangerous than average, especially to children, the elderly, and the immunocompromised. Here I report my findings on two less-studied aspects of HAdV biology. First, I show that the smallest three splicing isoforms of the HAdV-C E1A protein are not properly generated when the E1A genomic region is supplied in *trans*, and that this reduces E1-deficient HAdV growth approximately twofold; an important discovery for generation of therapeutic HAdV vectors, as these are almost always E1-deficient. Second, I compare IFN resistance in HAdVs C (mild) and B (severe), revealing that HAdV-B is superior at preventing host cell ISG expression. I theorize that this may be in part due to a novel mechanism in which the virus sequesters away the host cell protein RuvBL1 to prevent its role in ISG expression. These results shed new light on two aspects of HAdV, both in terms of its role as a pathogen and as a therapeutic vector.

# 1. Introduction

## 1.1 Overview of Study

First discovered in the early 1950s, HAdVs are causative agents of pink eye, the common cold, and various gastrointestinal diseases[1], as well as useful tools for cancer research, thanks to the oncogenic properties of their replication cycle[2]. More recently, they have been valuable as a medical tool, both as vectors for delivery of gene therapy and vaccines, and as backbones for oncolytic virus treatment of certain cancers[3]. As such, one would expect the genomic and proteomic profile of these viruses to be well-documented, and to an extent, this is true. There is a sizeable body of research regarding nearly every aspect of HAdV-C, the model species. However, this is not the case for the remaining six discovered species of HAdV – A, B, D, E, F, and G. While the general genomic and functional pattern is the same between species – noncoding virus-associated RNA expressed first, followed by five functional early transcription units, then one late, structural transcription unit, with variation provided by alternative splicing[4] – the specifics are much more varied.

Take, for example, the E1A protein – specifically the largest and earliest-expressed of the five different proteins alternatively transcribed from the *E1A* transcription unit. This is the first protein expressed during adenovirus infection, its primary purpose being the reprogramming of the host cell in favour of viral replication (forcing quiescent/$G_0$ cells into S-phase to take advantage of their DNA replication machinery, among many other changes[2]), by way of its various binding partners. E1A is substantially different between various HAdV species, containing sizeable insertions or deletions that likely have some effect on the protein's function[5], shifting some binding sites in relation to one another, adding some, and removing others. Additionally, even within the

purview of species C E1A, the majority of existing knowledge is on the largest two isoforms. The smallest three, which express later in the infection, still possess no definitively-assigned functions[4].

The recent SARS-Cov2 pandemic has revealed just how dangerous a common nuisance virus can become, given the right circumstances, and so it is in our best interest to develop as wide a knowledge base as possible. As such, I set out to investigate the lesser-known functions of E1A by two routes: Determining the function of the smaller, later-expressing E1A isoforms, and examining a difference between the well-understood E1A protein of HAdV-C and that of the much more dangerous[6–9] HAdV B.

### 1.2 Research Questions

In the first of the two studies presented here, I observed that an E1A-deficient adenovirus mutant did not replicate to the same degree as wild-type in HEK-293 cells, despite these cells providing E1A in *trans*[10]. As E1A has five different splice isoforms[2], three of which are relatively unknown in terms of function, I theorized that the source of this difference in growth rates may be due to the failure of E1A supplied exclusively in *trans* to splice properly, leading to downstream consequences on viral titre yields. I investigated this idea by means of electrophoresis of cDNA generated from E1A mRNA backed up by western blots and qPCR to observe relative abundance of E1A isoforms as well as other viral proteins at various timepoints, immunofluorescent microscopy to observe subcellular localization of E1A mRNA relative to viral replication centres, and creation of cell lines individually expressing all E1A isoforms to attempt a rescue of the phenotype.

In the second study, I observed a large difference in the binding affinity of E1A to AAA+ protein (ATPase associated with diverse cellular activities) RuvBL1 between species B and C

HAdV. The interaction of E1A and RuvBL1 is for the purpose of innate immune suppression, specifically prevention of interferon-stimulated gene expression[11], and as such I theorized that a difference may exist between the two species in terms of resistance to the effects of interferon. I started by investigating the effect of interferon on each species by way of viral growth assays and qPCR examinations of interferon-stimulated genes (ISGs) and viral genes, concluding that species B HAdVs are indeed more resistant to interferon than HAdV-C. I examined the molecular mechanisms underpinning this difference by way of immunoprecipitation (IP) and chromatin immunoprecipitation (ChIP) to observe protein-protein and protein-DNA interactions respectively, and immunofluorescent microscopy to view subcellular localization of RuvBL1 in cells infected with each of the two species of HAdV. In addition, I had 2D-liquid chromatography tandem mass spectrometry (2D-LC-MS/MS) performed on cells treated with IFN and infected with species B and C HAdVs, and performed proteomic analysis to present a broad-spectrum picture of the differences between these two species.

### 1.3 Hypotheses

1. E1A supplied in *trans* does not splice properly into all five of its isoforms, negatively affecting viral propagation.
2. The increased morbidity of HAdV-B strains 7 and 14 is, at least in part, the result of differing binding affinity of E1A to RuvBL1, which drives more efficient shutdown of the interferon response pathway.

## 2. Literature Review

### 2.1 *Adenoviridae* and Human Adenovirus

Originally identified as a causative agent of cellular degradation in adenoid tissue extracted from children[12], *Adenoviridae* is a family of mid-sized (90-100 nm), icosahedral, non-enveloped double-stranded (ds) DNA viruses within the order *Rowavirales*[13]. Taxonomically, it divides into six genera: *Aviadenovirus*, which infects birds (>14 species); *Atadenovirus*, which infects a wide variety of hosts including reptiles, birds, marsupials, and ruminants (>9 species); *Ichtadenovirus*, which infects white sturgeon (1 species); *Mastadenovirus*, which infects mammals (>50 species); *Siadenovirus*, which infects frogs, tortoises, and birds (>7 species)[14]; and *Testadenovirus*, which infects red-eared sliders (1 species)[15,16].

Of interest here is the genus *Mastadenovirus*, which contains species infecting a wide variety of mammals (bats, mice, chimps, etc.) and includes every known species of HAdV[17]. HAdV is divided into seven species, named A through G based on serology, hemagglutination, oncogenicity in rodents, transformation of primary cells in culture, and genome sequence[14]. These are further divided into over 100 numbered types, originally defined exclusively as cross-neutralization serotypes up to type 51[18], beyond which types have been categorized based on whole-genome sequence (discussed in more detail by Seto et. al.[19]).

While HAdV is generally considered a common cold virus, the specific outcomes of infection vary between species. For example, species A, D, F, and G are often associated with gastroenteritis, while species B, D, and E are known to cause conjunctivitis. Species B, C, and E all commonly infect the upper respiratory tract, but only species B and E infections routinely extend to the lower respiratory tract as well. Species B and E are also uniquely associated with

pharyngoconjunctival fever; a combination of pharyngitis, keratoconjunctivitis, and fever[14]. Even species B adenovirus can be divided into two subspecies, B1 and B2, based on genetic clustering. While B1 (HAdVs B3, B7, B16, B21, and B50) primarily causes respiratory infection, B2 types (HAdVs B11, B14, B34, and B35) are also associated with urinary tract and renal infections[20,21].

| *HAdV Species* | Types[22] | Primary Mode(s) of Infection[23] |
|---|---|---|
| ***A*** | 12, 18, 31, 61 | Gastrointestinal, respiratory, urinary |
| ***B*** | 3, 7, 11, 14, 16, 21, 34, 35, 50, 55, 66, 68, 76–79 | Keratoconjunctivitis, gastrointestinal, respiratory, urinary |
| ***C*** | 1, 2, 5, 6, 57, 89 | Respiratory, gastrointestinal including hepatitis, urinary |
| ***D*** | 8, 9, 10, 13, 15, 17, 19, 20, 22–30, 32, 33, 36–39, 42–49, 51, 53, 54, 56, 58–60, 62, 63, 64, 65, 67, 69–75, 80–88, 90–103 | Keratoconjunctivitis, gastrointestinal |
| ***E*** | 4 | Keratoconjunctivitis, respiratory |
| ***F*** | 40, 41 | Gastrointestinal |
| ***G*** | 52 | Gastrointestinal |

**Table 2.1. HAdV types and the species to which they belong.**

While HAdV infections are usually mild and self-clearing[4], certain strains can result in severe infections in young children, the elderly, the immunocompromised, and occasionally in healthy individuals[23–26]. Outbreaks tend to occur in crowded populations, such as those in hospitals[27,28], nursing homes[29], military bases[30,31], and schools[32,33]. The HAdV types B3, E4, B7, D8, B14, and B55 are most commonly associated with outbreaks, and tend to be the most virulent[24]. It is worth noting that four out of six of these types belong to HAdV species B, making it the most consistently dangerous out of the seven. Indeed, epidemiological reports suggest that

nearly all severe or fatal incidences of adenovirus disease in children are associated with HAdV-B7[9], and it is one of the two HAdV types routinely vaccinated against by the US military, along with HAdV-E4. HAdV-B14 also has a long history with military barracks and recruits[20], dating back to its initial discovery in 1957[34]. HAdV-B55, another of the more dangerous strains, is almost functionally identical to HAdV-B14, the only difference being a short recombination event in its genome replacing a section of its hexon gene with that of HAdV-B11[35].

Additionally, a recent link has been suggested between HAdV-F41 and cases of severe acute hepatitis of unknown etiology (SAHUE), starting in Alabama in October 2021[36], and since then from all over the world, including Ireland[37], Japan, Spain, and Italy[38].

**2.2 The Adenovirus Genome**

The adenovirus genome (Fig. 2.1) is made up of a single strand of dsDNA, anywhere from 24,630 to 48,395 base pairs in length, containing inverted terminal repeats (ITRs) of 26-721 bp in length[16]. A terminal protein, which serves as a primer for new strand synthesis, is covalently attached at the 5' end of each strand[4]. The left end (the end containing the E1A transcription unit, by convention) of the genome also contains a *cis*-acting packaging domain, from base pairs ~200-400, that is indispensable for packaging of the viral DNA into the capsid during the final stages of virion assembly[39]. The remainder of the genome is made up mostly of five early transcription units (E1A, E1B, E2, E3, and E4), four intermediate transcription units expressed around initiation of viral DNA replication (pIX, IVa2, L4 intermediate, and E2-late), and a single late transcription unit that is processed post-expression to generate five distinct families of mRNAs (L1 – L5)[4]. Each early transcription unit is governed by its own promoter, with the exception of E2 which has two alternative promoters (E2-early and E2-late, controlling expression of its early and intermediate isoforms, respectively), and the entirety of the late region is controlled by a single major late

promoter (MLP). Host RNA polymerase II (RPII) transcribes each of these genes into mRNA, and except for IVa2 and pIX, all are alternatively spliced to generate several different proteins. Indeed, it was adenovirus from which the concept of RNA splicing was initially discovered[40–42]. With some exceptions, the goals of adenoviral proteins can be sorted into one of six groups: S-phase initiation in an otherwise quiescent host cell, shutdown of host cell innate immunity, evasion of host adaptive immunity, further expression of viral genes, viral genome replication, and construction/packaging of the progeny virions.

It is worth noting that most of the work over the years has been performed on species C adenoviruses, making the layout and functionality of their genome into a sort of "adenovirus canon." As such, the following descriptions of the various transcription units will use species C as a model, and a visual representation of its genome is presented in Fig. 2.1. Given the topics of this thesis, the E1 proteins and their functions will be discussed at length, whereas the remaining sections will not be exhaustive.

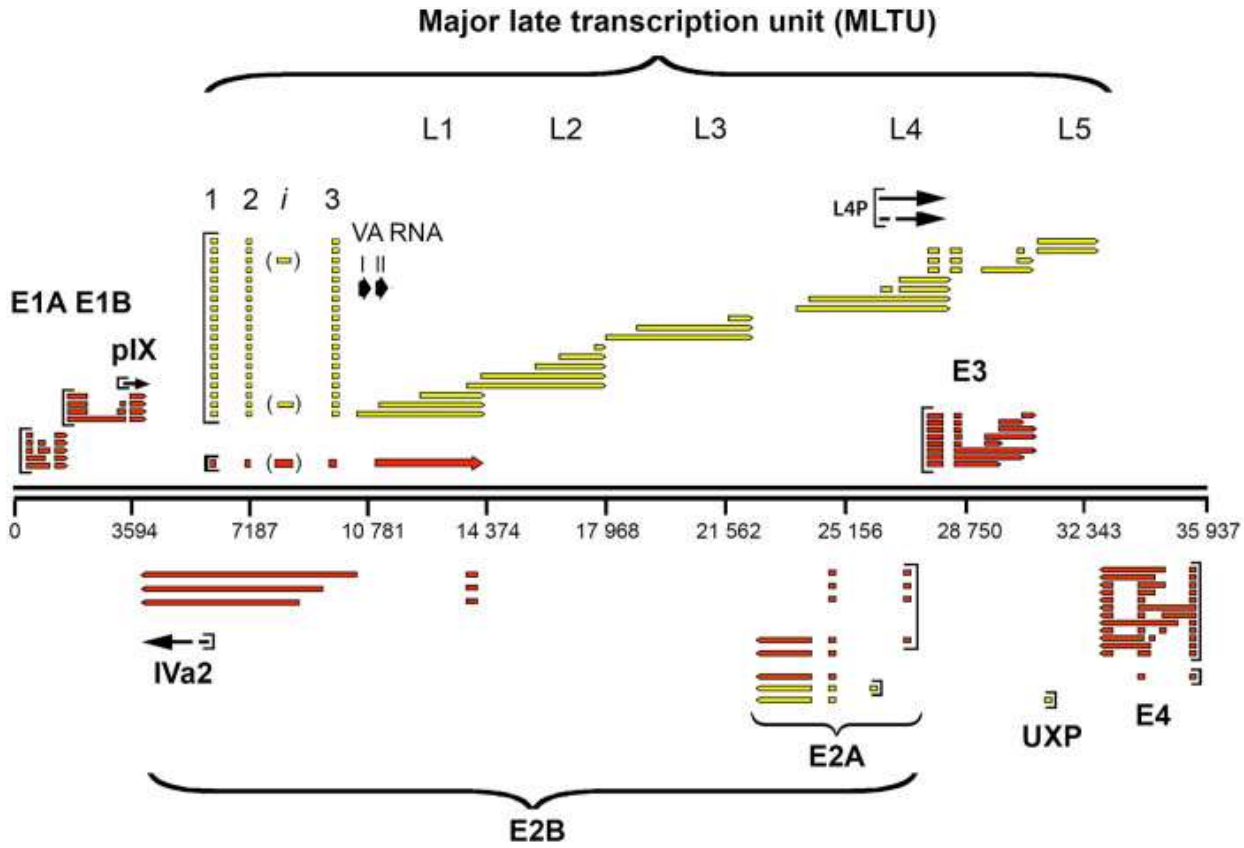


**Figure 2.1. Schematic representation of the HAdV genome and all transcription units contained therein.** Figure reproduced under Creative Commons Attribution 4.0 International license without alteration. Originally produced by Westergren Jakobsson et al. (2021)[40]. https://creativecommons.org/licenses/by/4.0/

### 2.2.1 The E1A Transcription Unit

Left-most on the HAdV genome, and expressed roughly six hours post-infection[43], the E1A transcriptional unit is a region coding for a pre-mRNA that, through alternative splicing, produces five different proteins, named for their sizes measured in amino acids residues: 289R, 243R, 217R, 171R, and 55R; from mRNA splice isoforms 13S, 12S, 11S, 10S, and 9S respectively (Fig. 2.2)[44,45]. E1A 289R, structurally, can be divided into small N- and C-terminal regions, along with four regions of amino acid sequence similarity, termed conserved regions – CR1, CR2, CR3, and CR4[2]. E1A 243R is near-identical in layout but missing the CR3 region in its entirety. While a plethora of functions have been attributed to these largest two isoforms, which appear relatively early in the course of infection, the smallest three, appearing later and eventually in greater quantity[46], currently have no clearly understood function[4], although it has been shown that mutant HAdV expressing only 217R or 171R E1A is unable to grow in HeLa cells, confirming that these species are not sufficient for viral growth[44]. The shift in splicing behaviour from expression of early (large) to late (small) E1A isoforms is governed by titration of serine/arginine (SR) splicing factors over the course of infection. Essentially, above a certain concentration, these splicing factors allow for the production of early E1A transcripts, but as the infection progresses, they are sequestered away to a point at which the splicing pattern shifts to production of the late isoforms[47]. Additionally, changing the specificity of the host cell U1 small nuclear ribonucleoprotein (snRNP) away from a position downstream of the 12S E1A splice site reduces levels of 12S and 13S E1A mRNA by 60% and 90% respectively, and induces the appearance of 10S and 11S mRNA far earlier in infection than normal[48].

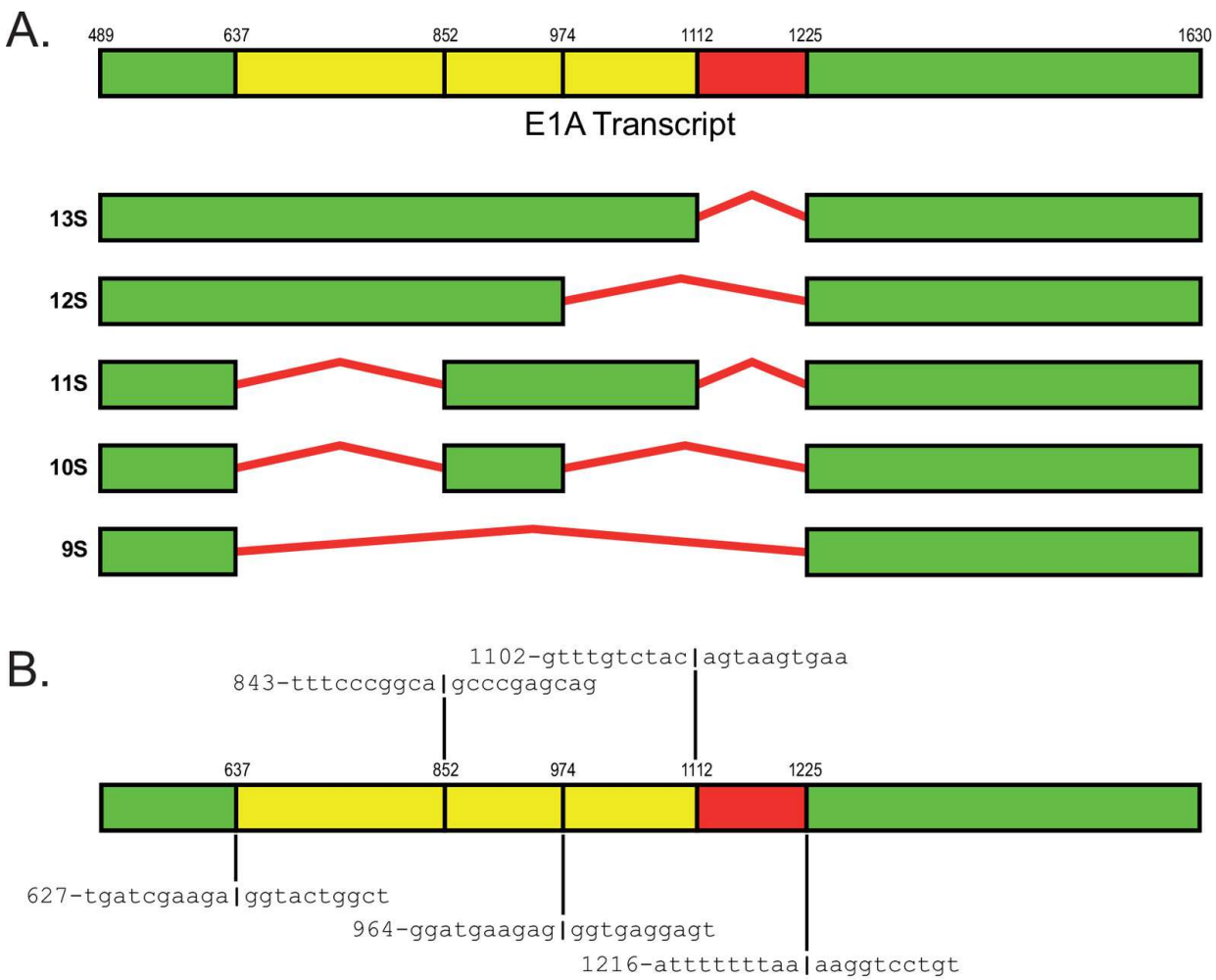


**Figure 2.2. Schematic representation of E1A splicing.** (A) HAdV5 E1A protein splice isoforms, with numbers representing nucleotides. (B) Nucleotide sequences at the splicing junctions of the HAdV5 E1A gene, where vertical lines represent the splice point.

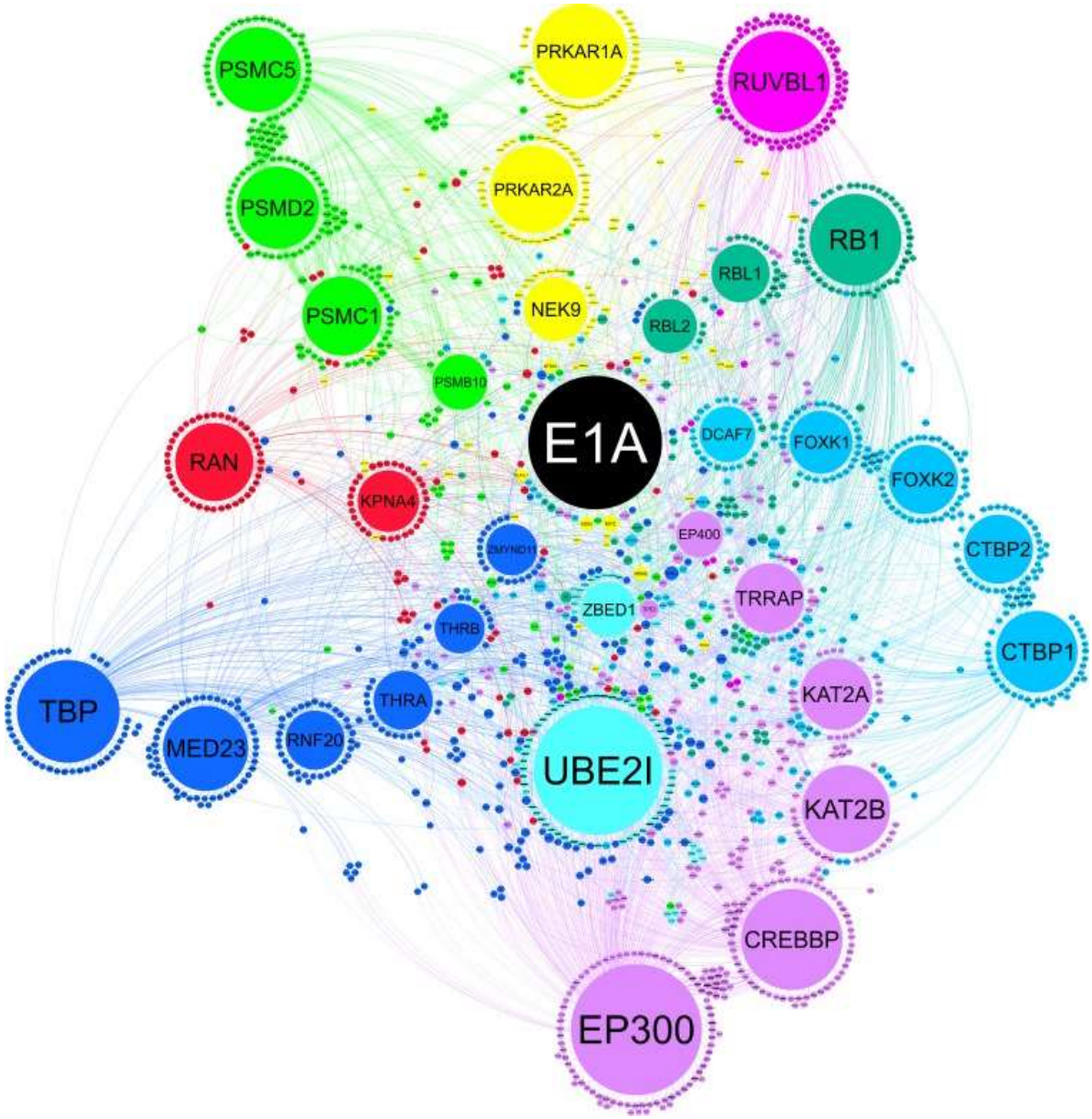


**Figure 2.3. Map of the HAdV-C5 interactome.** Direct binding partners represented by large circles emanating out from E1A, with their protein networks in turn represented by the small circles surrounding them. Figure reproduced under Creative Commons Attribution 4.0 International license without alteration. Originally produced by King et al. (2018)[2]. https://creativecommons.org/licenses/by/4.0/

E1A's main, though not only, function is to stimulate the host cell (usually arrested in $G_0$ or $G_1$) to enter S phase, even in the absence of mitogenic signals[49,50]. This is necessary as while HAdV encodes a sizeable amount of its own replication machinery, it still requires some level of host cell support to replicate its own genome. This function, along with every other known role that E1A plays, is accomplished through its staggeringly large network of interaction partners. Indeed, one could describe the E1A protein as little more than a collection of binding sites for other proteins, here referred to as molecular recognition features (MoRFs). These include, but are not limited to, sites for binding to host retinoblastoma protein (pRb), p300, C-terminal binding protein (CtBP), and FoxK1/K2[2]. A more complete picture of the interactome of E1A is presented in Fig. 2.3.

Being the first protein expressed from the viral genome and given that the majority of its roles are carried out within the nucleus, E1A must be responsible for making its own way from its site of translation in the cytoplasm back into the nucleus. It accomplishes this through a bipartite classic nuclear localization signal (cNLS) present in CR4[51,52], as well as two noncanonical NLSs in CR1 and CR3[53], ensuring proper nuclear entry under all splicing conditions.

The largest E1A isoform, 289R, is uniquely responsible for enhancing early viral protein expression across the board[54]. It stimulates a roughly fivefold increase in transcription of the E1A region itself, and increases transcription of the other early regions by anywhere from 10- (E1B) to 100-fold (E2-early, E3, E4)[4]. This is based on an interaction between a MoRF in E1A CR3 (spliced out in E1A 243R) and MED23 (a subunit of the human mediator transcription complex)[55], which results in higher levels of preinitiation complex assembly at viral promoters and stimulates transcriptional elongation[56,57]. It makes use of the host cell acetyltransferases p300 and CBP to upregulate these viral genes as well, acetylating H3K18 and H3K27 within their promoter

regions[58]. Additionally, a site immediately C-terminal to CR3 (auxiliary region 1 – AR1, a glutamate-proline repeat) is necessary for this viral transactivation[59]. E1A 289R's methods of transcriptional regulation do not ever involve it binding directly to DNA, instead accessing these promoter regions through interactions with several cellular transcription factors, such as members of the ATF family[60,61], AP1[62], and SP1[63]. It then activates or represses gene expression by recruiting positive (p300 or CBP) or negative (Rb family) transcriptional regulators to these promoters.

The 243R isoform, which contains all of the same regions as the 289R isoform with the exception of CR3, is also responsible for up- and downregulation of various host cell genes, and does so in a specific temporal order[64]. The first group includes genes involved with the cell cycle, as well as synthesis of DNA, RNA, and proteins, adding up to roughly 30% of all host cell genes, and specifically involves enrichment of p300/CBP and PCAF acetyltransferases at activated genes that drive H3K18 acetylation, and downregulation of the Rb protein family of tumor suppressors[64,65]. It also deregulates the promoters of genes involved in inflammation, innate immunity, and cell cycle inhibition, accounting for roughly 20% of cellular genes[66,67]. E1A 243R represses these genes by inducing acetylation of H4K16[64]. The second group of genes makes up the remaining ~50% of the host genome, and is universally downregulated starting at 12 hours post-infection[64]. Interestingly, as this isoform binds mostly to the same proteins as E1A 289R and lacks only the CR3 region, which is involved in transactivation of viral and cellular genes, an overabundance of E1A 243R by even a slight amount titrates away enough of 289R's binding partners to interfere with E1A 289R-mediated transactivation, suppressing gene expression[68].

E1A's initiation of S-phase requires interactions with pRb, p107 (Rb-like 1) and p130 (Rb-like 2), p300, and CBP[2]. Binding sites for p300 and CBP can be found in the N-terminus and CR1[4], while the Rb family binds in CR1 and CR2[69], which contain similar Rb binding sites to those found

in the polyomavirus large T antigen and the papillomavirus E7 protein[70]. By binding to pRb, E1A displaces its usual binding partners, the E2F family of transcription factors[71], freeing them to carry out their usual action of transcriptionally regulating cell cycle activation[72]. Further, E1A takes advantage of the acetyltransferase functions of p300 and CBP to acetylate pRb, hindering its phosphorylation and further contributing to its oncogenic properties[73]. Independently of this, E1A 289R also binds to the protein DP1, which is part of a complex with E2F protein E2F4. This was shown to help override Rb-mediated transcriptional repression, leading to increased S-phase induction[74].

In mouse cells, promoters of cell cycle regulation genes Cdc6 and cyclin A are bound by the E2F protein E2F4, which associates with p130 and the HADC1/2-mSin3B histone deacetylase complex, in order to prevent their expression[75]. This is in addition to the H3K9 methylase protein that also interacts with this promoter, Suv39H1, which further reduces expression of Cdc6 and cyclin A[76]. Expression of HAdV E1A (specifically the 243R isoform) in these cells was shown to disrupt E2F4-p130 complexes, replacing the promoter-bound repressive E2Fs, such as E2F4, with the activating E2Fs 1, 2, and 3[75,77]. This leads to acetylation of H3K9, which activates transcription and reduces methylation at these sites, further preventing heterochromatinization. Removal of the CR2 region of E1A containing the high affinity Rb-binding site, and by extension prevention of its interaction with the Rb protein family, prevented each step of this interaction, while an N-terminal mutation to E1A that prevented binding to a histone acetyl transferase/chromatin remodeling complex containing TRRAP-PCAF-p400 still allowed for the displacement of E2F4-p130, but not the subsequent H3K9 acetylation[77]. Essentially, E1A binds p130, preventing its interaction with E2F4 and blocking the formation of a repressive complex at the promoters of Cdc6

and cyclin A (cell cycle regulation genes), while simultaneously recruiting a histone acetylation complex (TRRAP-PCAF-p400) to these same promoters, encouraging stronger transcription[4].

Host cell transformation by E1A has been shown to be reduced by its CR4 region, as mutants missing this section exhibit stronger transformative properties than observed in wild type[78]. This region, notably, contains binding sites for host cell proteins FOXK1/2, DCAF7, and CtBP, and conflicting reports exist on which interaction is responsible for this effect. Originally, it was attributed mostly to interaction between E1A and CtBP[78,79], but the DCAF7[80] and FOXK1/2[81] interactions have since been shown to contribute as well, with at least one study showing CtBP interaction to be dispensible[80]. These findings may be due to variations in experimental methodology and mutant construction, and overall likely reflect some functional redundancy between each of these interaction targets[4]. The CR4 region interactions have also been identified as contributors to host innate immune suppression, repressing a subset of ISGs that would otherwise express 12 hours post infection, even in the absence of IFN stimulation[82]. It was shown that CR4 must interact with all three binding partners to demonstrate this effect.

E1A interferes with ISG expression by other means as well, specifically blocking it in response to stimulation by IFNα[83], thanks to reduced levels of the component parts of the ISGF3 complex[84,85]. This reduction correlates with the E1A-p300/CBP interaction[86]. This phenotype seems to vary depending on the cell type in which it is tested[4], as in primary human airway epithelial cells, it is a result of E1A-STAT1 interaction, resulting in downregulation of STAT1 phosphorylation[87]. Another protein that E1A uses to suppress ISG expression is the multipurpose ATPase protein RuvBL1[11]. RuvBL1, in addition to its participation in protein complexes governing chromatin remodeling, transcription, DNA repair, and apoptosis[88,89], is involved in expression of ISGs in response to type I IFN[90]. E1A binds RuvBL1 with its C-terminus, recruiting it to ISG

promoters to suppress ISGs[11]. More recently, E1A was found to target RuvBL1 and 2 in order to prevent IRF3 stabilization (necessary for ISG expression) by forming a complex with CRL4 E3 ubiquitin ligase and DCAF10[91].

Finally, E1A, through its interaction with the cellular ubiquitin ligase hBre1/RNF20, has a role in preventing ubiquitination of histone protein H2B[92], a modification that generally results in the transcriptional activation of chromatin[93]. This modification takes place both during infection with an E1A-null HAdV mutant and following treatment of cells with type I IFN, implying that it may be another viral mechanism of innate immune suppression[92]. Furthermore, it seems that E1A is able to essentially "recycle" hBre1/RNF20, not only preventing it from ubiquitinating H2B, but also causing it to recruit the RNA polymerase-associated protein hPaf1 to help stimulate early viral gene expression[94].

Interestingly, a pair of studies on the smallest E1A isoform, E1A 55R, have revealed a number of characteristics that are unique to it. While E1A primarily localizes to the nucleus, the 55R isoform was shown to be present in the cytoplasm as well[95]. Additionally, it is able to weakly stimulate viral gene expression during infection and interacts with the S8 component of the proteasome[95]. Finally, it is capable of binding to and modulating the activity of the unliganded thyroid hormone receptor (TR) by way of a signature CoRNR box motif[96].

### 2.2.2 The E1B Transcription Unit

Next to the E1A region on the viral genome is the E1B region. Despite the physical proximity, the genes encoded here do not begin to express until much later in the infection (12-13 hours)[43]. This region encodes for two proteins, each named for their weight in kilodaltons: E1B 19K and E1B 55K. The primary function of both of these proteins is to interfere with cellular

responses to viral gene expression: Primarily apoptosis, by p53-dependent or independent means, and the DNA damage response.

The cellular protein p53 is a major tumour suppressor coded for by the gene *TP53*. Normally present at low levels, p53 is stabilized and activated in response to various stimuli, such as oncogene activation and DNA damage, resulting in direct changes in regulation of ~500 genes, and indirect changes in many more. This affects various cellular functions, but most critically for the interests of adenovirus, it is able to trigger host cell apoptosis, through means both direct and indirect[97]. To prevent this, E1B 55K binds to p53 on the same site as its normal binding partner, MDM2[98], a ubiquitin ligase that normally controls proteasomal degradation and keeps p53 levels low[99]. While this interaction does serve to stabilize p53, it also prevents p53-mediated transcriptional activation[100,101]. E1B 55K then proceeds to serve as a SUMO1 (small ubiquitin-like modifier) ligase for p53, SUMOylating about 1% of p53 present in the nucleus[102,103]. This results in localization of the majority of p53 to nuclear promyelocytic leukemia protein (PML) bodies, as E1B 55K is recruited to PML in a SUMO-dependent manner[104], while simultaneously binding to p53 tetramers and forming homodimers with itself. These cross-linked networks are then exported from the nucleus into large inclusion bodies called aggresomes, that are targeted for degradation[105,106]. E1B 55K also targets the chromatin remodeling factor Daxx for proteasomal degradation[107] and interferes with the cellular response to type I IFNs[108,109].

Additionally, E1B 55K forms a complex with fellow viral protein E4orf6 to further interfere with the function of p53. The complex associates with cellular proteins Elongin B and C, Cullin 5, and Rbx1 to form a ubiquitin ligase that polyubiquitinates p53, targeting it for proteasomal degradation[110]. E1B 55K also binds to the Mre11-Rad50-Nbs1 (MRN) complex, a host cell sensor of DNA damage, that it both poly-ubiquitinates and re-localizes into PML bodies

to prevent a cellular DNA damage response (DDR)[105,111,112]. Other targets of the E1B 55K/E4 Orf6 complex include integrin α3[113], TIP60 (a lysine acetyltransferase involved in gene expression, DNA damage response, apoptosis, and cell cycle regulation)[114], SPOC1 (an epigenetic reader protein with a role in DNA damage response)[115], SMARCAL1 (a cellular DNA replication protein and ATR substrate)[116], ALCAM, EPHA2, and PTPRF (three proteins involved in regulating cell-cell contacts)[117]. While not all the reasons for each of these interactions have been determined yet, the common factor seems to be that the targets in some way limit early viral genome replication.

Finally, the E1B 55K-E4 Orf6 complex is involved in regulation of mRNA export from the nucleus; both inhibiting host mRNA export[118] and encouraging export of late viral mRNA[119], though the mechanism by which this takes place remains a mystery.

In response to expression of E1A and unscheduled entry of cells into S-phase, the host cell begins to degrade the protein MCL-1, likely as a DNA damage response[120]. MCL-1, a member of the cellular BCL2-related family of proteins (cBCL-2s), normally binds to another cBCL2 protein, BAK, preventing it from co-oligomerizing with a third cBCL2 protein, BAX. The result of BAK/BAX interaction is permeabilization of the mitochondrial membrane and a subsequent release of cysteine proteases that serve as the point of no return for the apoptosis pathway[97]. The role of the smaller viral E1B protein, E1B 19K, is to prevent this brand of p53-independent apoptosis, doing so through host protein imitation. E1B 19K is a structural and functional homolog of the cellular BCL2 protein[121], and as such is able to bind to and sequester both BAK and BAX from one another, preventing their interaction and subsequent initiation of the apoptosis pathway.

The E1B also produces at least five additional proteins through alternative splicing, these being 433R, 422R[122], 156R, 93R, and 84R[123]. These proteins are relatively minor species[124], and their functions are mostly unknown. That said, the 433R protein is sufficient for viral replication,

even at low levels of expression[122], and the 156R protein has demonstrated the capability to transform rat cells in culture, though this transformation was independent of p53-stimulated transcription repression[123].

### 2.2.3 The E2 Transcription Unit

To the right of the E1B region, encoded on the complementary strand, lies the E2 transcription unit. With genes expressing at 11-12 hours post-infection, and proteins detectable six hours later[43], the gene products of this region are dedicated to the replication of the HAdV genome. These gene products are precursor terminal protein (pTP), DNA-binding protein (DBP), and adenovirus DNA polymerase (Ad-Pol).

While the distinct mechanisms of adenovirus DNA replication will not be discussed at length here, it should be noted that initiation requires five proteins in total: The three viral proteins previously mentioned, as well as the cellular transcription factors Nuclear Factor I and III (NFI and NFIII)[125]. NFI homodimerizes and binds strongly to a specific sequence within the HAdV origin of replication[126,127], also interacting directly with Ad-Pol, which in turn forms a heterodimer with pTP[128]. This serves to guide the replication complex to its proper starting point in the origin of replication. NFIII similarly binds to pTP[125], also contributing to sequence-specificity of the replication complex[129]. Ad-Pol, as its name suggests, is a DNA polymerase that directly synthesizes a new HAdV genome from a template strand; it is expressed from the E2B region of the genome. Also from the E2B region, by alternative splicing, comes pTP, a protein responsible for maintaining the termini of the viral genome through multiple rounds of replication[14]. Catalyzed by Ad-Pol, it forms a direct bond with the 5' end of the first nucleotide (dCMP) in the nascent strand, which serves as a primer for new strand synthesis, and melts the end of the DNA duplex, allowing room for Ad-Pol[130]. Upon completion of DNA replication, pTP is proteolytically cleaved

into the adenovirus terminal protein (TP), which remains covalently linked to viral genome at each 5' end[130]. Finally, the sole output from the E2A region is DBP, which binds to DNA, both ss and ds[131], and serves primarily to protect the DNA strand being displaced by new strand synthesis from nucleocytic degradation[132]. It also stimulates binding of the Ad-Pol-NFI complex to the origin of replication[133] and works with cellular topoisomerase I to unwind the viral genome[130].

### 2.2.4 The E3 Transcription Unit

The E3 genomic region begins detectable gene expression about 10 hours post-infection[43], and codes for eight known proteins in total, the majority of which are named for their weights in kDa: In order from left to right, these are 12.5K, 6.7K, gp19K, adenovirus death protein (ADP), receptor internalization and degradation proteins α and β (RIDα and RIDβ), and 14.7K. With one known exception, the function of this transcription unit is primarily to protect the virus from the host immune system, both innate and adaptive[134].

6.7K[135] and 14.7K[136,137] both help to inhibit apoptosis of the host cell. E3-6.7K is a transmembrane protein localized mostly to the ER[138], and is theorized to inhibit intrinsic apoptosis by maintaining cytosolic $Ca^{2+}$ homeostasis[134], while E3-14.7K is a cytosolic protein that prevents extrinsic apoptosis in response to tumour necrosis factor α (TNFα), through interaction with three "14.7K-interacting proteins," (FIPs). It does this by interfering with the synthesis of arachidonic acid[134], and by preventing internalization of the TNFα receptor[139].

E3-gp19K[140,141] binds to the host protein major histocompatibility complex (MHC1) and localizes it to the ER, leaving it unable to perform its standard function of presenting the antigens of invading pathogens for pickup by the adaptive immune system at the cell membrane, and protecting the cell from destruction *via* cytotoxic T lymphocytes. While this does leave the cell

more vulnerable to recognition and destruction by natural killer (NK) cells, gp19K also counters this by also binding to and sequestering the NK cell ligands major histocompatibility complex class 1 chain-related proteins A and B (MICA and MICB), also to the ER[141].

The receptor internalization and degradation complex (RID)[135,142–144] is a dimer of two E3 proteins (10.4K and 14.5K or RIDα and RIDβ respectively) that – as its name suggests – internalize and trigger the lysosomal destruction of various cell membrane-bound death receptors. These receptors include epidermal growth factor receptor (EGFR)[142,144], Fas[143], TRAIL receptor 1[135], and TNF receptor 1. It also works in concert with E3-6.7K to down-regulate cell surface presentation of TNF receptor 2[135]. Finally, it interferes with lipopolysaccharide (LPS) and interleukin-1 beta (IL-1β) mediated responses in a way that does not involve removal of the related cell surface receptors[145].

Adenovirus death protein (ADP)[146] is an 11.6K integral membrane protein that is expressed late in infection, from the major late promoter. Its function is to promote lysis of the host cell to aid in viral spread.

Only the function of the 5'-most gene in the E3 transcriptional unit, E3 12.5K[147], remains a mystery.

### 2.2.5 The E4 Transcription Unit

At the right-most point in the adenovirus genome, encoded on the complementary strand, is the E4 genomic region. The seven proteins encoded here, expressed at nearly the same time as E1A (~6 hours post-infection)[43], have a variety of functions, making this transcriptional unit a "Swiss army knife" of sorts for the virus. Each protein from this location is named for the open reading frames (ORFs) from which they are translated, numbered one through seven from right to

left on the genome. Most arise from a single ORF, but two are from multiple ORFs spliced together. They are named E4orf1, E4orf2, E4orf3, E4orf4, E4orf3/4, E4orf6, and E4orf6/7. Orf 5 does not express a protein product.

E4orf1 works alongside E4orf4 to activate the cellular protein kinase mammalian target of rapamycin (mTOR), even without the presence of nutrients or necessary signals[148]. This in turn stimulates greater levels of protein synthesis, leading to higher rates of glycolytic metabolism, glucose consumption, and lactate production in the host cell, while reducing levels of oxygen consumption[149,150]. This boost in metabolism enhances viral DNA replication, possibly due to the availability of more nucleotides for genome synthesis[150].

E4orf3 is a multifunctional protein, sharing some redundancy with E4orf6. It is necessary and sufficient for the reorganization of PML bodies from their usual globular organization into filamentous nuclear "tracks[151–153]." The reasons for this are twofold: PML bodies themselves possess antiviral properties[154], so by disrupting them, the outcome for the virus is improved; and these nuclear tracks can then be used by the virus to trap and sequester other host cell proteins to interfere with their functions. It can also induce heterochromatinization at p53-induced promoters, another method of p53 activity suppression[155]. It also serves as a SUMO E3 ligase[156], SUMOylating specifically the Mre11 and Nbs1 proteins[157] (components of the MRN complex) and more broadly a large set of proteins involved in DDR[158]. As discussed in the section on E1B, in the context of a HAdV infection, SUMOylation often leads to sequestration within these modified PML bodies. The aforementioned functional redundancy of E4orf3 is found in this role in DDR suppression, redirecting the MRN complex into PML tracks in the same way as the E1B 55K/E3orf6 complex[159]. Finally, E4orf3 has been recently shown cooperate with E1A to help fine-tune later viral gene expression. E4orf3 was shown to increase nucleosome density across the

board within the viral genome, restricting gene expression, which is then rescued as needed by an interaction between E4orf3 and E1A[160].

E4orf4 binds to the β-subunits of protein phosphatase 2A (PP2A) family proteins[161], the downstream effects of which all eventually inform its multitude of functions, affecting both viral and cellular gene expression[162,163], mRNA splicing[164,165], protein translation[148,166], and cell death[167–169]. As mentioned earlier, E4orf4 is redundant with E4orf1 in terms of mTOR activation. This raises levels of cellular protein translation and leads to more dNTPs for use in viral genome replication[148]. It remains unclear how this outcome is achieved through E4orf4/PP2A interaction, but it has been suggested to be a result of the interaction altering PP2A substrate specificity[170]. Additionally, E4orf4 can dephosphorylate DDR effector kinases ATM and ATR, inhibiting DDR[171]; and when expressed alone in transformed cells, E4orf3 causes apoptosis *via* a non-canonical pathway, independent of p53[172].

E4orf6 is another anti-apoptotic protein, working through inhibition of p53. As discussed in the E1B section, E4orf6 pairs with E1B 55K to form a ubiquitin ligase complex that polyubiquitinates p53, marking it for cellular degradation[110], in addition to various other functions. E4orf6 also interacts with and inhibits p53[173] and p73[174,175] independently of E1B 55K, p73 being a member of the p53 family of proteins that activates transcription through alternative p53 promoters[176].

E4orf6/7 (formed from alternate splicing generating a fusion protein of ORFs 6 and 7) dimerizes and binds to cellular transcription factor E2F, increasing its affinity for the HAdV E2-region promoter, helping to activate E2-region transcription[177]. As E4orf6/7 competes with host protein Rb for its E2F binding site, it can functionally substitute for E1A in terms of preventing E2F-Rb interaction[178]. By the same method, it activates cellular E2F1 promoters as well[179].

The newly-discovered E4orf3/4 fusion protein has been recently characterized as a promoter of E1A/E1B-induced transformation of primary rodent cells[180]. On the other hand, while expression of E4orf2 has been confirmed for decades now[181], its function still remains unknown.

### 2.2.6 Virus Associated (VA)-RNAs

VA-RNAs are the products of the first adenovirus genes transcribed following infection[43], by host RNA polymerase III, rather than II. In 80% of HAdVs (HAdVs C2 and C5 included), two VA-RNA sequences are transcribed, but the other 20% have only one[182]. These RNA transcripts, referred-to as VA-RNA$_I$ and VA-RNA$_{II}$, are never translated, accumulating in the cytoplasm over the course of the infection, eventually reaching copy numbers of $10^8$ and $10^6$ per cell, respectively[183]. Starting early in infection, VA-RNAs significantly reduce the expression level of host cell hepatoma-derived growth factor (HDGF) which inhibits HAdV growth when overexpressed[184]. VA-RNAs also interact with several host proteins, the most well-known of which is protein kinase R (PKR), an innate immune protein activated by the presence of dsRNA[185], whose function VA-RNA inhibits, contributing to adenovirus's resistance to interferon[186]. However, they also activate other dsRNA-detecting proteins: RIG-I[187] and OAS1[188], resulting in downstream type I IFN induction. By late infection, they occupy the endoribonucleases Dicer[189] and Argonaute-2 (Ago-2)[190], components of the RNA-induced silencing complex (RISC), serving as competitive substrates to inhibit host cell RNA interference, and generating virus-associated micro-RNAs (mivaRNA), which serve to inhibit host cell protein expression.

### 2.2.7 The Late Transcription Unit

Depending on the source, protein-producing adenoviral genes are divided into either two or three categories: Early and late; or early, intermediate, and late. This is because the line between

early and late transcripts tends to blur in a real infection scenario, as despite the general pattern of E genes first, L genes second, the single promoter responsible for transcription of the L genes (major late promoter or MLP) does direct some level of transcription early in infection. As well, the L genes for proteins IVa2, pIX, L4-22K, and L4-33K are expressed in sizable quantities somewhat earlier than the remaining late proteins, creating a soft intermediate category[4]. Regardless, the MLP begins to express its transcription unit to a meaningful extent around the onset of viral genome replication. At this point, the only things left for the virus to do are to assemble capsids, package their genomes, and lyse the host cell, and as such, the functions of the late proteins mostly fall into one of these categories.

Proteins II, III, and IV are the major capsid proteins: Hexon, penton base, and fiber respectively. As an icosahedral *pseudo* T = 25 virus[191], each face of the adenovirus capsid is made up of 72 hexon units, and at each vertex, a trimeric strand of fiber protein projects out from the centre of five penton units. The knob domain of fiber binds to the host cell transmembrane coxsackie adenovirus receptor (CAR) protein as the first step of viral attachment[192], leading to interaction between the cellular αvβ3/αvβ5 integrins and the RGD loop domains of the penton base, allowing for viral entry[193].

The minor capsid proteins, IIIa, VIII, and IX, are responsible for stabilizing non-equivalent interactions between hexon trimers. This allows the same hexon trimer to be used in four different chemical environments on the capsid surface[194]: The group of six connections (penton to each of the five hexon units it touches) at each vertex are stabilized by protein IIIa, groups of nine hexon units are lashed together by protein IX “ropes,” which also connect each group of nine to its adjacent groups of nine, and the groups of six are stabilized in their connection to groups of nine by a combination of proteins IIIa and VIII[194].

The viral core proteins, VII, VI, V, IVa2, adenovirus protease (AVP), terminal protein, and μ, are found inside the capsid, and have more varied functions. The major core protein is VII, with the function of condensing viral DNA into clusters inside the capsid[195], referred to as adenosomes. It also helps prevent the viral genome, upon release into the nucleus, from being recognized by the cellular Mre11-Rad50-Nbs1 (MRN) DNA repair complex[196]. Protein VI slots into cavities on the inside surface of hexon trimers[197], while binding to protein V[198], which is associated with the viral DNA, the pair serving as a tether between the capsid and genome. Protein μ (also known as protein X) contributes to the organization of the viral genome as well, aiding in DNA condensation[199] and interacting with protein V, which in turn interacts with protein VII, resulting in a μ-V-VII multimer[200]. It also plays a role in E2 protein expression. Specifically, if transiently expressed in its precursor form prior to or shortly following infection, the appearance of pre-terminal protein (but no other E2 proteins) is prevented, leading to a lack of late protein expression[201]. Protein IVa2 is present at a low copy number per virion, binding to the aforementioned packaging domain (see section 2.2 – The Adenovirus Genome), while localizing to the inside of a single vertex of the viral capsid[202]. It is required for the packaging of adenovirus DNA[4].

The AVP protein is a viral endopeptidase that is packaged, complete, into the viral capsid[203]. It is synthesized in an inactive state[204], but achieves maturity within the viral capsid through a series of interactions within the capsid, such that it is fully functional by the start of the infection cycle[204–206]. This is necessary for proper disassembly of the viral capsid following infection[207], and assembly of new capsids following genomic replication[208]. Its function is to cleave precursor forms of various other viral proteins, those being IIIa, VI, VII, VIII, μ, and terminal protein[209], as well as the non-structural 52K/55K protein[210], required for genome packaging.

The last of the adenovirus core proteins, terminal protein, has already been discussed (see the section on the E2 transcription unit).

The L4 proteins 22K and 33K are somewhat miscellaneous in their function, both falling into the small intermediate category of viral proteins. L4-22K is a multi-functional protein with roles in multiple aspects of infection: It regulates late gene expression, both through activation of the late genes and through suppression of the early; it is required for packaging of the genome, binding to packaging sequences and recruiting IVa2 and L1-52/55K (two other packaging proteins); and it regulates expression of the E3 protein ADP (Adenovirus Death Protein), contributing to the process of host cell lysis[211]. L4-33K is less complex in function, serving as an RNA splicing factor that affects transcripts with a weak 3' splice site sequence context (common among late sequence transcripts), critical to the proper splicing of late protein IIIa[212].

**2.3 Human Adenovirus as a Therapeutic Vector**

HAdV has long had a role as a vector for delivery of therapeutic genes[3] due to its high transduction efficiency in most cells, ability to persist within a host cell without integrating into its genome, broad host range, and decades of pre-existing research allowing for scalable production systems[213]. These constructs can be divided into three generations of design (pictured in Fig. 2.4)[3]. The first removes the E1 and E3 regions[3], the second removes either the E2 or E4 region as well[214–218], and the third removes everything except the packaging sequence[219], replicating only with the aid of a helper virus (HV) [220]. In all cases, the E1 region must be provided in *trans* to allow for proper growth of the construct, through cell lines such as HEK 293[10], HER 911[221], and Hela-E1[222].

The first attempts at gene therapy in humans using HAdV vectors attempted to express the cystic fibrosis transmembrane conductance regulator (CFTR) in cystic fibrosis patients[223] and

vascular endothelial growth factor (VEGF) to combat peripheral vascular disease[224]. Following the discovery of the strongly immunogenic properties of these vectors (even those lacking all viral genes)[3,225] and the unfortunate death by cytokine storm of Jesse Gelsinger (1999), a participant in a gene therapy pilot study for the treatment of ornithine transcarbmaylase (OTC) deficiency[226], research slowed on this avenue of treatment for a time. Now, any gene therapy treatment using HAdV-based delivery systems must be wary of the strong innate immune response that the vector will likely induce.

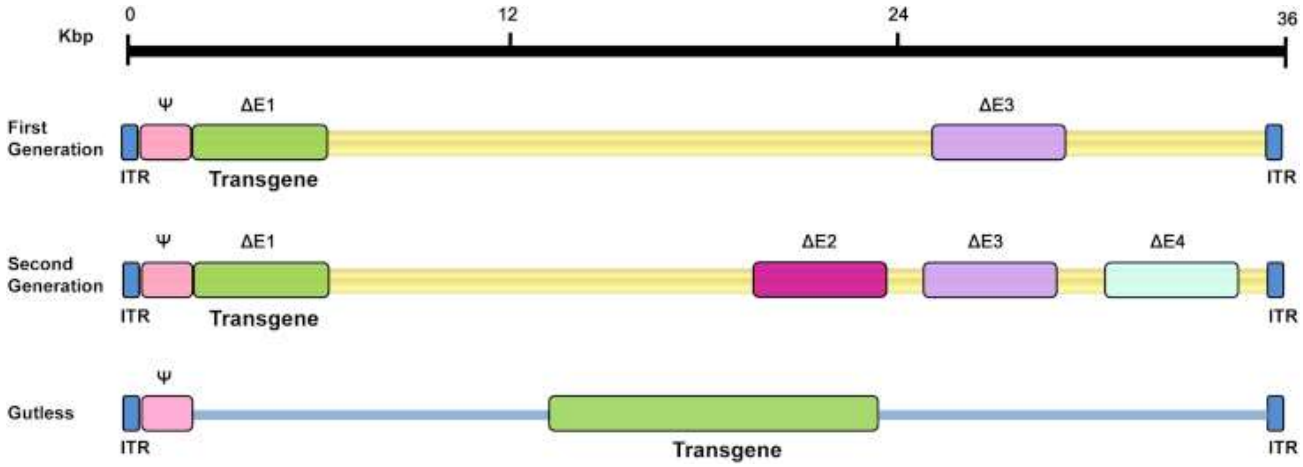


**Figure 2.4. Genomic layout of adenoviral transgene vectors by generation.** Δ regions represent areas of the genome that have been removed. Ψ represents the packaging domain. Figure reproduced under Creative Commons Attribution-Noncommercial-Noderivatives 4.0 International license without alteration. Originally produced by Lee et al. (2017)[213], copyright Chongqing Medical University. https://creativecommons.org/licenses/by-nc-nd/4.0/

Despite their flaws, Ad-based vectors are still an important avenue of research in the field of gene therapy, occupying 50% of total worldwide clinical trials[3]. The most relevant example almost goes without saying: Adenovirus vectors were recently used for a sizable number of SARS-CoV-2 (the causative agent of COVID-19) vaccines, such as ChAdOX1 nCoV-19[227], Sputnik V[228], Ad5-nCOV[229], and Ad26.COV2-S (Johnson & Johnson)[230]. All of these function by providing a transgene for the SARS-CoV-2 spike protein, inducing a humoral immune response as infected cells generate and present this antigen. The Johnson & Johnson vaccine uniquely contains a recombinant version of the spike gene altered to maintain its prefusion orientation[230]. In 2021, it was approved in over 40 countries, Canada and the USA included, for individuals 18 or over[231], though administration was later paused due to 15 reports of severe thrombosis with thrombocytopenia out of 7.98 million doses that had been administered[232]. The following investigation concluded that development of this condition, now called thrombosis with thrombocytopenia syndrome (TTS), was low enough to justify resumption of vaccine administration[232,233]. Other Ad-based vaccine vectors include Ad26.ZEBOV (Ebola virus)[234], Ad26.ZIKV.001 (Zika virus)[235], Ad26.Mos.HIV (HIV)[236], and ChAdOx1 (influenza virus)[237,238]. Several Ad-based vaccine vectors also exist for the purpose of cancer prevention as well, providing transgenes that code for tumour-associated antigens (TAAs), generating a humoral immune response to certain types of cancer within the recipient. These target a number of different tumour types, and are reviewed in detail by Shaw and Suzuki[239].

One approach taken by certain groups in construction of therapeutic Ad constructs, both for gene therapy and oncolysis, is to alter the host specificity of the viral particle. The first step in normal Ad entry into a host cell is binding of the viral fiber protein to receptor protein CAR[192], and as not all cells in the human body express these receptors in great quantities, certain targets

are harder to infect than others[3]. DNX-2401, for example, is an E1A CR2-deleted oncolytic virus with an RGD-4C sequence inserted into the HI loop of its fiber knob. This allows for direct targeting of αvβ3 and αvβ5, independently of CAR, and greatly enhances virus tropism[240]. The HAdV5/3 chimeric vector is another example, based on HAdV-C5, but swapping out the fiber knob domain for that of HAdV-B3[241]. As species B HAdVs uniquely target a different receptor than all other HAdV species[4], this has been shown to improve transgene expression in certain cancer types[241].

### 2.4 Interferon: Production and Response

Type-I interferons (IFN-I) – specifically IFN-α and IFN-β – are defined as cytokines that confer resistance to viral infections, named in 1957[242]. They are components of the innate immune system, essentially chemical messengers allowing virally-infected cells to "warn" other nearby cells of incoming danger. The antiviral state they initiate when detected by the cell has earned them a historical role in treatment of viral infection[243]. Most cells produce IFN-I, but sources can vary with different infections. For example, when the infection is localized to the mucosa, epithelial cells and alveolar macrophages provide the majority of the interferon[244,245] (the local cells available to internalize the virus in the first place), while infections of the brain see IFN being secreted by neuron cells[246]. That said, immunity is complicated, and so sources of IFN can vary wildly depending on the type, location, and severity of the infection in question, reviewed in detail by Swiecki and Colonna[247].

A major example of a variant IFN source is the plasmacytoid dendritic cell (pDC). pDCs are derived from bone marrow and secrete IFN-I in large quantities. Generally, while cells local to the infection secrete IFN initially, when that line of defence is broken and the infection becomes systemic, the balance shifts to favour pDCs[248]. Various individual cell types have been identified

as unique and important providers of IFN-I during infections with different viruses[247], though describing each individually would be beyond the scope of this review. Of note, however, is that splenic dendritic cells produce sizable quantities of IFN-I during systemic infections by adenoviruses[249].

Multiple receptors are responsible for detecting invaders, the two most common examples being toll-like receptors (TLRs 1 through 13)[250], which detect proteins containing molecular patterns commonly associated with pathogens, and RIG-I-like receptors (RLRs – RIG-I, MDA5, LGP2)[251], which bind to common viral RNA structures that accumulate during infection. Additionally, DExD/H box-containing helicases (DHX1, DDX21, DDX36) detect viral cytosolic dsRNA (in classic dendritic cells), forming a sensor complex with TRIF[252]. Some more widely-distributed (that is to say, present outside of specialized dendritic cells) molecular sensors for the detection of viral DNA are DNA-dependent activator of IFN-regulatory factors[253] (DAI, also known as ZBP1 or DLM-1), stimulator of interferon genes[254] (STING), and IFI16[255]. Each of these sensors, as well as others still, trigger a different signaling cascade leading to the production and secretion of IFN.

These IFNs, once secreted, are detected by receptors on nearby cells. These are dimers of different proteins, triggering different responses depending on the IFN type they are designed to detect, but as this project only investigated the effects of type I IFN, the specifics of types II and III will not be discussed here. The type I IFN receptor is a heterodimer composed of transmembrane proteins IFNAR1 and IFNAR2 which, when activated by the binding of IFN, recruit the proteins tyrosine kinase 2 (TYK2) and Janus Kinase 1 (JAK1). Now activated, these kinases phosphorylate signal transducer and activator of transcription 1 and 2 (STAT1 and STAT2), which form a heterodimer with one another and in turn recruit the protein interferon regulatory

factor 9 (IRF9)[256,257]. This complex, now dubbed interferon-stimulated gene factor 3 (ISGF3), is then translocated to the nucleus, wherein it binds to recurring promoter elements called interferon-stimulated response elements (ISREs – consensus sequence TTTCNNTTTC[257]), common to the promoter regions of interferon-stimulated genes (ISGs)[258], driving the recruitment of chromatin remodelers and the RPII complex to the ISG promoter, activating transcription[259]. This is in contrast to the more common pattern among cytokines of generating STAT homodimers which bind to a distinct gamma-activated sequences (GAS – consensus sequence TTCNNNGAA)[257]. As such, type I IFN signalling triggers the transcription and subsequent translation of a unique subset of ISRE-driven ISGs, which possess many and varied functions, though the overall effect is the induction of the aforementioned antiviral state that IFN is meant to cause[260]. This response is depicted in Fig. 2.5.

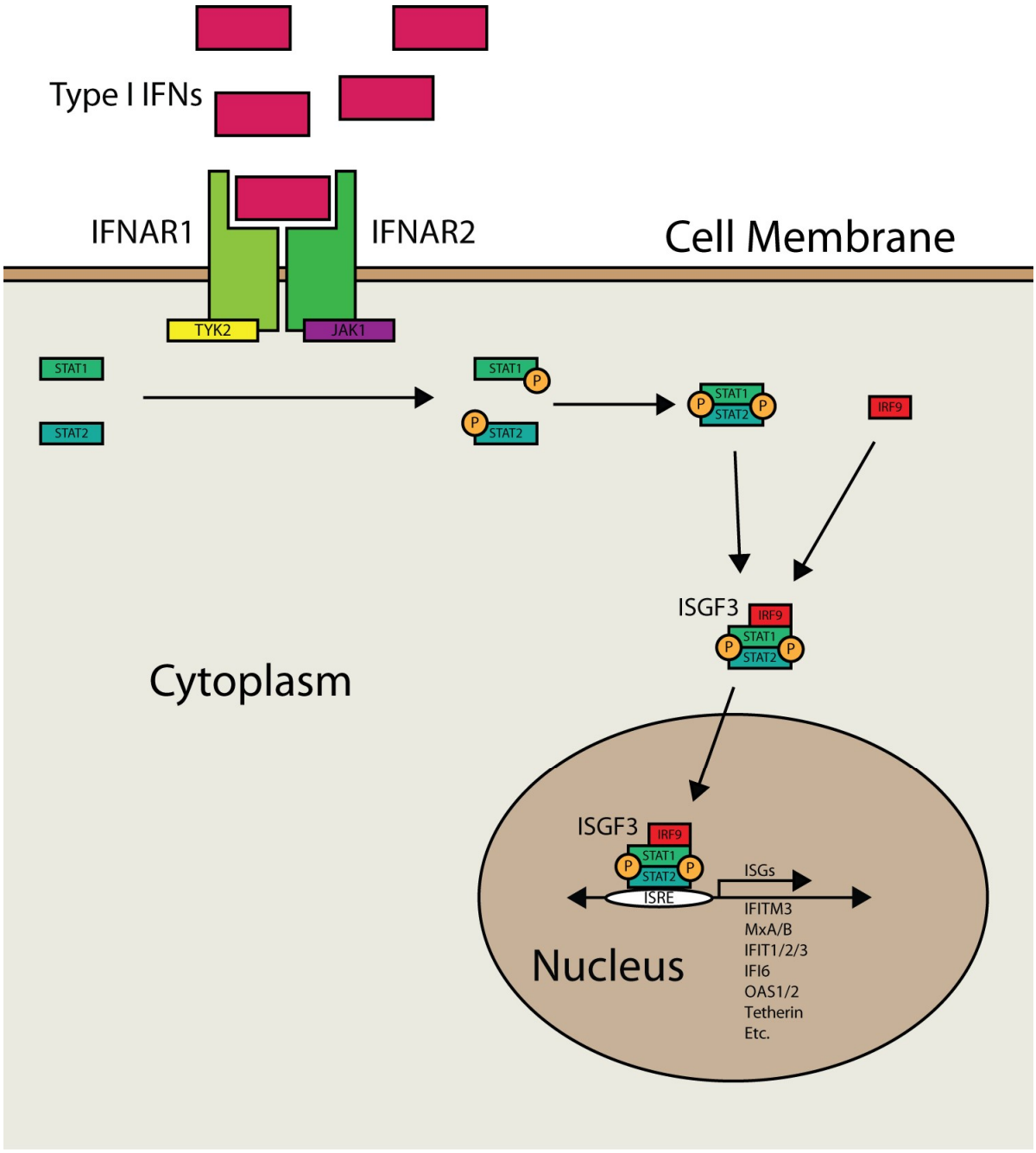


**Figure 2.5. Diagrammatic representation of the type I IFN response.** Type I IFNs are detected by dimeric receptor IFNAR1 and IFNAR2, which recruits kinases TYK2 and JAK1. Kinases phosphorylate STAT1 and 2, which dimerize and recruit IRF9, forming the ISGF3 complex, which is translocated to the nucleus, binding to ISG promoter elements (ISREs) to trigger their expression.

Immune cells are equipped to respond quickly to even small amounts of IFN, thanks to an autocrine loop within the body maintaining a basal level of IFNβ. This maintains a steady level of STAT1 and IRF9, which are themselves ISGs[261]. Interestingly, this basal expression is driven in part by commensal microflora, which are able to help calibrate type I IFN responses[262]. IFNAR signal induction is also up- and down-regulated by a number of factors. The protein immunoreceptor tyrosine-based activation motif (ITAM) and its associated immunoreceptors express tonic signals that augment IFNAR signalling in response to binding a set of endogenous ligands that provide a "picture" of the cell's external environment, to fine-tune the immune response to the situation at hand[263]. ITAM signalling activates protein tyrosine kinase 2 (PYK2, or PTK2), which amplifies IFN-induced JAK activation[257]. Basal IFNAR signalling is also opposed by other mechanisms, such as RPII pausing on genes encoding components of the IFN pathway[264], downregulation of IFNAR[265], or miRNAs interfering with translation of these gene products[266]. Part of the type I IFN response is induction of proteins such as SOCS1, SOCS3, and USP18, which serve as negative regulators and limit its extent and duration[267].

It has recently been shown that the multi-purpose ATPase proteins RuvB-like 1 and 2 (RuvBL1 and RuvBL2) interact with the transactivation domain of STAT2 in the nuclei of IFN-treated cells, and by knockout both were confirmed to be major requirements for the expression of ISGs[90]. Interestingly, knockdown of any of their known complex partners (other members of the Tip60, BRD8, Ino80, SRCAP, and URI complexes) had no effect on ISG expression, implying an as-of-yet unidentified RuvBL complex to be involved here. Chromatin IP assays demonstrated that while RuvBL1 and RuvBL2 were necessary for recruitment of RPII to ISG promoters, they were not needed for recruitment of STAT2 to the same regions. This implies the RVB-containing

complex to be brought assembled and localized by the ISGF3 complex, where it in turn performs some action to initiate ISG transcription.

From the first microarray studies of the effect of IFN on cells, the number of ISGs has been estimated to exceed 300. One early meta-analysis of ISG transcriptomes estimated around 450 genes to be induced by type I IFN alone[268], and with time, this number has only grown. A more recent RNA-Seq experiment has shown that around 10% of the human genome is in some way regulated by the presence of IFN[269], though admittedly many of these genes are not induced very strongly. Additionally, by comparing the results of multiple RNA-Seq experiments across a diverse collection of vertebrate cells, this study found that despite the large cohort of ISGs within human cells, only 62 genes seemed to be widely evolutionarily conserved[269]. Generally, the function of a given ISG is to interfere with some aspect of the viral replication cycle, from entry into the host cell all the way through final release of assembled virions.

As the subject of this thesis primarily focuses on the induction of ISG expression, rather than the effects of the ISGs themselves, I will not provide a detailed description of all their functions. However, to estimate overall ISG expression levels, I routinely measured the quantity of a representative suite that I will quickly describe here, consisting of *IFI6*, *IFIT1*, *IFIT2*, *OAS1*, and *OAS2*.

IFITs 1 and 2 represent half of the *IFIT* genes present in humans (the other two being 3 and 5). The goal of this protein family is to interfere with the translation of viral proteins. IFIT1 has been demonstrated to strongly bind to viral triphosphorylated mRNA[270], with IFITs 2 and 3 binding similarly, though as part of a complex rather than directly, suggesting a role in sequestration of viral mRNA. This feature of IFIT1 has also proven true for viral RNA lacking 2'-O methylation of its cap, with similar results[271]. In both cases, the presence or absence of IFIT1 was not a major

factor for viruses lacking the mentioned mRNA cap variants. These IFIT proteins also bind to eukaryotic translation initiation factor eIF3, globally reducing the rate of protein translation[272], and interfering with viruses that rely on internal ribosome entry sites for cap-independent translation, as this process requires eIF3[273].

The roles of IFI6, OAS1, and OAS2 are all to interfere with viral genome replication. IFI6 targets flavivirus replication in the ER, in combination with heat shock protein 70 chaperone BiP, by preventing the formation of flavivirus's characteristic ER membrane invaginations (within which it copies its genome)[274]. The protein family of oligoadenylate synthetases (OAS1, OAS2, OAS3, and OASL), on the other hand, take a more general approach. These proteins are pathogen recognizers that search for viral dsRNA, at which point they activate cellular RNase L, an endoribonuclease for viral ssRNA, targeting RNA genomes for direct destruction[275]. The cleavage products, whether from viral or cellular RNA, can then in turn be picked up by RIG-I-like receptors, resulting in the further production and secretion of IFN[276,277]. RNase L is also a critical component in IFN induction in response to herpes simplex virus, a dsDNA virus[278].

Each ISG has a limited pool of viral targets, and while some target multiple steps, others are quite specific. The outcome of their united, simultaneous expression and activation, however, is the generation of a potent antiviral state within the cell. As such, it is within the interest of any invading virus to overcome the IFN response to as great a degree as possible.

## 3. Differential Splicing of Human Adenovirus 5 E1A RNA Expressed in *cis* versus in *trans*

### 3.1 Introduction

The discovery of eukaryotic gene splicing can be credited to Richard J. Roberts[41] and Philip A. Sharp[42], both of whom did so while working with HAdV. This critical feature allows for an organism to produce far more varied proteins than the size of its genome would let on[279], and HAdV is one such virus. The gene for HAdV E1A encodes five possible proteins from one pre-mRNA[280], these being E1As 289R, 243R, 217R, 171R, and 55R, encoded by 13S, 12S, 11S, 10S, and 9S mRNAs respectively[44] (see Fig. 2.2). Expression levels of these isoforms change with time post-infection, with the two largest primarily expressing first, and the smaller three appearing later. The 10S-derived 171R protein ultimately expresses to the highest level[43,46].

While the functions of the early/large E1A isoforms are well-characterized[2,280], the small/late isoforms are less-so. What is known is that HAdVs mutated to express the 217R or 171R isoforms instead of proper E1A are defective for growth in HeLa cells and transformation of rodent cells[44], and that the 55R isoform uniquely localizes both to the nucleus and the cytoplasm[95], weakly activates viral gene expression[95], interacts with the S8 component of the proteasome[95], and functions as a transcriptional activator, binding to the unliganded thyroid hormone receptor[96].

This section presents a study, published in the Journal of Virology under the same name[281], comparing the generation of late E1A transcripts in 293 cells during infection with viruses that normally express E1A from their genomes (*dl*309 and *wt*300/HAdV-C5) to a virus deleted for E1A (*dl*312), expressing E1A only in *trans*, from the cell line. While these scenarios are nearly identical in terms of the genotypes present, E1A late transcripts were only produced in sizable amounts when the infecting virus provided its own E1A gene. When the virus was E1A-deleted, late E1A

transcripts and proteins were nearly non-existent, and this had overall negative effects on viral fitness and growth.

While the majority of the work here was performed by myself, the genomic sequencing in section 3.3.2, the making of panel C of Fig. 3.8, and the generation of cell lines referenced in section 3.3.7 were performed by my fellow students Nikolas Akkerman and Scott Bachus, and my supervisor Peter Pelka respectively.

## 3.2 Materials and Methods

**3.2.1 Antibodies.** Mouse monoclonal antibodies against E1A M1, M37, M58, and M73 have been described previously[282] and were grown in-house and used as the supernatants of hybridoma cells. A cocktail of all hybridomas was used for E1A detection to maximize sensitivity at a 1:50 dilution of the supernatant from hybridoma cells. The mouse monoclonal anti-72K DBP antibody has been described previously[283] and was used at a dilution of 1:10 for immunofluorescence and 1:400 for Western blotting. Anti-adenovirus type 5 antibody was purchased from Abcam (catalog no. ab6982; Abcam, Cambridge, MA, USA). Actin and digoxigenin (DIG) antibodies were purchased from Abcam (actin catalog no. ab3280; DIG catalog no. ab76907). Horseradish peroxidase-tagged secondary antibodies were acquired from Jackson ImmunoResearch (West Grove, PA, USA) and were used at a dilution of 1:200,000 for Western blotting. Alexa Fluor 488- and 594-conjugated secondary antibodies were purchased from Thermo Fisher Scientific and were used at a dilution of 1:600 for immunofluorescence.

**3.2.2 Cell and virus culture.** Human embryonic kidney 293 cells (ATCC CRL-1573) were grown in Dulbecco's modified Eagle's medium (HyClone) and supplemented with 10% fetal bovine serum (VWR Seradigm) and streptomycin and penicillin (HyClone). Cells were incubated at 37°C

and 5% $CO_2$. All virus infections were carried out in serum-free medium for 1 h, after which complete medium was added without removal of the infection medium. For all infections, viral stocks were prepared by infecting HEK-293 cells with the virus at MOI 10 until total cell death was observed. Cell remains and media were then harvested and freeze-thawed three times, debris was removed from suspension by centrifugation (1,400 RPM for three minutes), and supernatant was aliquoted (1.5 mL) and titred *via* plaque-forming assay on 293 cells.

**3.2.3 Co-immuno-FISH.** 293 cells were plated at a low density (40,000 cells per chamber) on four-chambered slides (Nalgene Nunc) and subsequently infected as described above. Twenty-four hours after infection, cells were fixed in 4% formaldehyde and permeabilized in 0.1% Triton before DNase I was applied at a concentration of 5 U/ml for 1 h to remove viral and cellular DNA. Cells were blocked in FISH blocking buffer (pH 7.4) (0.1 M maleic acid, 0.15 M NaCl, 1% FISH blocking agent [Roche]) and prehybridized in hybridization buffer (50% deionized formamide, 2× SSPE [1× SSPE is 0.18 M NaCl, 10 mM $NaH_2PO_4$, and 1 mM EDTA {pH 7.7}], 5× Denhardt's reagent, 1 mg/ml baker's yeast tRNA [Roche]). Probes (made using a New England Biolabs HiScribe T7 high-yield RNA synthesis kit by following manufacturer instructions) were applied at a concentration of 10 ng/μl in hybridization buffer and were left in a 42°C humidified chamber overnight. Chambers were washed with a 50% deionized formamide–2× SSPE solution at 42°C and were blocked with FISH blocking solution. Cells were stained with primary antibodies: anti-DIG at a dilution of 1:100 and anti-DBP at 1:10. Secondary antibodies were conjugated with Alexa Fluor 488 and Alexa Fluor 594 and were applied at a dilution of 1:600. After staining and extensive washing, slides were mounted using ProLong Gold with 4′,6-diamidino-2-phenylindole (DAPI) (Invitrogen) and were imaged using a Zeiss LSM 700 confocal laser scanning microscope. Images were analyzed using the Zeiss ZEN software package.

**3.2.4 PCR primers.** All primers and probes were purchased from Integrated DNA Technologies, and an annealing temperature of 60°C was used. All primer sequences are listed below in table 3.1.

| *Category* | *Name* | *Sequence* |
|---|---|---|
| ***E1A*** | *Total E1A F* | ATGAGACATATTATCTGCCACGG |
| | *Total E1A R* | CCATGTGCTAGCTTATGGCCTGGGGCGTTT |
| | *E1A 13S F* | TTTTGAACCACCTACCCTTC |
| | *E1A 13S R* | CCACAGGTCCTCATATAGCAAA |
| | *E1A 12S F* | TTTTGAACCACCTACCCTTC |
| | *E1A 12S R* | GGAGTCACAGCTATCCGTACTACT |
| | *E1A 11S F* | GATCGAAGAGCCCGAGCA |
| | *E1A 11S R* | CCACAGGTCCTCATATAGCAAA |
| | *E1A 10S F* | GATCGAAGAGCCCGAGCA |
| | *E1A 10S R* | GGAGTCACAGCTATCCGTACTACT |
| | *E1A 9S F* | TGATCGAAGAGGTCCTGTGTCT |
| | *E1A 9S R* | TCAGGATAGCAGGCGCCA |
| ***Non-E1A Early Genes*** | *E1B-19K F* | TTCTGCTGTGCGTAACTTGC |
| | *E1B-19K R* | ACTAACTTTGCCTGGGATGAGC |
| | *E1B-55K F* | AACTGTCACCTGCTGAAGACC |
| | *E1B-55K R* | ACCCAAATGCAAGGAACAGC |
| | *E2-DBP F* | TTTCTTCTTGGGCGCAATGG |
| | *E2-DBP R* | AAGACTCATCACAAGACGCG |
| | *E3 F* | TTGTTGCCATCTCTGTGCTG |
| | *E3 R* | AAAGTACCAGGTAAGGTTCGCC |
| | *E4orf6/7 F* | AAGTTCATGTCGCTGTCCAG |
| | *E4orf6/7 R* | GTGGACTTCTCCTTCGCCG |
| ***Late Genes*** | *HEXON F* | AGCATTTGCCTTTACGCCAC |
| | *HEXON R* | TGTCGTTTCTAAGCATGGCC |
| | *Fiber F* | ATGCTTGCGCTCAAAATGGG |
| | *Fiber R* | TTTTTGAGAGGTGGGCTCAC |
| ***VA-RNA*** | *VAI F* | AAGGGTATCATGGCGGACG |
| | *VAI Probe* | ACCGCCCGCGTGTCGAACCCAGGTGT |
| | *VAI R* | GAGCACTCCCCCGTTGTC |
| | *VAII F* | TTTTCCAAGGGTTGAGTCGC |
| | *VAII Probe* | TCGAGTCTCGGACCGGCCGGAC |
| | *VAII R* | AATTTGCAAGCGGGGTCTTG |
| ***Housekeeping*** | *GAPDH F* | GAGTCAACGGATTTGGTCGT |
| | *GAPDH R* | TTGATTTTGGAGGGATCTCG |

**Table 3.1. PCR primer sequences used in E1A splicing analysis.**

**3.2.5 Real-time gene expression analysis.** 293 cells were infected with the different viruses at multiplicity of infection (MOI) 10 for 16, 24, and 48 h. Total RNA was extracted using the NucleoZOL reagent (Macherey-Nagel) at the time points indicated in the figures according to the manufacturer's instructions. One microgram of total RNA was used for the reverse transcriptase reaction using SuperScript VILO reverse transcriptase (Invitrogen) according to the manufacturer's guidelines by using random hexanucleotides for priming. The cDNA was subsequently used for real-time expression analysis with the Bio-Rad CFX96 real-time thermocycler (Bio-Rad) and the Applied Biosystems SYBR Select Master Mix for CFX in all cases except for analysis of VA RNA I and II, which used IDT PrimeTime Gene Expression Master Mix for probes. Expression data were normalized to *glyceraldehyde-3-phosphate dehydrogenase* (GAPDH) mRNA levels.

**3.2.6 Sequencing of genomic E1A from 293 cells.** Cells were lysed in alkaline lysis buffer (25 mM NaOH and 0.2 mM EDTA). The lysate was incubated at 95°C for 10 min, cooled to 4°C, and neutralized with 0.5 M Tris (pH 8.0) according to the procedure described by Truett *et al*[284]. A total of 5 µg DNA in the neutralized lysate was diluted into 100 µl Tris-EDTA (TE) buffer (Invitrogen) and sonicated in a Covaris M220 focused ultrasonicator using the default 1,000-bp fragmentation program in a Covaris microtube AFA fiber preslit snap cap to break up the genomes. PCRs were run using a Phusion High-Fidelity PCR kit (New England Biolabs) with 2 µl of sonicated lysate as the template, 2.5 mM (final concentration) $MgCl_2$, and a 60°C annealing temperature with forward primer CCATGTGCTAGCTTATGGCCTGGGGCGTTT and reverse primer ATGAGACATATTATCTGCCACGG. Amplified *E1A* genomic DNA was purified using an EZ-10 gel extraction kit (Bio-Basic). Purified PCR products were sent to The Centre for Applied Genomics in Toronto, ON, Canada, for sequencing using the same forward and reverse primers,

and 12 independent PCR products were analyzed pairwise. Sequences were analyzed using ContigExpress software (Invitrogen).

**3.2.7 Stable cell lines expressing the 217R, 171R, and 55R E1A isoforms.** E1A 9S and 10S RNAs were amplified 72 h after infection from total RNA of A549 cells infected with *wt*300 at MOI 10 by using the OneTaq One-Step RT-PCR kit (New England Biolabs) with forward primer AGCTCGXXXXXXACCATGAGACATATTATCTGCCACGGAG (where XXXXXX is the sequence of the restriction site used for cloning, which differed for the 10S and 9S mRNAs [HindIII and BamHI, respectively]) and reverse primer ACGTCGCTCGAGTTATGGCCTGGGGCGTTTAC and were cloned into the pVITRO2 (Invivogen) dual-expression plasmid. E1A-11S RNA was a generous gift from Dr. Joe Mymryk (Victoria Hospital – London, Ontario) and was cloned out of pcDNA-HA-E1A-11S into pcDNA3.1 with removal of the hemagglutinin (HA) tag. Low-passage-number 293 cells (passage 27; a generous gift from Dr. Frank Graham – McMaster University) were transfected with either pVITRO2-E1A-9S/10S or pVITRO2-E1A-9S/10S and pcDNA3.1-E1A-11S. Cells were selected 48 h after transfection with 150 μg/ml of hygromycin B (Millipore-Sigma) for single-plasmid transfection or 40 μg/ml of hygromycin B and 160 μg/ml Geneticin (Invitrogen) for dual-plasmid transfection. Cells were selected for 4 weeks until colonies were well defined, pooled, and used as a pool of all colonies for further assays to avoid specific clonal differences.

**3.2.8 Statistical analysis.** Statistical analysis was conducted using unpaired Student *t*-tests of viral genes from *wt*300 infection versus *dl*312 virus infection. Viral growth assays were also subjected to unpaired *t*-tests comparing *dl*312 to *wt*300. *P* values were two-tailed, and values of $<0.05$ were considered statistically significant in gene expression assays and viral growth assays.

**3.2.9 Virus growth assay.** 293 cells were infected with *wt*300 and *dl*312 at MOI 10 as specified above. Virus titers were determined at 24, 48, and 72 h after infection by plaque assays performed on 293 cells by serial dilution.

**3.2.10 Splice isoform analysis.** 293 cells were infected with *wt*300 and *dl*312 at MOI 10 in serum-free medium as specified above. RNA was extracted 12, 16, 24, 48, and 72 h after infection using NucleoZOL reagent according to the manufacturer's instructions. cDNA was generated from E1A transcripts using One*Taq* One-Step RT-PCR Kit from NEB, which were PCR amplified with Bio-Rad PCR Supermix. The resultant DNA was resolved on an agarose DNA gel and visualized.

## 3.3 Results

### 3.3.1 E1A is differentially spliced when provided in *trans* by 293 cells

I observed that E1-deleted viruses, *dl*312 specifically (a partial E1A deletion mutant null for E1A protein expression[285]), grew poorly in 293 cells when compared to similar viruses that do express E1A (such as *dl*309, a partial E3-deletion mutant), despite 293 cells fully complementing the HAdV E1 region. I hypothesized that this was due, at least in part, to potential differences in the splicing patterns of early proteins expressed from the cellular genome, rather than the viral genome. The primary early transcripts provided in *trans* by 293 cells are E1A and E1B proteins, as well as the late protein IX[10]. E1B is known to produce at least five additional proteins beyond its classical 55K and 19K proteins[122,123], but these are likely minor species during infection[124]. As such, I chose to investigate E1A, a genomic region known to produce five separate proteins by alternative splicing (Fig. 2.1) [44,45]. I compared the splicing patterns of E1A in 293 cells infected with a virus either expressing E1A (*wt*300 (HAdV-C5) or *dl*309) or lacking E1A (*dl*312). In *wt*300- and *dl*309- infected 293 cells, I saw all five E1A mRNA species at levels that shifted with time

post-infection (large isoforms started plentiful and then dropped off, corresponding to an increase in the presence of smaller isoforms), as expected. In *dl*312-infected cells, however, the smaller E1A mRNA species were observed at much lower levels, consistently across all observed timepoints post-infection (Fig. 3.1A). Additionally, I observed an absence of 13S and 12S E1A mRNA at later timepoints in both E1A-expressing viruses, though this was likely a PCR artifact, as smaller products are already favoured for amplification, eventually allowing them to "out-compete" larger transcripts for limited PCR primers.

The observed changes in E1A mRNA levels were also seen in protein as well. I clearly saw 171R E1A (from 10S mRNA) expressed in both E1A-expressing infections, but it was nearly non-existent in the *dl*312 infection (Fig. 3.1B). All told, this suggests that the precise source of gene transcripts has a major impact on the splicing patterns of E1A and possibly other viral genes.

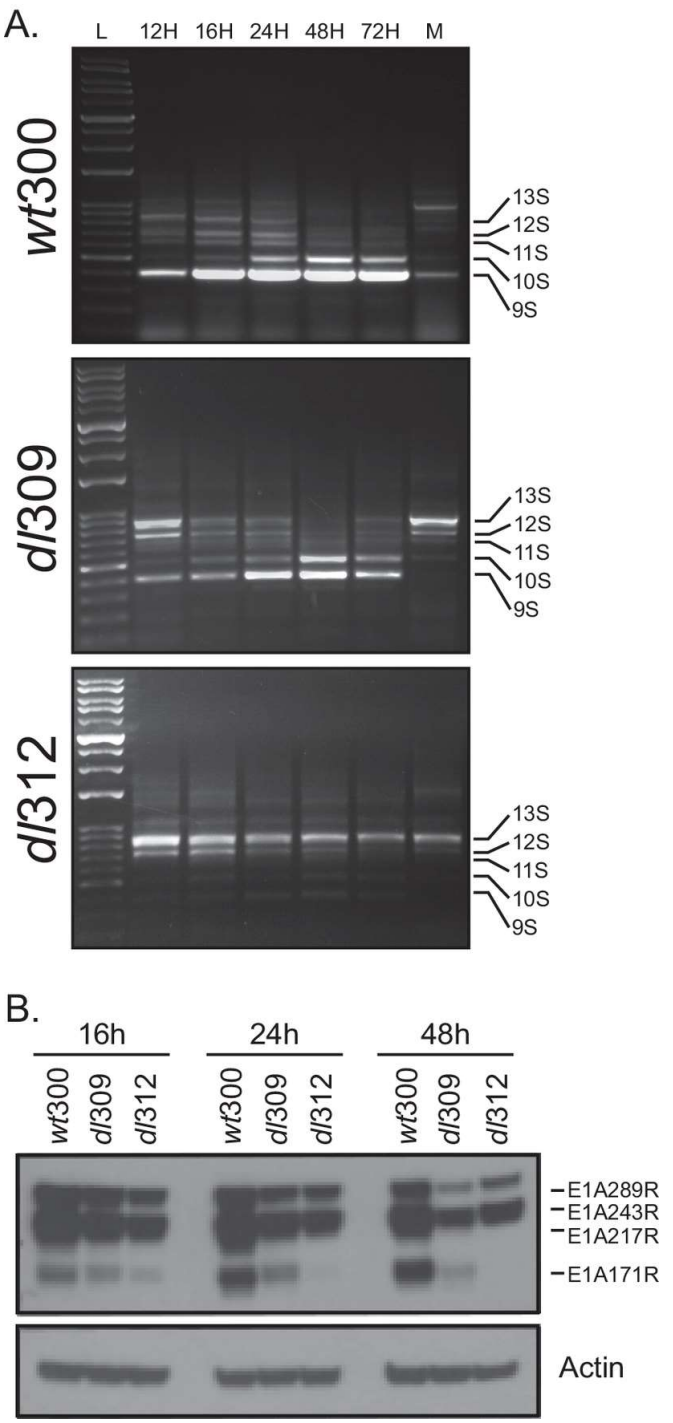


**Figure 3.1. Splicing of E1A pre-mRNA differs when it is expressed from the host genome.** (A) 293 cells were infected with adenovirus mutant strains at MOI 10, and RNA was extracted at the indicated time points. cDNA was generated from E1A transcripts, which was PCR amplified, resolved by agarose gel electrophoresis, and visualized with ethidium bromide staining. (B) 293 cells were infected with adenovirus mutant strains at MOI 10, and protein was extracted at the indicated time points. Twenty micrograms of the total-cell lysate was resolved by SDS gel electrophoresis, blotted for E1A or actin, and visualized using film.

### 3.3.2 The E1A gene in 293 cells is not mutated

It is worth noting the possibility that these differences in splicing patterns may be due to some mutation to the E1A provided in *trans* by the 293 cells in question, possibly in one of the splice junction sites (Fig. 2.1), preventing proper splicing, with the *wt*300 and *dl*309 viruses simply providing the wild type E1A gene. If such a mutation were able to affect splicing of the intra-exonic intron in the first E1A exon, this would completely explain away the previously-observed phenotypes. To account for this, I PCR amplified the genomic E1A region from the 293 cells that were used in all growth experiments and sequenced the E1A gene. Twelve separate PCR products were sequenced from both ends, providing a total of 24 sequencing runs, encompassing the E1A region in its entirety, including both introns. Compared to the HAdV-C5 reference genome, no mutations were present within the introns or exons of the E1A gene, leaving only its subnuclear location as an explanation for the observed splicing differences.

### 3.3.3 E1A RNA localizes to viral replication centres when expressed in *cis*, but not in *trans*

Having observed a difference in E1A transcript levels depending on whether it was expressed from both the virus and the cells or only the cells, I sought to determine whether the subnuclear localization of E1A RNA differed between cells infected with *wt*300/*dl*309 (E1A-expressing) and cells infected with *dl*312 (E1A-deleted – relies entirely on E1A provided in *trans* by the cell line). To observe the subnuclear localization of E1A RNA, I performed a co-immuno-FISH assay in 293 cells infected with *wt*300, *dl*309, or *dl*312 HAdV: This consisted of fluorescence *in situ* hybridization (FISH) for E1A RNA combined with an immunostain for the 72 kDa E2 DNA binding protein. As E2 DBP binds to viral ssDNA during viral genome replication[132], it localizes to viral replication centres, allowing for their visualization.

In *wt*300- and *dl*309-infected cells, E1A RNA was highly abundant in the nucleus, alongside punctate cytoplasmic localization (as is to be expected of mRNA). The nuclear E1A mRNA bodies fell into two distinct categories: Those that colocalized with the DBP-visualized replication centres (indicated by arrowheads in Fig. 3.2), and those that did not. Interestingly, in *dl*312-infected cells, I observed only the second category of E1A mRNA (non-colocalized), whereas *wt*300- and *dl*309-infection saw colocalization in around a quarter to a third of these bodies. Please note that even mock infections stain for E1A mRNA here, as 293 cells supply it from their genome.

To verify that the FISH probes detected only RNA, I probed *wt*300-infected 293 cells with a probe for the same sequence as the mRNA, referred to as the coding strand probe (CS probe). This is not complementary to the mRNA, meaning that any signal it picked up would have to come from the E1A sequence present in the viral or cellular genomic DNA. CS probe staining did not, however, present any signal, which indicated that any staining these probes observed came from mRNA specifically.

The results here indicate that E1A RNA expressed in *cis*, from the viral genome, colocalizes with viral replication centres, as one would expect. E1A expressed in *trans*, from the cellular genome, however, does not.

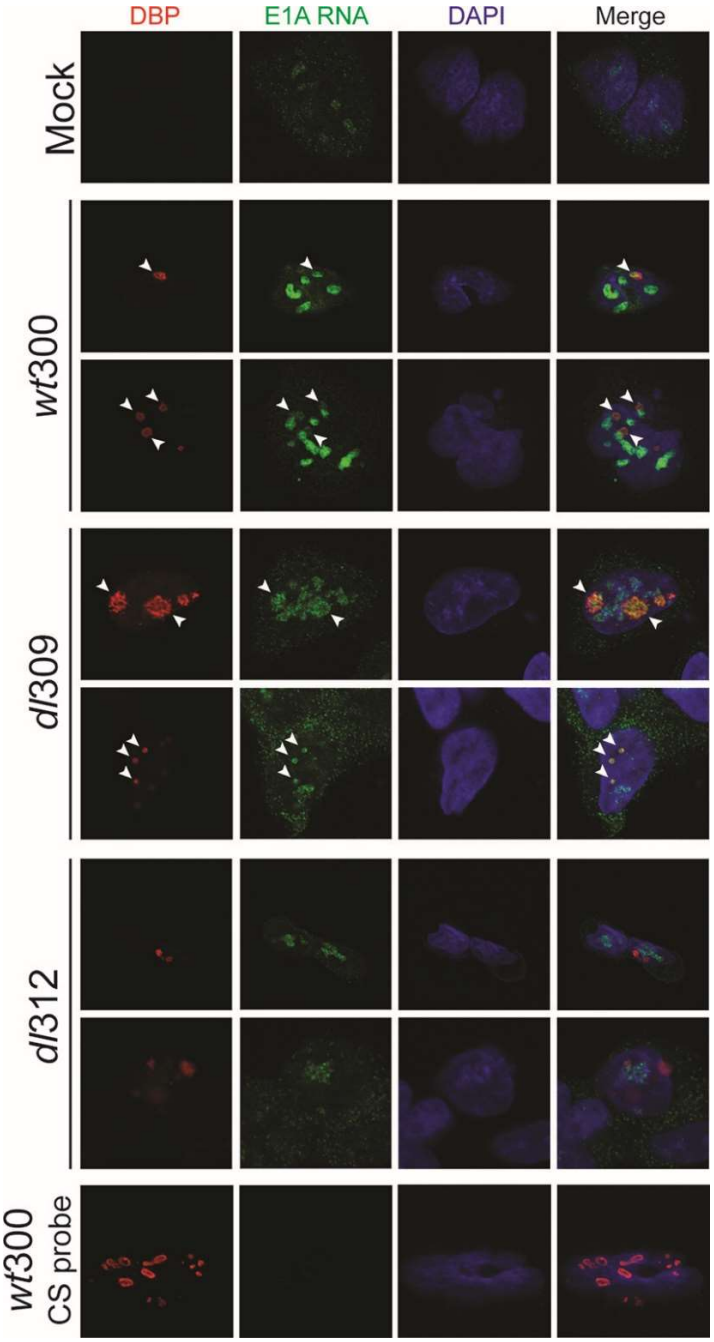


**Figure 3.2. E1A RNA expressed from the 293 cell genome does not localize to viral replication centers.** 293 cells were infected with adenovirus mutant strains at MOI 5 for 24 h. Cells were fixed and permeabilized, and internal RNA was hybridized to anti-E1A DIG probes. Cells were then stained with anti-DIG and anti-DBP antibodies and were further stained with Alexa Fluor 488-conjugated anti-goat and Alexa Fluor 594-conjugated anti-mouse secondary antibodies. CS probe, coding strand probe with the same sequence as E1A mRNA. DAPI was added as a nuclear counterstain. Arrowheads indicate points of colocalization between E1A RNA and viral DBP. Images were acquired on a Zeiss LSM 700 laser confocal microscope using a 63× objective lens.

### 3.3.4 The lack of smaller E1A species affects viral growth

While I had previously observed the poor growth of *dl*312 in comparison to *dl*309 (unpublished results), I still wanted to directly compare the growth of *dl*312 to the wild-type strain *wt*300 (HAdV-C5), which does not have the same E3 deletion as *dl*309[286]. Of note, *wt*300 has been previously shown to grow slightly worse than *dl*312, by a factor of around 50%[285]. Whether this difference is biologically significant remains to be determined, but it provides a good comparison point for our studies. Regardless, I observed that *dl*312 grew significantly worse than *wt*300 in 293 cells, despite their near-identical genetic profiles (Fig. 3.3A). *dl*312 grew more slowly overall, taking longer to reach a similar titre to *wt*300. 24 hours after infection, we observed a difference of nearly two orders of magnitude in titre between the two strains, which proceeded to diminish over time. By the endpoint of the assay, when all cells were dead, *dl*312 still showed a roughly 2-fold growth deficit compared to *wt*300.

These results were consistent with an additionally observed later onset of cytopathic effect (CPE) in the *dl*312-infected cells (Fig. 3.3B), along with an overall reduction in expression of viral late proteins (Fig. 3.3C). Interestingly, DBP expression was visibly higher in *dl*312-infected cells than *wt*300, with the appearance of greater levels of small DBP derivatives.

This observed reduction in growth demonstrates that the smaller E1A species play a meaningful role in the viral replicative cycle.

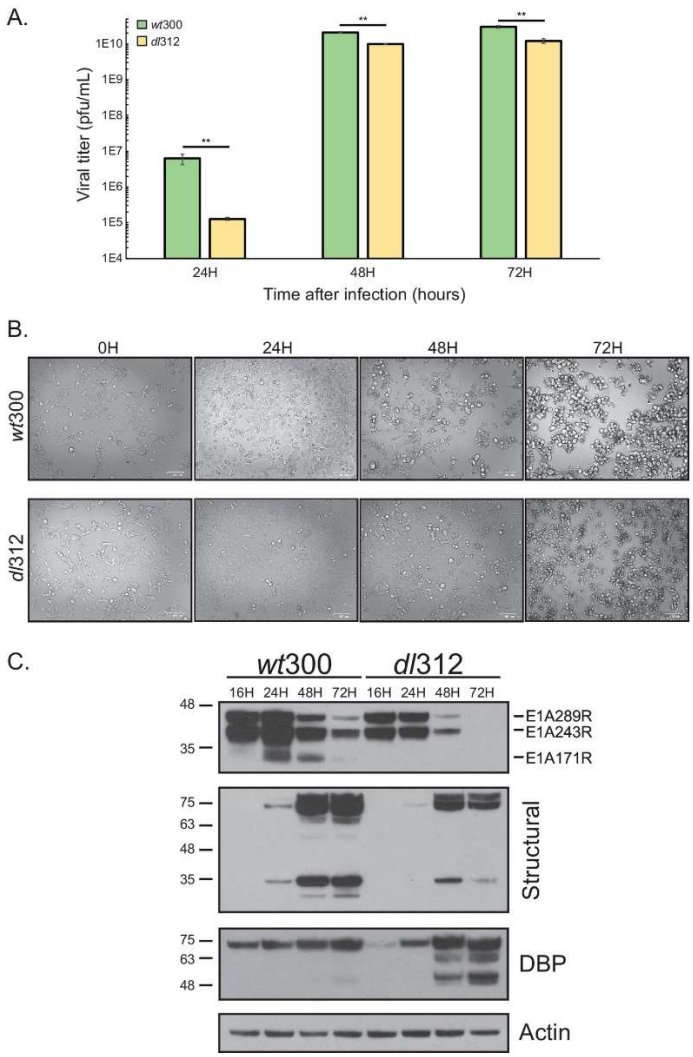


**Figure 3.3. HAdV5 *dl*312 shows delayed growth relative to that of the wild type.** (A) 293 cells were infected with the indicated HAdV5 strains at MOI 10. Titers were determined at the indicated time points by performing plaque assays on 293 cells. Statistical significance was determined by an unpaired *t* test. Results were significant at all time points with a *P* value of <0.01 (**). Data represent results for three biological replicates. (B) The infected cells for which results are shown in panel A were imaged with a 20× objective lens at each harvest time point. (C) 293 cells were infected with the indicated HAdV5 strains at MOI 10, and protein was extracted at the indicated time points. Twenty micrograms of the total-cell lysate was resolved by SDS gel electrophoresis, blotted for E1A, adenovirus structural proteins, or DBP, and visualized using film. Actin was used as a loading control.

### 3.3.5 Late E1A transcripts are weakly expressed during infection of 293 cells with *dl*312

Each experiment performed thus far had been primarily qualitative in nature. As such, I wanted to investigate whether the results we observed *via* nonquantitative reverse transcription-PCR (RT-PCR) (Fig. 3.1A) could be replicated and quantified. Therefore, I performed reverse transcriptase quantitative PCR (RT-qPCR) on 293 cells infected with *wt*300, *dl*312, or nothing at all (mock) (Fig. 3.4).

Uninfected 293 cells showed high levels of 12S and 13S E1A mRNA which, as expected, remained relatively consistent throughout the assay. The same could not be said for the later E1A transcripts (11S, 10S, and 9S), which were expressed at a much lower level. Similar results were observed in the *dl*312-infected cells as well. Levels of late E1A transcripts never increased, and levels of early E1A transcripts began to drop off later in the course of the infection, as one would expect due to cell death as a result of the completion of the viral replicative cycle.

In the *wt*300-infected cells, however, I observed steady increases in all E1A transcripts, as would be expected from a healthy viral infection. Most critically here, we saw a significant upregulation of late E1A transcripts that occurred 24 and 48 hours post-infection. The 9S and 10S transcripts were the most abundant of the late variants, while 11S mRNA remained low. That said, 11S was still expressed at higher levels than in *dl*312-infected cells.

All of this is consistent with our previous observations with *dl*309-infected 293 cells (Fig. 3.1) as well. The results demonstrate that levels of late E1A mRNA transcripts are consistently low when expressed in *trans* from the cellular genome and not in *cis* from the genome of the infecting virus.

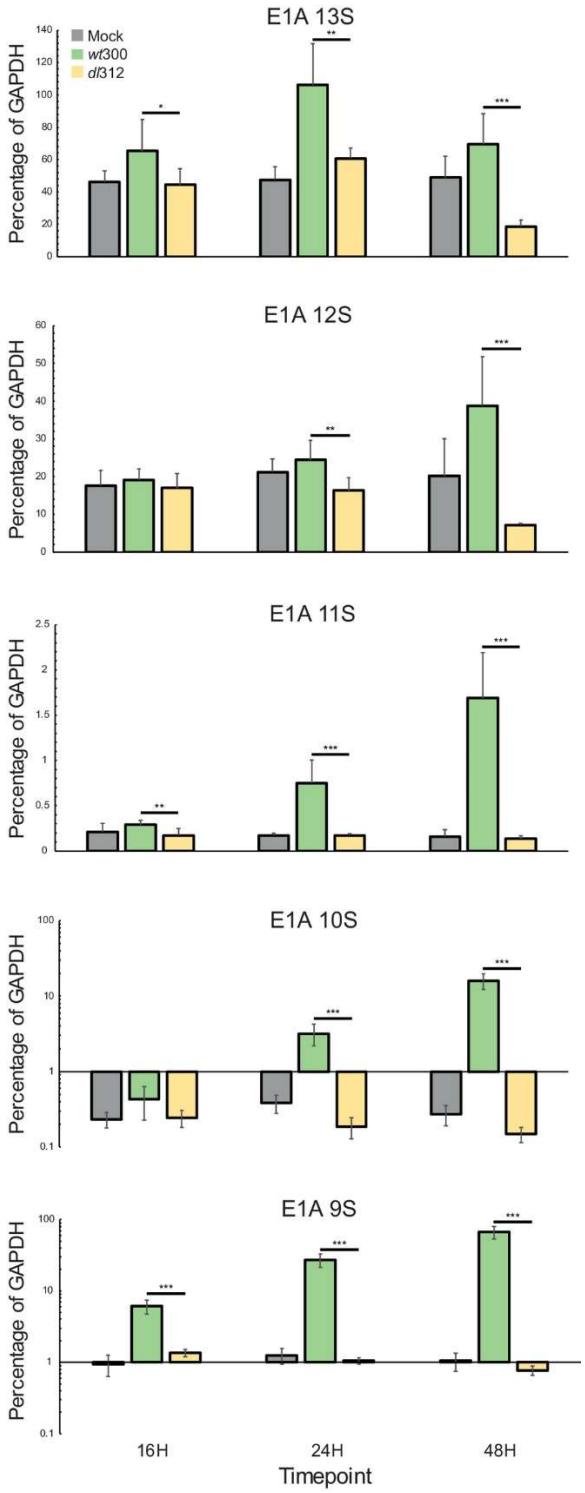


**Figure 3.4. Infection of 293 cells does not drive the splicing of late E1A transcripts.** RNA was extracted using NucleoZOL reagent and was treated with DNase at the indicated time points. cDNA was produced using VILO Master Mix reverse transcriptase. Levels of the indicated viral RNAs were measured by qPCR using a Bio-Rad CFX96 system with Applied Biosystems SYBR master mix for CFX. GAPDH was used as a reference. Asterisks indicate statistically significant results (*, $P \leq 0.05$; **, $P \leq 0.01$; ***, $P \leq 0.001$). Data represent results for three biological replicates.

### 3.3.6 Reduction of late E1A transcripts and proteins affects viral gene expression

To gain a broader view of the effects of in *trans* E1A expression, I sought to determine how these reduced late transcripts affected the expression of other viral genes over the course of infection. To do so, I examined expression levels of representative genes from all viral transcriptional units *via* RT-qPCR in 293 cells infected with *dl*312 or *wt*300 HAdV, or vehicle only (mock) (Figs. 3.5, 3.6, and 3.7).

I started by investigating the expression of noncoding RNAs; VA-RNAs that express shortly (roughly 3 hours) after infection[43]. Levels were very low in uninfected cells, as any detection here was nothing but a background reading (Fig. 3.5). In infected cells, I saw higher levels of VA-RNA expressed by *wt*300 than by *dl*312, with VAII expression appearing multiple log units higher than VAI expression, regardless of virus.

Interestingly, VAI expression is known to be compromised in *dl*309 compared to wild-type[287], and *dl*309 has a similar genetic backbone to *dl*312. One would expect, therefore, to see little to no VAI expression from *dl*312. Surprisingly, this was not the case; while VAI expression was reduced in *dl*312, it was still readily detectable, implying either the existence of unknown alterations within the genome of *dl*312 that restore VAI expression, or some negative regulation of VAI expression by the E1 region in *dl*309.

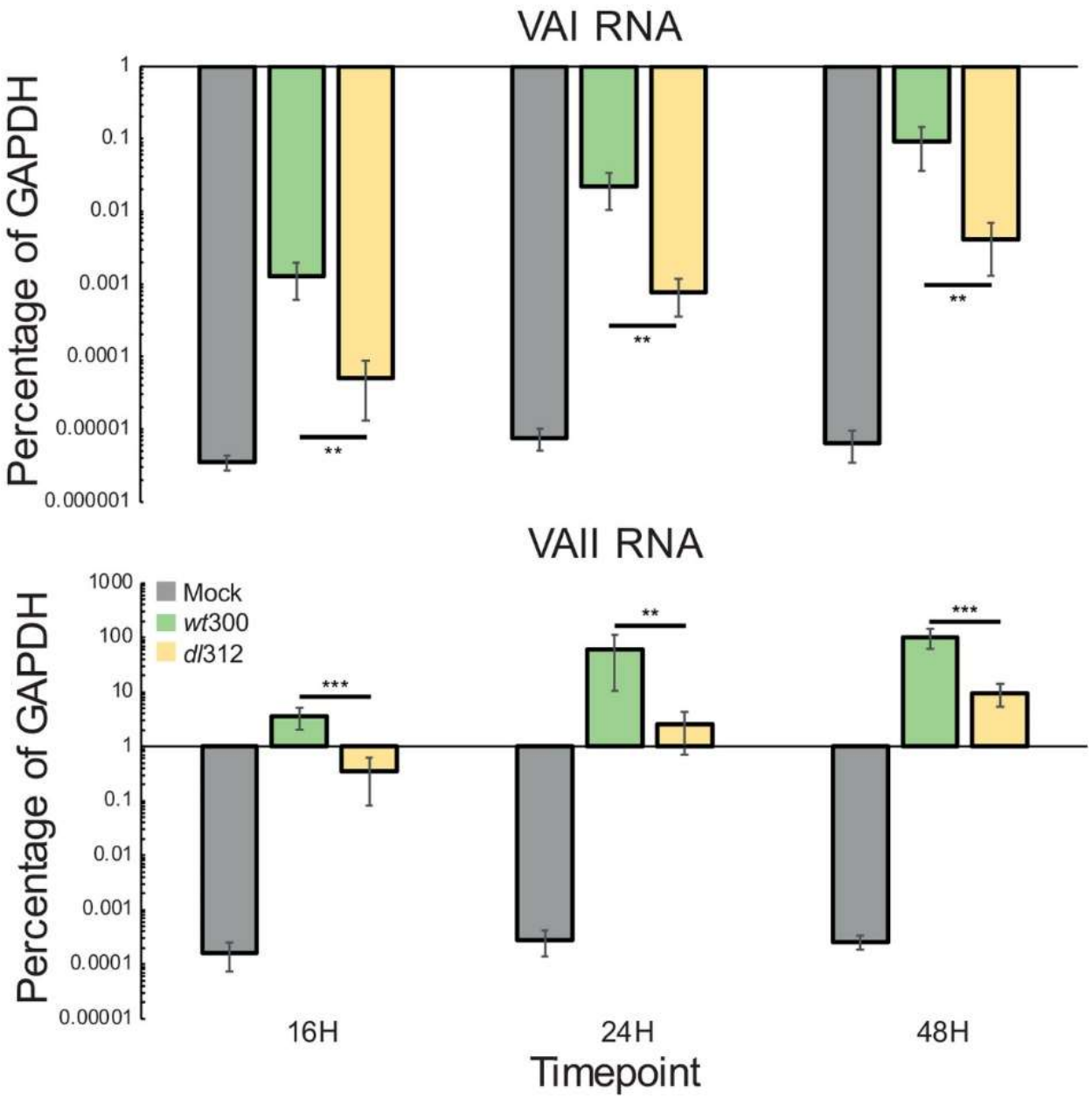


**Figure 3.5. HAdV5 *dl*312 VA RNA expression is lower than that of the wild type.** 293 cells were infected with the indicated HAdV5 strains at MOI 10. RNA was extracted using NucleoZOL reagent and treated with DNase at the indicated time points. cDNA was produced using VILO Master Mix reverse transcriptase. Levels of the indicated viral RNAs were measured by qPCR using a Bio-Rad CFX96 system with PrimeTime Gene Expression master mix (IDT). GAPDH was used as a reference. Asterisks indicate statistically significant results (**, $P \leq 0.01$; ***, $P \leq 0.001$). Data represent results for three biological replicates.

Next, I investigated the expression of other early transcription units by measuring levels of representative gene(s) of each: E1B (19K and 55K), E2 (DBP), E3 (E3A/Adenovirus Death Protein), and E4 (E4orf6/7) (Fig. 3.6). Expression of E1B was, for the most part, the same between *wt*300 and *dl*312, implying that these transcripts are unaffected by the presence or absence of certain E1A variants. E1B levels were also similar between infected and uninfected cells, which is not surprising as 293 cells contain the entire HAdV E1 transcription unit, which includes both E1A and E1B[10]. The remaining transcription units (E2, E3, and E4) all showed higher expression in *wt*300 infections than in *dl*312 infections (Fig. 3.6). These transcripts were also absent in mock-infected cells (any bars present represent the background level of the assay).

Finally, I examined the expression levels of late viral proteins, using the genes *hexon* and *fiber* as representatives (Fig. 3.7). In line with previous results, we observed consistently higher expression levels of these genes in *wt*300-infected cells than in *dl*312-infected cells.

These results, in combination with my previous experiments, show that levels of E1A isoforms, specifically the smallest three (11S, 10S, 9S), affect the expression of most viral transcriptional units, and may play a role in driving late viral gene expression.

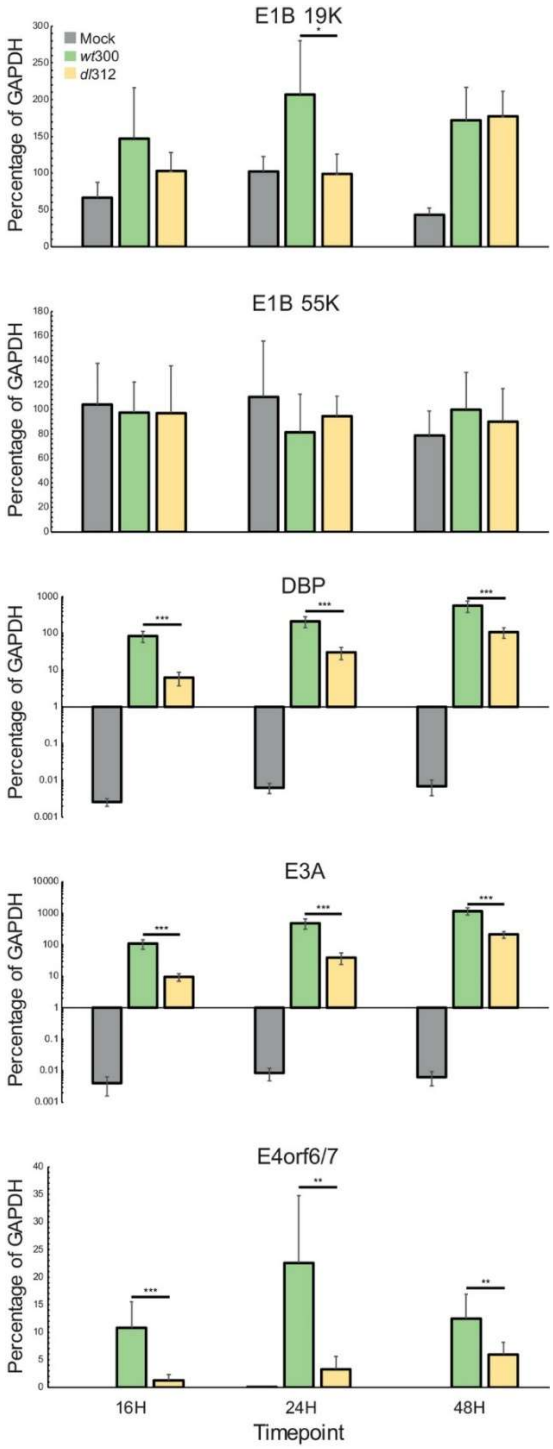


**Figure 3.6. Expression of various replication genes is reduced in HAdV5 *dl*312 from that in the wild type.** RNA was extracted using NucleoZOL reagent and treated with DNase at the indicated time points. cDNA was produced using VILO Master Mix reverse transcriptase. Levels of the indicated viral RNAs were measured by qPCR using a Bio-Rad CFX96 system with Applied Biosystems SYBR master mix for CFX. GAPDH was used as a reference. Asterisks indicate statistically significant results (*, $P \leq 0.05$; **, $P \leq 0.01$; ***, $P \leq 0.001$). Data represent results for three biological replicates.

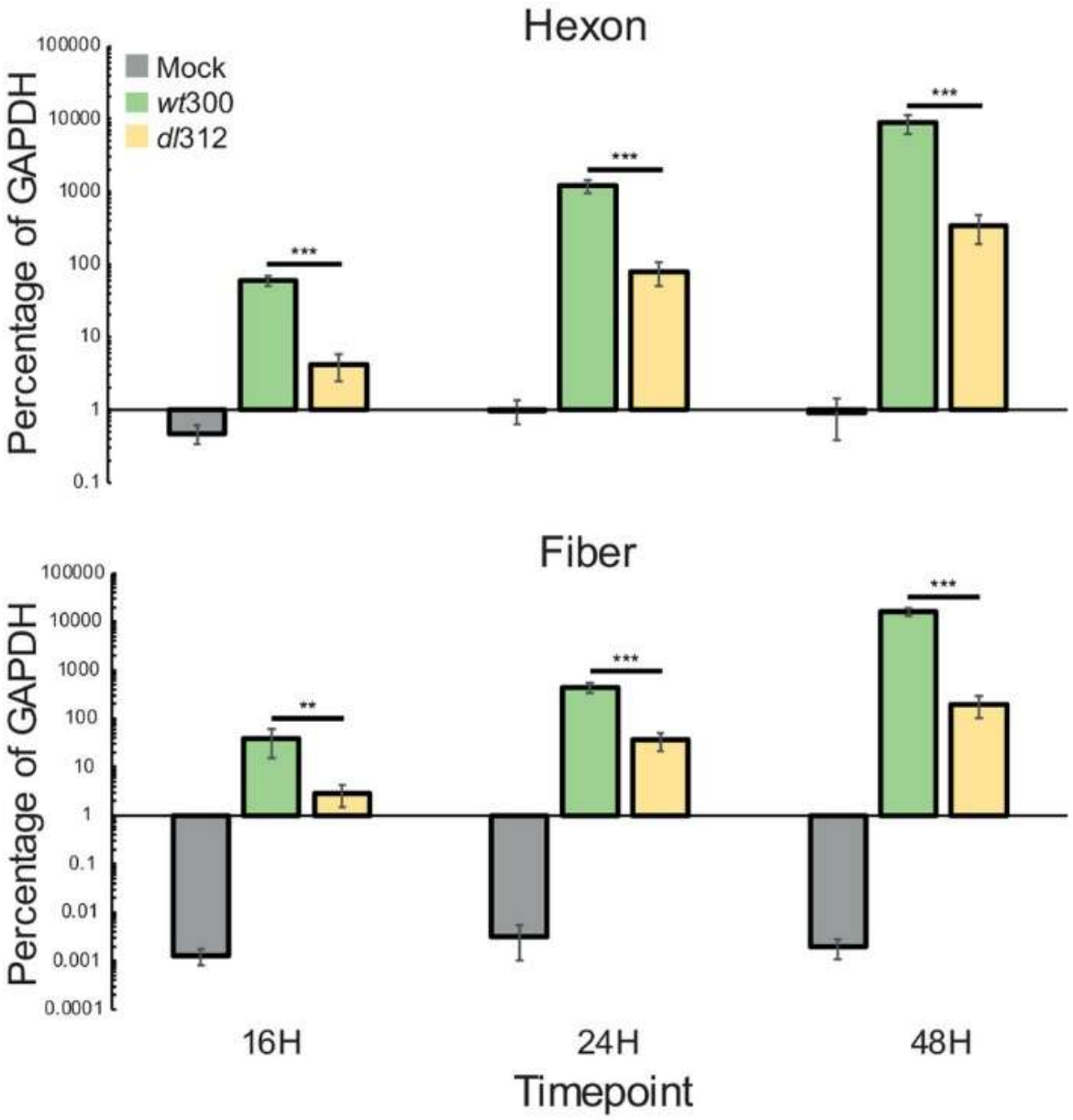


**Figure 3.7. Structural protein mRNA expression in HAdV5 *dl*312 is diminished from that in the wild type.** RNA was extracted using NucleoZOL reagent and treated with DNase at the indicated time points. cDNA was produced using VILO Master Mix reverse transcriptase. Levels of the indicated viral RNAs were measured by qPCR using a Bio-Rad CFX96 system with Applied Biosystems SYBR master mix for CFX. GAPDH was used as a reference. Asterisks indicate statistically significant results (**, $P \leq 0.01$; ***, $P \leq 0.001$). Data represent results for three biological replicates.

### 3.3.7 Complementation of late E1A transcripts in 293 cells enhances virus growth

Lastly, I investigated how the late E1A mRNA transcripts affect the growth of HAdV. To do so, I generated two 293-based cell lines, one of which complemented only the 9S and 10S E1A transcripts (293 9S/10S), while the other provided all three (293 9S/10S/11S). The expression of these transcripts was verified by Western blotting for 171R and 217R E1A (Fig. 3.8A) and by quantitative PCR (qPCR) for 11S, 10S, and 9S mRNA (Fig. 3.8B). No Western blot was performed for the product of 9S mRNA, as no antibody could be found for E1A55R.

Viral protein expression of *dl*312 over the course of a 72-hour infection was analyzed in both of these cell lines as well as in normal 293 cells by Western blot (Fig. 3.8C), revealing that levels of E1A protein dropped steadily over the course of the infection, while DBP and late protein levels increased. Interestingly, each complementing cell line showed lower levels of DBP expression compared to standard 293 cells at the 24-hour timepoint, though this difference was minimized by 48 hours. Late protein levels were mostly similar between each of the cell lines, though levels of penton and smaller structural proteins were slightly elevated in 293 cells, while hexon was slightly more abundant in 293 9S/10S/11S cells at the 72-hour timepoint. Quantification and normalization of the hexon band showed a comparative expression level in the 9S/10S line of 21% of that in standard 293 cells. The comparative level in the 9S/10S/11S line at the same timepoint was 170%.

Finally, I performed a growth assay on HAdV *dl*312 infecting 293, 293 9S/10S, and 293 9S/10S/11S cells over the course of 72 hours (Fig. 3.8D) in order to further investigate the effects of late E1A isoforms on the growth of HAdV. To correct for variance emerging from possible different growth rates of the various cell lines, resulting viral titres were determined on a per-cell basis by counting and averaging the cells in three sacrificial wells for each cell line immediately

prior to initial infection (timepoint zero). At the 48- and 72-hour timepoints, there was no significant difference between the titres obtained in 293 and 293 9S/10S cells; however, when all three late isoforms were present (293 9S/10S/11S cells), growth was significantly enhanced over that in standard 293 cells. One final note here is that 293 9S/10S cells showed a significant reduction of viral growth compared to 293 cells early on in infection (24-hour timepoint), which suggests that these late isoforms may have some negative effect on the early viral replication cycle. This would agree with the decreased levels of early DBP in the complementing cell lines we observed previously (Fig. 3.8C).

In conclusion, these results indicate that individual complementation of each of the five E1A isoforms (rather than just provision of the E1 region) to E1-deficient HAdV mutants, increases their overall viral fitness.

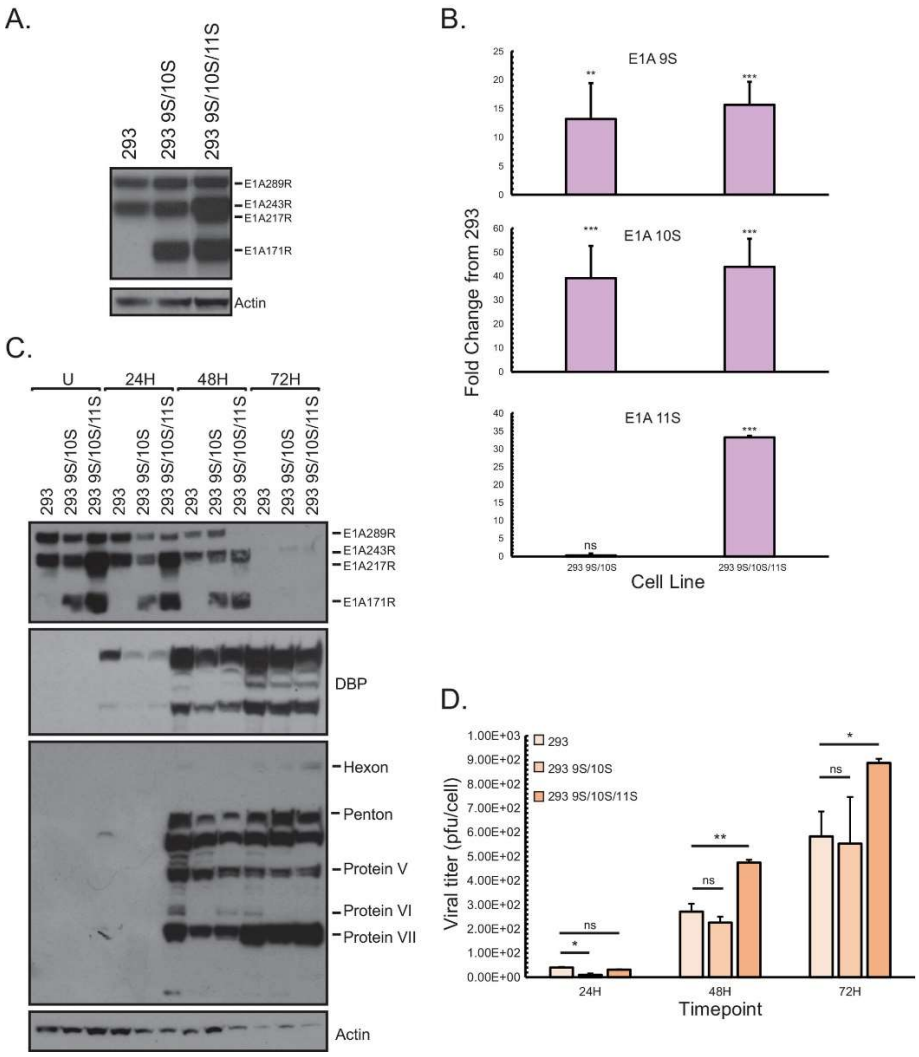


**Figure 3.8. Complementation of late E1A isoforms enhances virus growth.** (A) Expression of E1A in 293, 293 9S/10S, and 293 9S/10S/11S cells was determined by resolving 20 µg of total-cell lysate on an SDS-PAGE gel and blotting for E1A using a monoclonal antibody cocktail of M73 and M58. Actin was used as a control, and the bands were visualized using enhanced chemiluminescence and exposure to film. (B) Expression of E1A mRNAs in 293, 293 9S/10S, and 293 9S/10S/11S cells was determined using qPCR after total-RNA extraction with NucleoZOL, followed by DNase treatment and cDNA synthesis using VILO Master Mix. Levels of the indicated E1A RNAs were measured by qPCR using a Bio-Rad CFX96 system with Applied Biosystems SYBR master mix for CFX. GAPDH was used as a reference. Asterisks indicate statistically significant results (**, $P \leq 0.01$; ***, $P \leq 0.001$); ns, not significant. Data represent results for three biological replicates. (C) The indicated cell lines were infected with *dl*312 at MOI 10 and allowed to grow for the indicated times prior to lysis using NP-40 lysis buffer. Twenty micrograms of the total-cell lysate was resolved on a 4-to-12% Novex Bolt gradient gel and blotted for E1A, DBP, structural proteins, or actin as indicated. Bands were visualized using enhanced chemiluminescence and were exposed to film. U, uninfected cells. (D) The indicated cell lines were infected with *dl*312 at MOI 10 and allowed to grow for the indicated times prior to virus harvest by freeze-thawing. Total viral titers were determined by plaque assays on 293 cells. Asterisks indicate statistically significant results (*, $P \leq 0.05$; **, $P \leq 0.01$); ns, not significant. Data represent results for three biological replicates.

## 4. Molecular insights into ISG suppression and enhanced pathogenicity by species B HAdV

### 4.1 Introduction

Certain types of HAdV, in contrast to the virus's normal pattern of mild, self-clearing infection[4], have unusually severe symptoms, especially in the very young, the elderly, and the immuneocompromised[23–25]. A number of these viral types are found within species B, and include HAdVs B7 and B14[9,20,288], of which little is known despite the severity of their symptoms. Outbreaks of these are often serious, and commonly result in fatalities[6,26], and as such it is in our best interest to improve our understanding of these pathogens. One avenue of research here is to investigate the mechanisms by which they suppress the innate immune system of their host cell.

A key aspect of the innate immune system is the production of ISGs in response to cellular detection of IFN. This occurs rapidly, and depends on recruitment of ISGF3 (a complex of STAT1, STAT2, and IRF9) to ISREs within the promoters of ISGs, *via* the canonical JAK-STAT pathway[257]. This results in the recruitment of chromatin re-modelers and the RPII complex to the promoter, which drives transcription[259]. The purpose of ISGs is to induce an antiviral state within the cell[260], and as such, suppressing IFN signaling is very important to viral immune evasion, including that of HAdV[4]. These viruses have multiple avenues by which to inhibit expression of ISGs, such as its VA-RNAs[186], E4-Orf3 protein[153], E1B-55K protein[108,109], and E1A by way of multiple binding partners, such as STAT1[289], FoxK, DCAF7[82], and RuvBL1[11].

Little research has been performed on the effect of IFN on HAdV-B. One study showed IFN-β to have little effect on HAdV-B3's replication, with IFN-γ having no effect at all[290]. Another study showed a more pronounced effect, but this was a result of co-treatment with IFN-β, IFN-γ,

and anti-HAdV-B3 antibody[291]. Yet another showed HAdV-C5 to be more sensitive to IFN-γ than HAdVs B3 or B7, with B7 once again being nearly unaffected[292].

Previous work from the Pelka lab revealed the interaction between HAdV-C E1A and AAA+ DNA helicase RuvBL1/pontin to be a mechanism of viral ISG suppression. Presented in this section is a follow-up to this study, published in the journal mBio under the title "Molecular insights into type I interferon suppression and enhanced pathogenicity by species B human adenoviruses B7 and B14"[293]. The goal here was to determine the role of RuvBL1 in the ISG suppression mechanisms of HAdV types B7 and B14, and it was revealed that while both of these strains were nearly unaffected in the magnitude of their replication by the presence of IFN, their E1As did not bind as strongly to RuvBL1 as did that of HAdV-C. HAdV-B ISG suppression was shown to result from suppression of STAT2 and RPII recruitment to ISG promoters. Proteomic analysis also revealed these viruses to have major differences in their overall approaches to infection, which may also contribute to their increased pathogenicity.

While I performed the majority of the work here myself, the quantification data presented in Fig. 4.22 and Fig. 4.23 and the processing of a number of IF slides were performed by my labmates Nikolas Akkerman and Lauren Fulham respectively, and a portion of the proteomics work presented in section 4.2.23 was performed with the help of another labmate, Rafe Helwer.

## 4.2 Materials and Methods

**4.2.1 Antibodies.** Mouse monoclonal anti-species C E1A M1, M37, M58, and M73 antibodies were previously described[282], as were mouse monoclonal anti-hexon 27F11 and 9C12 antibodies[294], and mouse monoclonal anti-hemagglutinin (anti-HA) antibodies[295]; all of which were grown in-house and used as hybridoma supernatant. Anti-histone H3 and anti-DCAF7

antibodies were purchased from Abcam (cast. ab180727 and ab138490, respectively), while anti-tri-methyl K4 H3 and anti-H2A.Z antibodies were purchased from Cell Signaling Technology (cats. C42D8 and E9M5G, respectively). Rabbit anti-RuvBL1 and RuvBL2 antibodies were ordered from Cell Signaling Technology (cat. D1L8J) and Abclonal (cat. A1905) respectively; and anti-STAT1, anti-STAT2 and anti-FoxK1 and FoxK2 antibodies were ordered from Cell Signaling Technology (cats. D1K9Y, D9J7L, 12025, and 12008 respectively). Anti-RPII antibody (CTD specific) and anti-adenovirus structural protein antibody were ordered from Abcam (cats. Ab26721 and Ab6982 respectively). Rat anti-HA antibody (Roche, cat. 11867423001), clone 3F10, was used at a dilution of 1:5,000 for western blot. Secondary antibodies were purchased from Jackson ImmunoResearch.

Rabbit polyclonal antibodies for HAdV-B7 and -B14 E1A and DBP proteins were newly generated by Pacific Immunology using the following peptide sequences:

Ad7/14 E1A – KLEDLLEGGDGPLDLSTRK

Ad7/14 DBP – QFRNVSLPAGHYDSRQNPFD

These antibodies were affinity purified using peptide columns before use. Note that for E1A detection and other viral proteins, the variable levels observed between the different viruses are not necessarily due to differences in viral protein levels but are rather due to the fact that different antibodies had to be used to detect the proteins of different viruses, and as such vary in terms of binding affinity for their target.

**4.2.2 Cell and virus culture.** A549 (ATCC# CCL-185) and HT1080 (ATCC# CCL-121) cells were grown in Dulbecco's Modified Eagle's Medium (Sigma) supplemented with 5% fetal bovine serum, streptomycin and penicillin (Corning). IMR90s (ATCC# CCL-186) were the same, but in

10% FBS media. Unless otherwise specified, all virus infections were carried out at MOI 10 in serum-free media for 1 hour after which fresh complete media was added without removal of the infection media. For most experiments, A549 cells were used; however, in cases where transfection was necessary I used HT1080 cells due to their favourable transfection properties.

Virus stocks were generated by infecting 15 cm plates of permissive cells (A549) and waiting for total cell die-off. The resultant suspension was harvested and freeze-thawed thrice before cellular debris was removed by centrifugation and the supernatant divided into aliquots of crude lysate. These stocks were titred *via* plaquing assay.

**4.2.3 Chromatin immunoprecipitation.** ChIP was carried out essentially as previously described[68,296]. Cells were infected with the indicated adenoviruses at MOI 10 and cross-linked with formaldehyde and harvested 24 hours after infection for ChIP analysis. Cells were lysed, nuclei pelleted, isolated, and lysed in turn, and DNA sonicated to roughly 150 bp *via* Covaris focused-ultrasonicator M220. Proteins were immunoprecipitated, cross-linking was reversed, and DNA was isolated for qPCR. IFN α-2A treatment (working concentration 1 U/mL) was performed when specified in figure legends.

qPCR was carried out for ISG promoters using PowerUp SYBR Green Master Mix (BioRad) according to manufacturer's directions using a BioRad CFX96 Real-Time System (BioRad). The annealing temperature used was 60ºC, and 40 cycles were run.

**4.2.4 Cross-linked immunoprecipitation.** 15cm plates of A549 cells transfected to express HA-RuvBL1 24 hours earlier were infected with HAdV-C2, -B7, or -B14 for 1 hour at MOI 10. 16 hours later, IFN α-2A was applied (final concentration 1 U/mL). Eight hours later (24 hours after initial infection), cells were cross-linked directly on the plate with 1% (final concentration) formaldehyde for 10 minutes. Glycine was then applied to a final concentration of 125 mM to stop

the cross-linking reaction. Cells were scraped and pelleted, and the pellets were washed with PBS three times. These pellets were lysed with NP-40 lysis buffer (0.5% NP-40, 50 mM Tris [pH 7.8], 150 mM NaCl), and immunoprecipitation was performed using 12-CA5 anti-HA antibodies. Samples were resolved on Invitrogen Bolt 4-12% Bis-Tris Plus gel in MOPS buffer (Invitrogen).

**4.2.5 Cytopathic effect imaging.** 6-well plates of A549 or IMR90 cells, pretreated with IFN α-2A by 16 hours where indicated, were infected with HAdV-C2, -B7, and -B14 at a MOI indicated in the figure legend, as described above. Images were taken *via* BioRad ZOE Fluorescent Cell Imager light microscopy setting at indicated timepoints.

**4.2.6 Cytoplasmic/Nuclear Fractionation.** A549 cells were plated on 10cm plates and infected with HAdV-C2, -B7, and -B14 at MOI 100. IFN was applied 16h post-infection, and cells were harvested 8h after that. Cells were pelleted and washed with cold PBS twice before being resuspended in hypotonic salt solution and left on ice for 15 minutes. NP-40 detergent was added and cells were lysed *via* vortex. Nuclei were pelleted and supernatant was isolated as cytoplasmic fraction, before nuclei were lysed in cell extraction buffer supplemented with protease inhibitor cocktail and PMSF. Remaining cell debris was pelleted and supernatant was isolated as nuclear fraction. Protein levels were quantified *via* Bradford assay and resolved *via* SDS-PAGE.

**4.2.7 Immunofluorescence.** A549 cells or HT-1080 cells, depending on the experiment, were plated at low density (~40,000 cells per chamber) on chamber slides (Nalgene Nunc), and subsequently infected as described above. Twenty-four hours after infection, cells were fixed in 4% formaldehyde, permeabilized in 0.1% Triton, blocked in blocking buffer (1% normal goat serum, 1% BSA, 0.2% Tween-20 in PBS) and stained with specific primary antibodies. M58, M73, 27F11, and 9C12 were used neat (hybridoma supernatant); RuvBL1, RuvBL2, STAT1, and STAT2 antibodies were used at a dilution of 1:400, and AlexaFluor-488 and -594 secondary antibodies

(Jackson ImmunoResearch) were used at a dilution of 1:600. After staining and washing, slides were mounted using Prolong Gold with DAPI (Invitrogen) and imaged using Zeiss LSM700 confocal laser scanning microscope. Images were analyzed using Zeiss ZEN software package.

**4.2.8 Immunoprecipitation.** A549 cells were lysed in NP-40 lysis buffer (0.5% NP-40, 50 mM Tris [pH 7.8], 150 mM NaCl) supplemented with a protease inhibitor cocktail (Sigma). Cell lysate was used for IP with the rabbit anti-RuvBL1, mouse anti-HA 12CA5, mouse anti-E1A (species C), or rabbit anti-E1A (species B) antibody depending on the specific experiment. For ubiquitination IPs RIPA buffer (150 mM NaCl, 1% NP-40, 0.5% deoxycholate, 0.1% SDS, and 50 mM Tris pH [7.4]) was used instead of the NP-40 lysis buffer, and additionally supplemented with N-Ethylmaleimide (Sigma).

**4.2.9 Interferon overlay assay.** Six-well plates of A549 cells were infected with serial dilutions of HAdV-C2, -B7, and -B14, measured for plaque separation. After infection, infection media was removed and 3 mL of half 2x DMEM and half agarose was applied to each well, as in a standard plaquing assay. Where indicated, this agarose-DMEM contained IFN α-2A at a concentration of 1 U/mL. Plates were incubated at 37°C, 5% $CO_2$ until plaques began to show. Wells were then topped off with 2 mL of 0.01% Neutral Red (Fisher Chemical cat. 553-24-2)-containing agarose-DMEM and incubated for 24 hours. Plaques were imaged *via* AlphaEaseFC software in a FluorChem 8900 (Alpha Innotech) gel imaging cabinet. Images were overlayed with a 3D effect for ease of plaque visualization.

**4.2.10 PCR Primers.** qPCR primers for adenovirus species C viral genes and *GAPDH* were described in table 3.1. All remaining primers (ISGs and promoters, all species B viral genes) are described in Table 4.1. All primers were generated through the services of Integrated DNA Technologies.

| *Category* | *Name* | *Sequence* |
|---|---|---|
| ***ISGs*** | *IFI6 F* | CTCGCTGATGAGCTGGTCT |
| | *IFI6 R* | TGCTGGCTACTCCTCATCCT |
| | *IFIT1 F* | AAAAGCCCACATTTGAGGTG |
| | *IFIT1 R* | GAAATTCCTGAAACCGACCA |
| | *IFIT2 F* | GCGTGAAGAAGGTGAAGAGG |
| | *IFIT2 R* | GCAGGTAGGCATTGTTTGGT |
| | *OAS1 F* | AGACCGACGATCCCAGGAGGT |
| | *OAS1 R* | TGGGGTGGATGCTGCCTGGA |
| | *OAS2 F* | GGGTGGAGGGGACCGTTGGT |
| | *OAS2 R* | CCTGGTGTCTGCATTGTCGGC |
| ***Promoters*** | *IFI6p F* | CTGGGCGGAGCTGGGAGAG |
| | *IFI6p R* | TGGGCACAGCAGCGAGTAAAC |
| | *IFIT1p F* | TTTCACTTTCCCCTTTCGGTTTCC |
| | *IFIT1p R* | GGCTCCTCTGAGATCTGGCTATTC |
| | *OAS2p F* | GCAAGGGGCGGGGAAGAG |
| | *OAS2p R* | CCCAGAGCCAGGAAACTGAAAC |
| | *ACTBp F* | TTTCGCAAAAGGAGGGGAGAG |
| | *ACTBp R* | GCCGCTCGAGCCATAAAAG |
| ***Viral Genes (Species B)*** | *7E1A F* | TGATGAGTCACCTTCTCCTGA |
| | *7E1A R* | TGGCAGTTTCCGGGTACTAA |
| | *14E1A F* | CTCCTGAGATTCAAGCACCTG |
| | *14E1A R* | TTATTGTCTTGGCCGTTTCC |
| | *7E1B F* | ACCGTGCATATCGTTTCACA |
| | *7E1B R* | GAAAAGGCATCTGGTTCCAA |
| | *14E1B F* | ACCGTGCATATCGTTTCACA |
| | *14E1B R* | GAAAAGGCATCTGGTTCCAA |
| | *7E2 DNA Pol F* | CTTTTCTGGGGTGATGCAAT |
| | *7E2 DNA Pol R* | CTTTGGCAAGCAGCTAATCC |
| | *14E2 DNA Pol F* | GTGCGATTGGGTTTTTCTGT |
| | *14E2 DNA Pol R* | GTACTTGTCACCGCCCAACT |
| | *7E3 F* | ATTAAGTGCGGATGGGACTG |
| | *7E3 R* | CTGGGAGGCCATAGGTCATA |
| | *14E3 F* | GCTTCTTCAACCCGGATTTT |
| | *14E3 R* | CTTCCACCCAAGGGTTTTCT |
| | *7E4 F* | GTTATTTTGCCTCCCCCTTC |
| | *7E4 R* | GCAGCAGTTGGACTGTGAAA |
| | *14E4 F* | GTTATTTTGCCTCCCCCTTC |
| | *14E4 R* | ATGACCGTGATCCAGACTCC |
| | *7Hexon F* | CAAAGCCGTCACCTTACCAT |
| | *7Hexon R* | GTTCTGTCCCAGGTCGGTAA |
| | *14Hexon F* | CAGATGCTCGCCAACTACAA |
| | *14Hexon R* | AGCCATGTAACCCACAAAGC |

**Table 4.1. List of qPCR primers used for gene expression and ChIP assays.**

**4.2.11 Plasmids.** The expression plasmid for HA-RuvBL1 was generated by PCR-amplifying the genetic sequence of RuvBL1 and cloning it into the pcDNA-HA expression vector. The HA-RuvBL2 expression vector was obtained from Addgene (plasmid #51636)[297].

**4.2.12 Proteomic Analysis.** A549 cells were infected with HAdV strains at MOI 10 for 16 hours, and then treated with IFN. After eight hours, cells were harvested and lysed in PBS using sonication, and total proteins were precipitated *via* trichloroacetic acid prior to analysis. Protein was sent to the Southern Alberta Mass Spectrometry Centre for unlabelled 2D-LC-MS-MS shotgun proteomics analysis, where raw reads were interpreted into Scaffold data. Results were analyzed broadly by Heatmapper software[298], and in detail by Cytoscape's[299] String function and clusterMaker app[300]. All proteomics data has been deposited into PRIDE database under accession # PXD045673, with a DOI: 10.6019/PXD045673.

**4.2.13 Real-time gene expression analysis.** Cells were infected with indicated viral strains at MOI 10 for 24 hours, with IFN α-2A applied to a final concentration of 1 U/mL eight hours prior to harvest. Total RNA was extracted using TRIzol Reagent (Sigma) according to manufacturer's instructions. 1 μg of total RNA was used for cDNA generation with SuperScript VILO reverse transcriptase (Invitrogen) according to the manufacturer's guidelines, using random hexanucleotides for priming. The cDNA was subsequently used for real-time expression analysis *via* BioRad CFX96 real-time thermocycler. Analysis of expression data was carried out and was normalized to GAPDH mRNA levels.

**4.2.14 SiRNA knockdowns.** Knockdowns were performed *via* siLentFect Lipid Reagent for RNAi (BioRad) according to manufacturer specifications. Knockdown conditions were maintained for

24 hours for H2A.Z, and 72H for RuvBL1, RuvBL2, and GCN5. Infections were then carried out as described below, with IFN α-2A application taking place eight hours prior to harvest. Gene expression analysis was then carried out as described above.

siRNAs for RuvBL1, RuvBL2, GCN5, and H2A.Z were obtained from Life Technologies (siRNA IDs s16369, s21307, s5657, and s6414 respectively).

**4.2.15 Statistical analysis.** Statistical analysis for all experiments was performed using a two-tailed Student's *t*-test using HAdV-C2-infected samples as the reference for comparison. *P*-values of $< 0.05$ were considered statistically significant. Statistical significance is indicated with asterisks when present.

**4.2.16 Transfections.** Media was changed on cells 20 minutes prior to transfection. Transfections were prepared by mixing 1 ml of serum-free DMEM, 10 µg of total plasmid DNA, and 20 µL of linear 1 mg/mL solution of polyethylenimine 25kDa reagent from Polysciences (cat. 23966-2). This was vortexed for 10 seconds and incubated at room temperature for 20 minutes. The complexes were then added to the cells and incubated for 24 to 48 hours. Note that reagent quantities assume application to a 10cm plate of cells (fill volume 10 mL). For other plate/well sizes, reagent quantities were altered proportionally to the fill volume.

**4.2.17 Viruses**. Viruses used in the study were HAdV-C2 (ATCC# VR-846), HAdV-B7 (ATCC# VR-7), and HAdV-B14 (ATCC# VR-15). All infections were carried out in serum-free medium for 1 hour at MOI 10 unless otherwise specified in figure legends.

**4.2.18 Virus growth assay.** A549 cells were infected with HAdV-C2, -B7, or -B14 at MOI 10 in serum-free media, 16 hours after the treatment with IFN α-2A (working concentration 1 U/mL). Virus was adsorbed for 1 h at 37°C under 5% $CO_2$. Virus titers were harvested 24, 48, and 72 hours

after infection, freeze-thawed three times, and titred by plaque assays performed on A549 cells by serial dilution.

**4.2.19 Western blot.** All protein samples were boiled in DTT-enriched protein loading dye at 100°C for 10 minutes. Samples were resolved on Invitrogen Bolt 4-12% Bis-Tris Plus gel in MOPS buffer or MES buffer (both from Invitrogen) depending on the size of the target protein. Gels were transferred to PVDF membrane *via* Genscript eBlot L1 blot transfer apparatus. Membranes were blocked for one hour in skim milk powder in TBST. Primary antibodies were applied in 3% BSA, shaking, overnight. Secondary antibodies were applied in blocking buffer, diluted 1:100,000.

## 4.3 Results

### 4.3.1 HAdVs B7 and B14 are minimally affected by IFN

I wanted to examine how much of an effect interferon had on the growth of species B HAdVs B7 and B14. As previous studies in *dl*309 (HAdV-C5-based) have shown, the virus is generally not affected by IFN when infecting HEK 293 or KB cells, growing to equivalent titres regardless[186]. As such, A549 cells were treated with IFN α-2a for 16 hours prior to infection with HAdVs C2, B7, or B14, and were harvested and titred 24, 48, and 72 hours afterward (Fig. 4.1A). IFN pre-treatment had a significant effect on the growth of HAdV-C2, reducing titres by nearly one log at all timepoints, but did not affect HAdV-B7 or B14 meaningfully. Plotting the ratios of IFN-treated over untreated titres (Fig. 4.1B) reveals the difference between viruses to be highly significant, with HAdV-C2 titres reduced to roughly 20% of untreated, HAdV-B7 unaffected, and HAdV-B14 affected only minimally (titres reduced to about 80%). Notably, HAdV-B14 replicated much more quickly than the other two strains, reaching relatively high titres even by 24 hours post-infection (Fig. 4.1A).

I also investigated whether the appearance of CPE was affected by the presence of IFN, with cells treated and infected as previously described (Fig. 4.2A). I saw no observable difference between treated and untreated cells on the course of infection, and saw similar results in IMR-90 (primary) cells (Fig 4.2B). Also unaffected were the expression levels of viral genes and proteins (Fig. 4.3 and Fig. 4.4 respectively), as well as viral entry into cells (Fig. 4.5) – tested by IFN treatment, infection, and immunofluorescence for viral particles. When we investigated the effect of IFN on viral plaque formation in A549 cells, we observed no effect in HAdV-C2 or HAdV-B7, but interestingly, saw a large plaque phenotype in HAdV-B14 (Fig. 4.6). This was later determined to likely be the result of apoptosis in HAdV-B14-infected A549 cells, based on laddering (genomic fragmentation) observed in cellular genomic DNA (data not shown).

Altogether, these experiments showed a significant IFN sensitivity in HAdV-C2, that is not present in HAdV-B7 or B14.

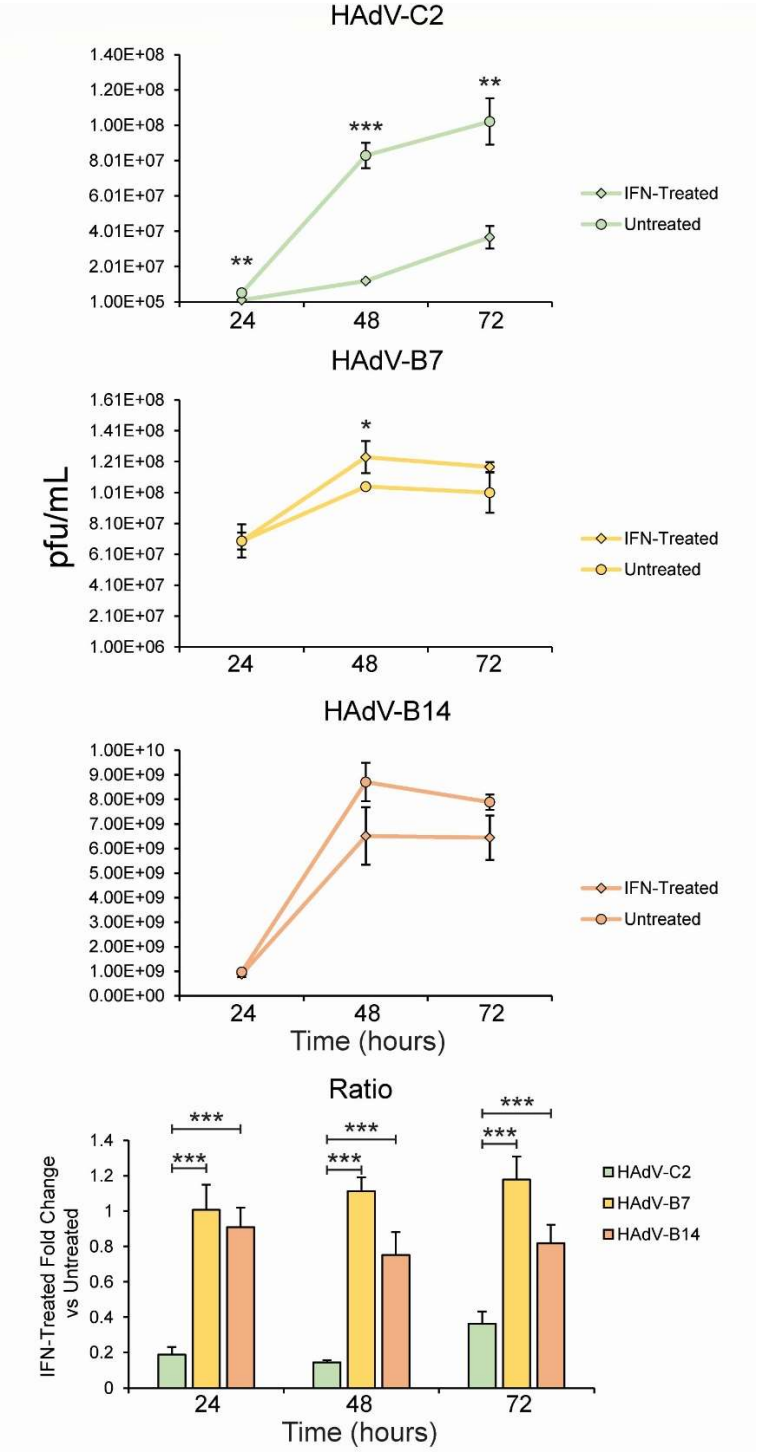


**Figure 4.1. HAdVs B7 and B14 grow better in IFN-treated cells than HAdV C2.** A549 cells treated 16 hours prior with IFN α-2A were infected with HAdV strains C2, B7, and B14, and harvested 24, 48, and 72 hours after infection. Viral titer was measured as pfu/mL *via* plaquing assay. The bar graph represents the same results as a ratio of IFN-treated samples to untreated samples. Statistical analysis was performed by unpaired student's *t*-test. One asterisk represents a *P*-value of <0.05, two represent <0.01, and three represent <0.001; $n = 3$.

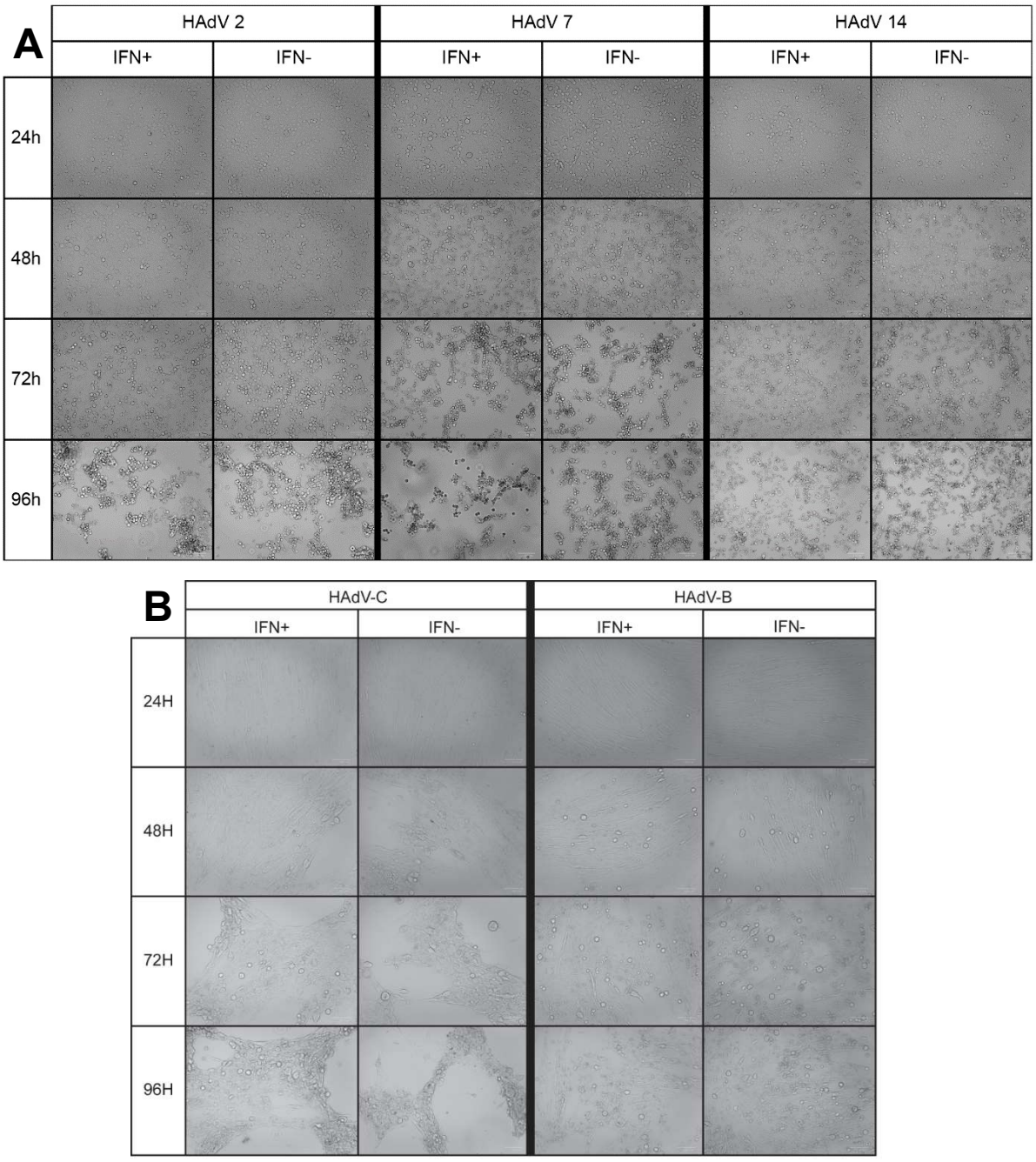


**Figure 4.2. IFN has little to no effect on HAdV cytopathic effect.** (A) A549 cells were treated with IFN 16 hours before infection with indicated HAdV strains at MOI 1. Cells were imaged at indicated timepoints. (B) IMR90 cells were plated and allowed to grow to confluency before infection with indicated HAdV strains at MOI 10. Cells were imaged every 24h following infection up to 96h.

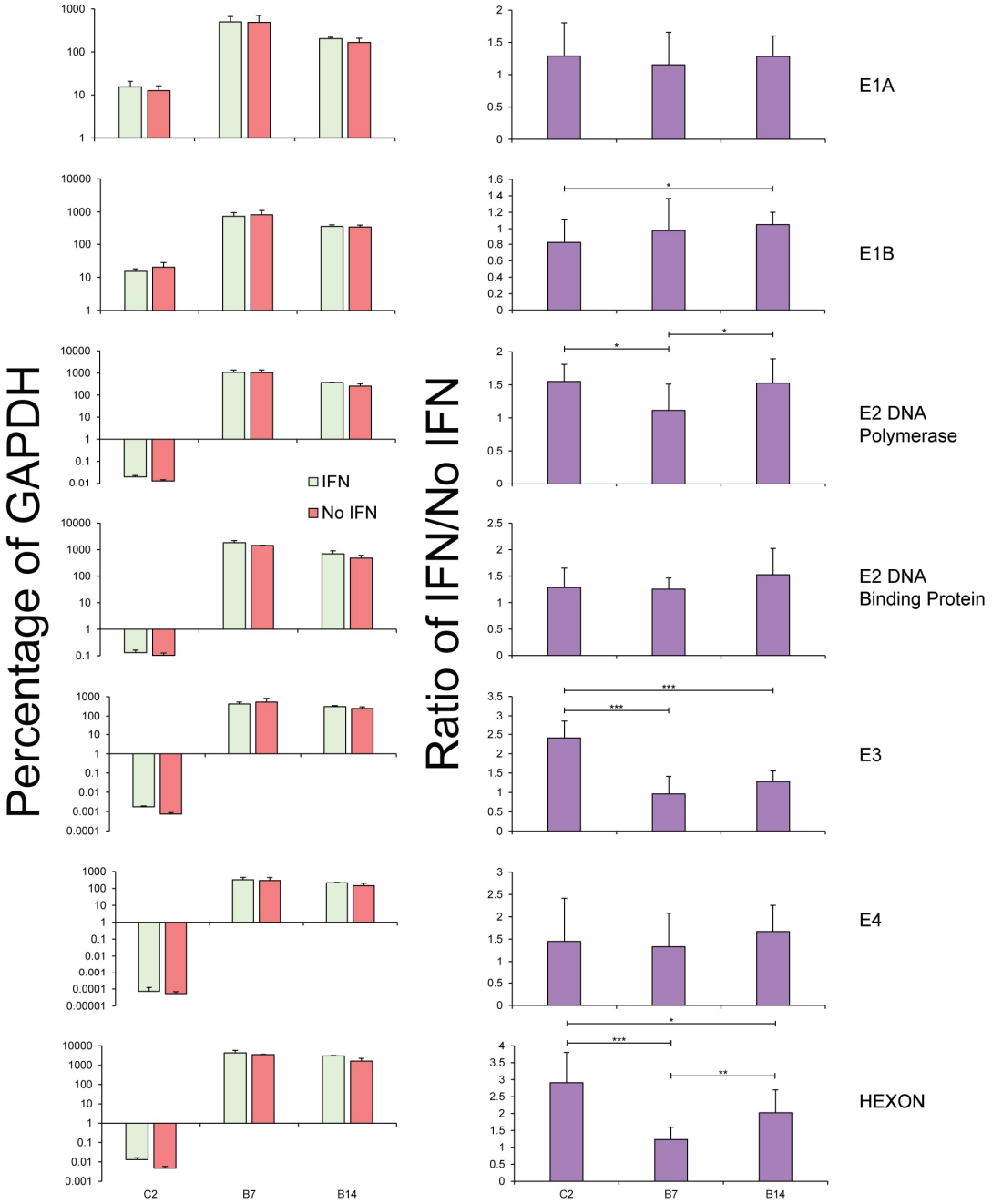


**Figure 4.3. Viral gene expression is not broadly affected by the presence of IFN.** A549 cells were treated with IFN α-2A 16 hours after infection with indicated HAdV strains. Eight hours later, the cells were harvested, RNA extracted, and cDNA generated. Viral gene expression was analyzed *via* real-time qPCR. Results were normalized to percentage expression of housekeeping gene GAPDH and presented as-is (A) and as a ratio of IFN-treated over untreated (B). All experiments were performed in triplicate. Statistical analysis was performed *via* unpaired t-test. One asterisk signifies a p-value of <0.05, two represent <0.01, and three indicate <0.001.

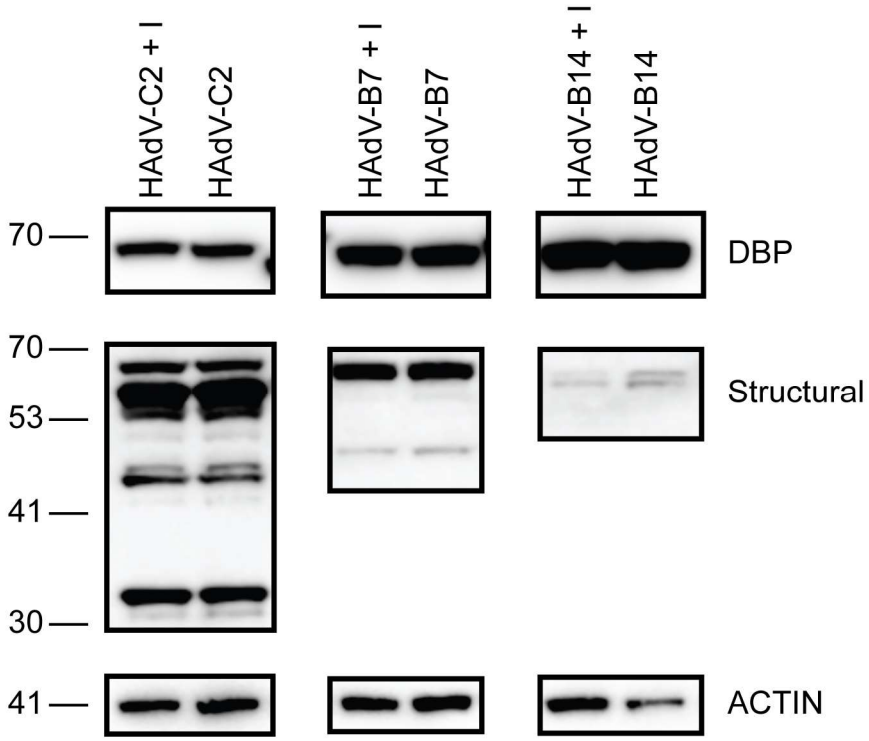


**Figure 4.4. Viral protein expression levels are unaffected by the presence of interferon.** A549 cells were infected with infected with indicated HAdV strains, treated with IFN 16 hours later, and harvested eight hours after that. Cells were lysed, protein levels measured, and equal protein volumes resolved on SDS gel, transferred to PVDF membrane, and blotted with indicated antibodies.

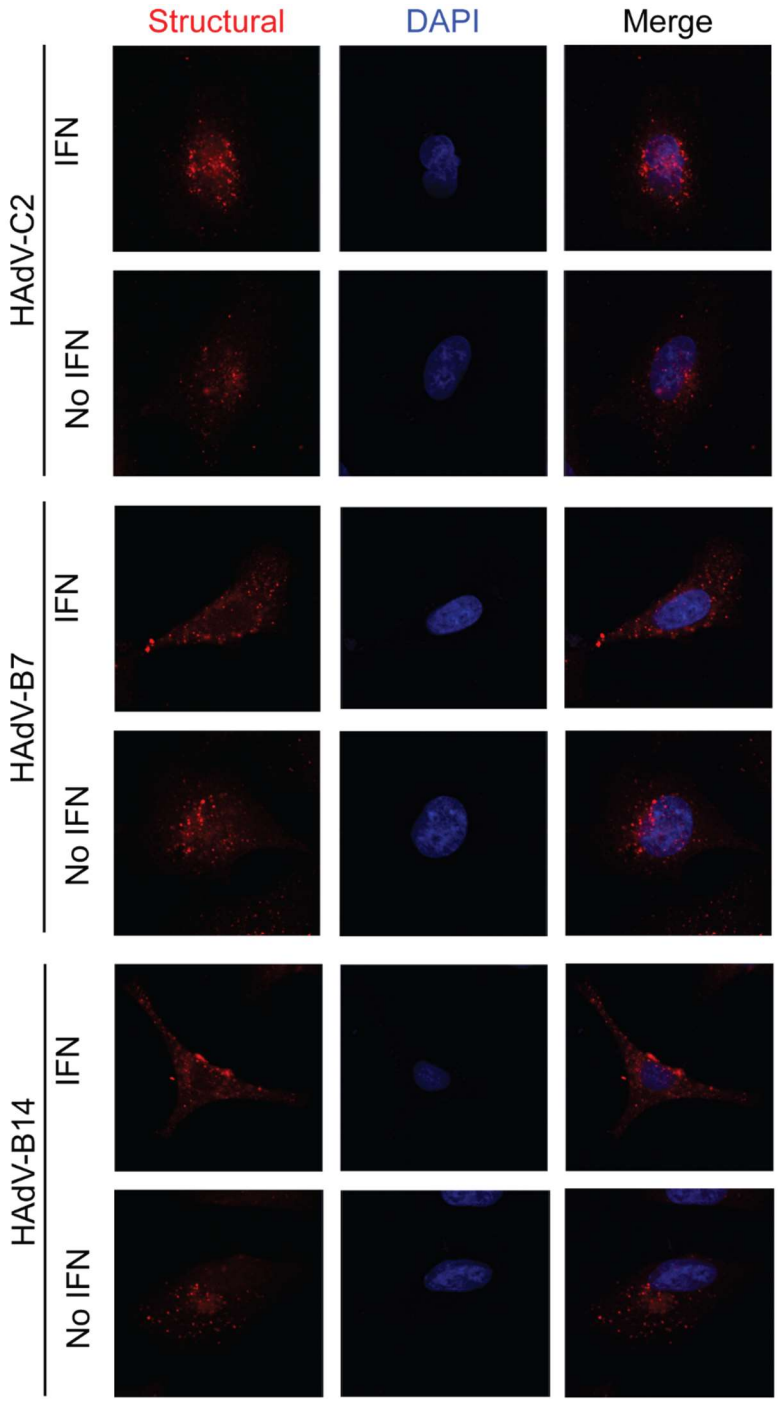


**Figure 4.5. Viral entry is unaffected by presence or absence of IFN.** A549 cells were seeded onto chamber slides and treated with IFN α-2a, as indicated, for 16 hours prior to infection with noted viral strains. After two hours, cells were fixed, permeabilized, and marked with antibodies targeting adenovirus structural proteins. Slides were visualized by confocal microscopy.

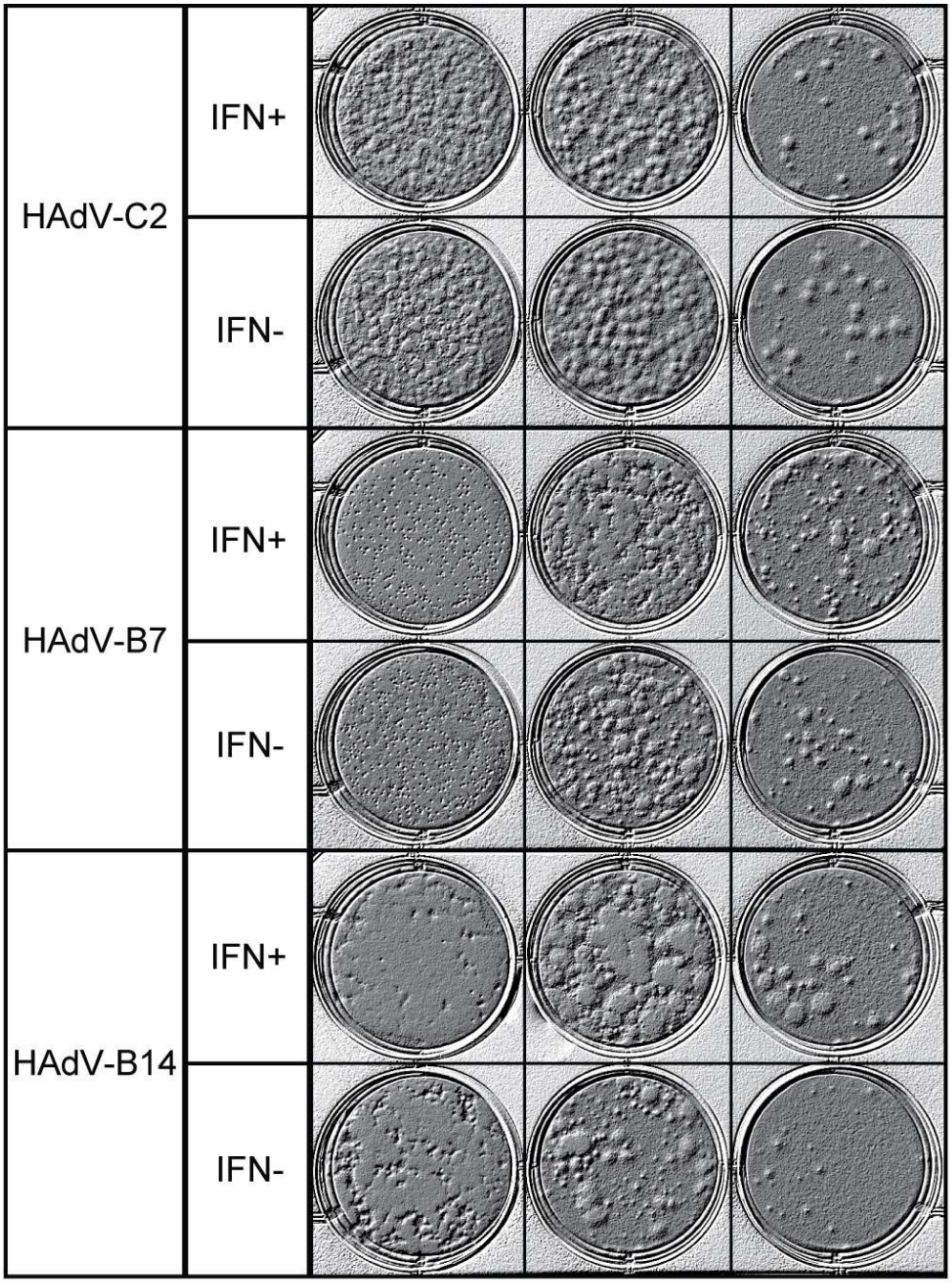


**Figure 4.6. Presence of IFN generates a distinct large-plaque phenotype in HAdV-B14-infected cells.** A549 cells were infected with serial dilutions of indicated HAdV strains and overlayed with agar-DMEM containing IFN where indicated. Once plaques had appeared, overall well appearance was visualized by neutral red dye.

### 4.3.2 Species B HAdVs efficiently suppress ISG expression

Previous work from the Pelka lab[11] showed HAdV-C5 to be reliant on RuvBL1 for efficient interferon-stimulated gene (ISG) suppression. It was further hypothesized that one of the reasons behind the enhanced pathogenicity of species B HAdV could be its ability to interfere with the IFN pathway, suppressing activation of ISGs. To investigate this idea, I infected A549 cells for 16 hours with HAdV-C2, B7, or B14, treated them with IFN α-2a, and harvested RNA eight hours after that. To gauge overall ISG expression, I looked at the RNA levels of five representative ISGs: *IFI6*, *IFIT1*, *IFIT2*, *OAS1*, and *OAS2* (Fig. 4.7). I observed that HAdV-C2 was significantly worse at ISG suppression than either species B representative, both of which could more efficiently suppress all measured ISGs, with *IFI6* being suppressed the least. This became even more clear when I took these results as ratios of IFN-treated vs. -untreated cells (right column). These ISG suppression patterns held true in IMR-90 (primary) cells as well (Fig. 4.8).

These results indicate that species B HAdVs are able to more efficiently suppress ISG expression in their host cell than their species C counterparts. Of note is that ISG suppression patterns observed here within HAdV-C2 were somewhat different than those previously seen by HAdV-C5 in HT-1080 cells[11]. This is far more likely to be due the use of a different host cell line, or variation in the timing of infection or IFN application than any difference in E1A protein sequence, as the three amino acid variances between HAdVs C2 and C5[5] lie well outside of the RuvBL1-binding region.

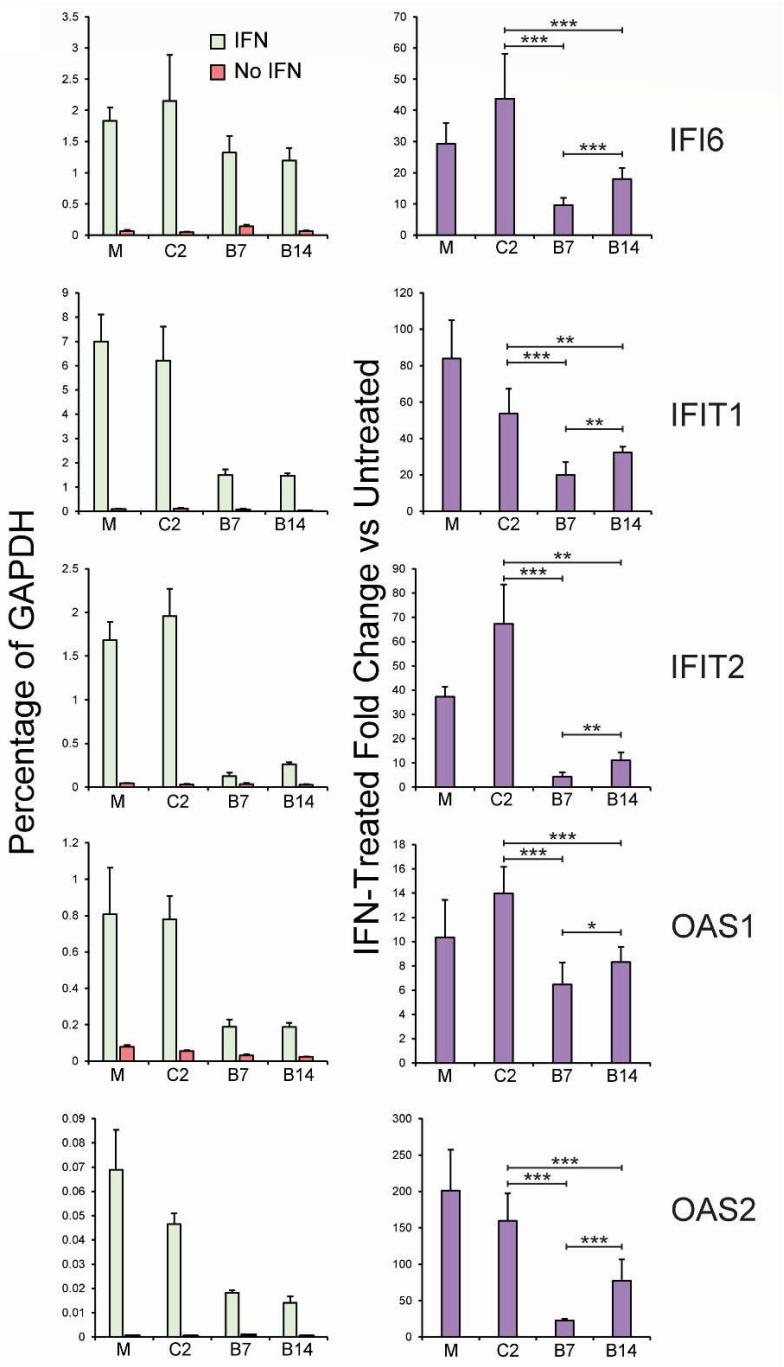


**Figure 4.7. ISG expression is severely hampered in cells infected with HAdVs B7 and B14 compared to those infected with HAdV-C2.** A549 cells were treated with IFN α-2A 16 hours after infection with indicated HAdV strains. Eight hours later, the cells were harvested, RNA extracted, and cDNA generated. Interferon-stimulated gene expression was analyzed *via* real-time qPCR. Results were normalized to percentage expression of the housekeeping gene *GAPDH* (left panel) and as a ratio of IFN-treated over untreated (right panel). M: mock infected, C2: HAdV-C2, B7: HAdV-B7, B14: HAdV-B14. Statistical analysis was performed by unpaired student's *t*-test. One asterisk represents a *P*-value of <0.05, two represent <0.01, and three represent <0.001; $n = 3$.

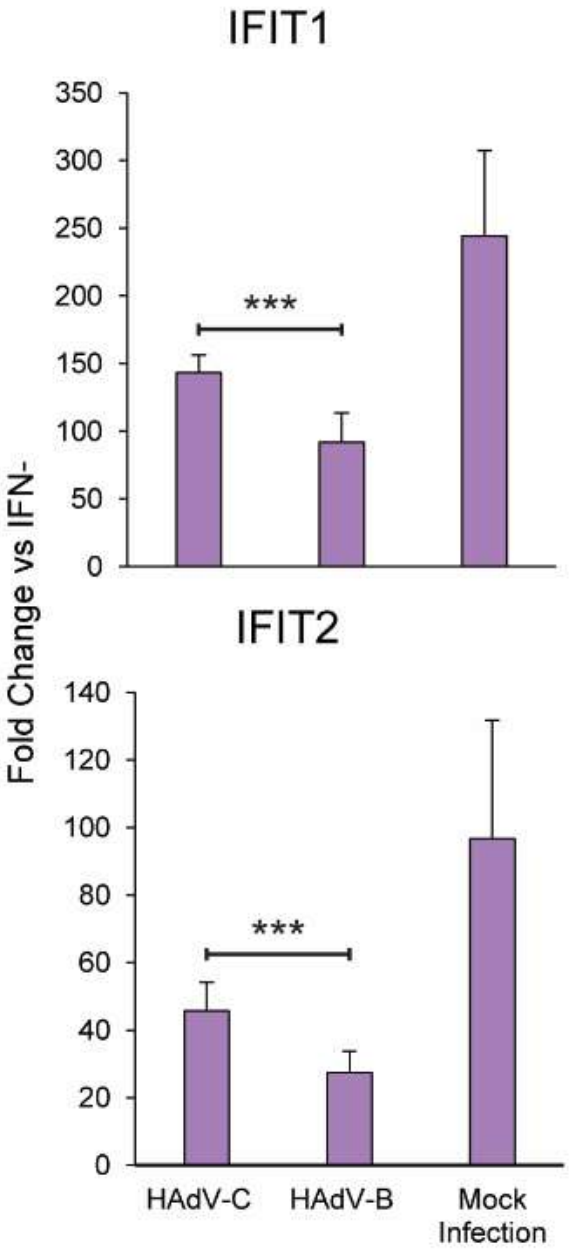


**Figure 4.8. ISG expression patterns are maintained in primary cells.** IMR90 cells were plated and allowed to grow to confluency before infection with indicated HAdV strains at MOI 10. Cells were IFN-treated 16h post-infection and harvested eight hours later. RNA was extracted, cDNA generated, and levels of indicated ISGs measured *via* qPCR. Bars represent three biological replicates each. Statistical significance determined by student's T-test. Three asterisks represent a p value<0.001.

### 4.3.3 Alignment of the E1A, E1B, E3, and E4 regions of HAdVs C2, B7, and B14

Next, I wanted to look for potential mechanisms by which species B HAdVs suppress the IFN response this efficiently. To do so, I performed sequence alignments of the regions of the HAdV genome known to be involved with innate immunity suppression: transcription units E1A, E1B, E3, and E4, though my focus was on E1A (Fig. 4.9). Alignments of the E1A genomic regions of HAdV-C2, B7, and B14 showed relatively high similarity to one another, though with a small deletion present in the second exon known to bind RuvBL1 in both species B viruses, but not species C. Such a deletion may have an effect on the way that E1A modulates RuvBL1 function, and therefore ISG suppression.

Our analyses of the other mentioned transcription units (Fig. 4.9B) turned up no major differences in E1B, or in the E4 region, between the three HAdVs, with no open reading frames unique to any of them. Interestingly, the E3 region had a sizable insert in only HAdV-B7, containing an open reading frame. The function of this ORF's putative protein product is unknown, but it is predicted to be glycosylated, with a transmembrane domain next to its C-terminus, and merits further investigation.

These results showed the most consistent difference between the early transcripts of these HAdVs to be present in E1A: deletions within or near the binding sites for RuvBL1, which previous research has shown to be involved in viral ISG suppression[11]. The largest difference was a full (albeit very small) ORF insertion in the E3 region, but this was present in only HAdV-B7, and so could not account for HAdV-B-wide differences. As such, I decided to focus on E1A and the RuvBL1 family for our initial investigation.

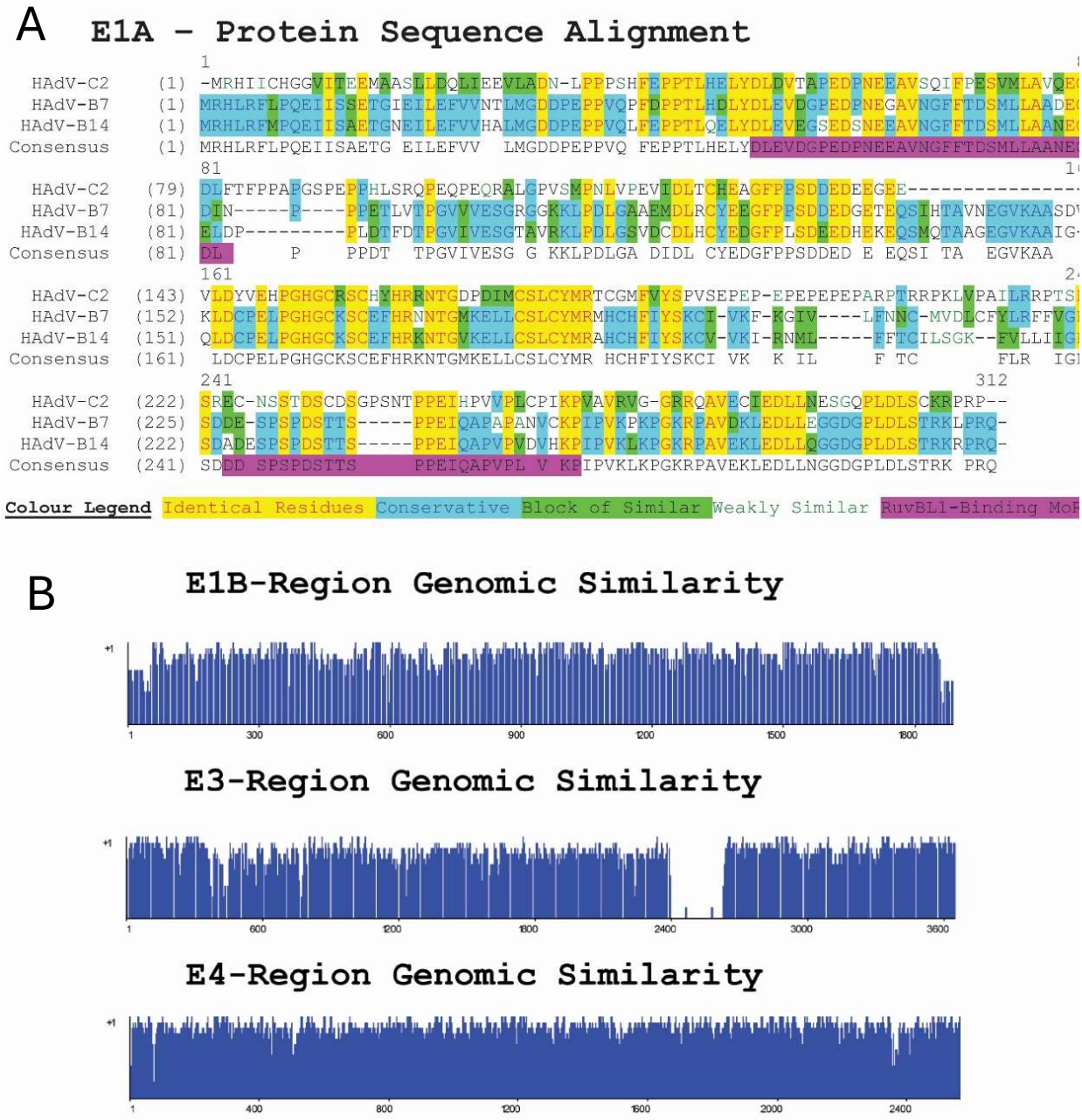


**Figure 4.9. Comparison of early genomic region similarity in HAdV-C2 to -B7 and -B14. (A) Strong conservation is present within the RuvBL1-binding site in HAdV-C2, B7, and B14 E1A.** Indicated E1A protein sequences acquired from Genbank were aligned *via* AlignX software. Residues are color-coded in accordance with the supplied color legend. **(B) General interspecies similarity levels in E1B, E3, and E4 early transcription regions.** E1B, E3, and E4 genomic regions of HAdV species C2, B7, and B14 were aligned *via* AlignX software. Histograms represent overall sequence similarity.

### 4.3.4 Species B HAdV E1As bind efficiently to RuvBL1 and RuvBL2

Previous sequence alignments showed fairly strong conservation within the regions of E1A that bind to RuvBL1 (Fig. 4.9A). As such, I hypothesized that species B HAdV E1A binds more strongly to RuvBL1 than that of species C, to better suppress ISG activation. To verify this, we looked at the interaction of RuvBL1, RuvBL2, and HAdV-C2, B7, and B14 E1A (Fig. 4.10) *via* immunoprecipitation. All E1As interacted with RuvBL1, though unexpectedly, the strongest interaction was with HAdV-C2 E1A, followed closely by B14, then distantly by B7, though all interactions were still readily detectible. All serotypes bound more strongly to RuvBL2 than RuvBL1, with both species B isoforms binding more strongly than species C, with roughly equal strength to one another (Fig. 4.10).

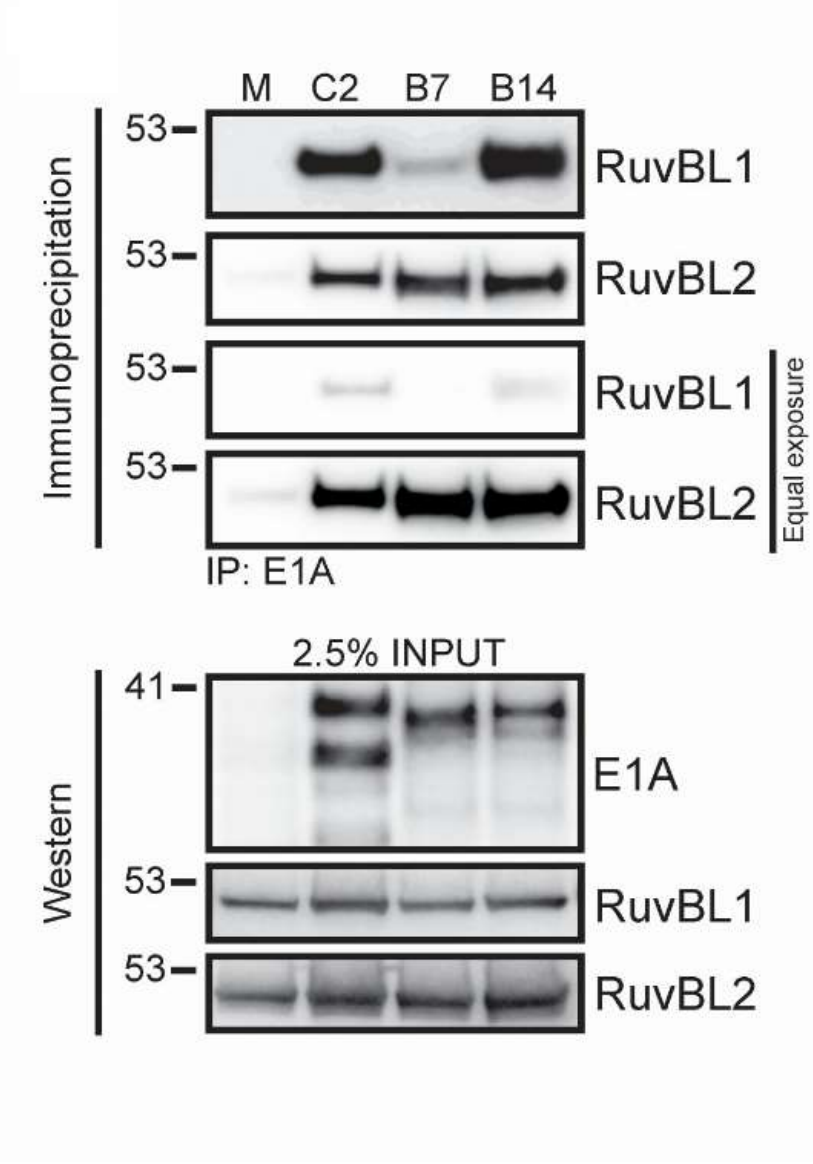


**Figure 4.10. HAdV E1As bind to RuvBL1 and RuvBL2.** A549 cells were infected with indicated viral strains for 24 hours, lysed, and indicated proteins were immunoprecipitated. Precipitates were resolved on SDS gel, transferred to the PVDF membrane, and blotted with indicated antibodies. M: mock infected, C2: HAdV-C2, B7: HAdV-B7, B14: HAdV-B14.

### 4.3.5 HAdV-B7 and B14 drive RuvBL1 into high molecular weight complexes

RuvBL1 is known to form HMW complexes with itself, RuvBL2, and other proteins[301]. Importantly, the previous results (Fig. 4.10) showed a higher binding affinity for RuvBL2 than RuvBL1 in all E1A isoforms. A possible method of ISG suppression is sequestration of RuvBL proteins into large complexes with little to no function. To test this idea, I performed immunoprecipitation in cells crosslinked with 1% formaldehyde immediately prior to harvest so as to stabilize existing protein complexes, as was done previously[68]. After lysing, I immunoprecipitated for HA-tagged RuvBL1, transfected previously, and blotted for RuvBL1-containing complexes (Fig. 4.11). High molecular weight complexes were present in cells infected with all HAdV species, though they were the most prevalent in B7, followed by B14, and with C2 showing by far the least. IFN treatment had minimal effect on complex formation. Mock infected cells contained no detectable levels of these complexes, but this could have been a result of lower expression of our tagged RuvBL1 plasmid in cells lacking a source of E1A to activate said plasmid's CMV promoter[302].

To confirm these results, we repeated the experiment above in A549 cells, immunoprecipitating and blotting for endogenous RuvBL1 in this case (Fig. 4.12). Given the less efficient antibody, results were weaker here, but overall, the pattern was the same: The HMW complex was present in its greatest quantities in HAdV-B7-infected cells, and less prevalent in those infected with the other HAdVs, and in uninfected cells.

These results clearly demonstrate that RuvBL1 is retained or stabilized in HMW complexes to a greater degree during species B infection compared to C2. This suggests that this complex might be aiding the virus in impairing host cell ISG expression.

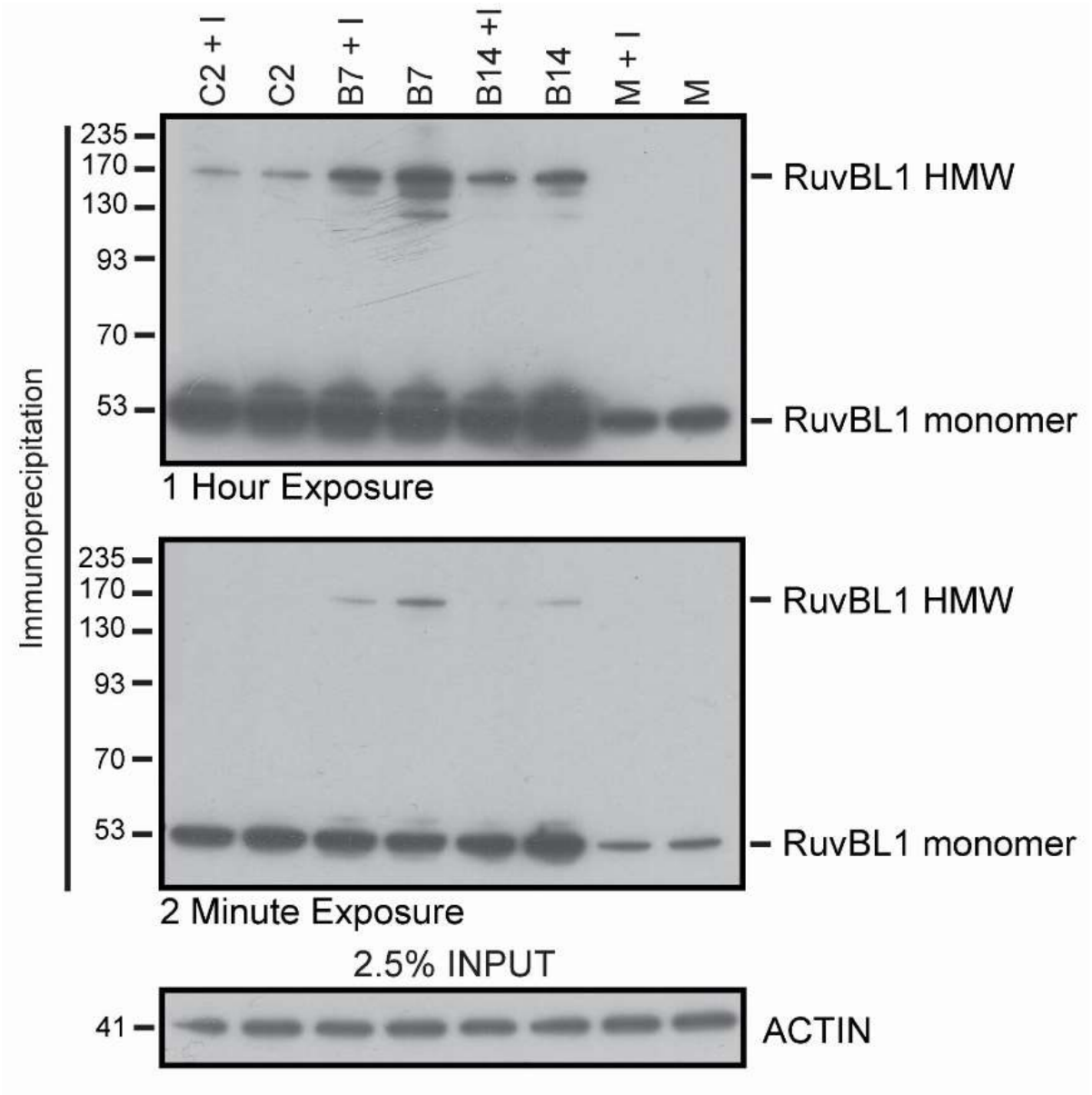


**Figure 4.11. HAdV-B7 and HAdV-B14 induce complex formation of RuvBL1 in infected cells.** A549 cells were transfected with HA-tagged RuvBL1 expression vector and infected with indicated viruses for 24 hours. Eight hours before harvest, indicated samples were treated with IFN α-2A. Cells were cross-linked with formaldehyde, harvested, and lysed, and HA-RuvBL1 was precipitated using 12CA5 anti-HA mouse antibody. Precipitates were resolved on precast, 4%–12% gradient SDS gel, transferred to the PVDF membrane, and blotted with the indicated antibodies (RuvBL1 was blotted with a rat anti-HA antibody different from that used to precipitate it); HMW, high molecular weight.

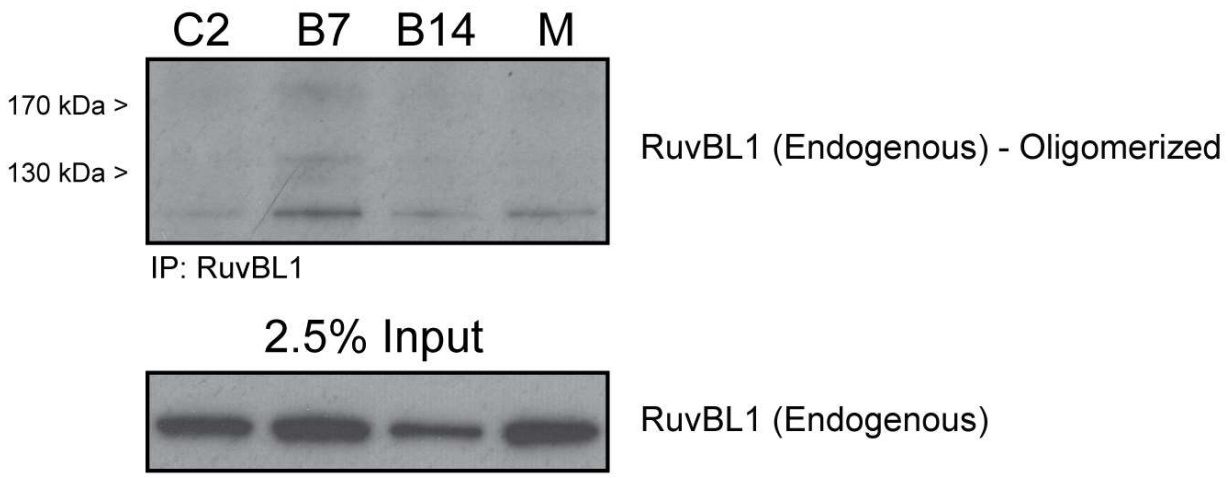


**Figure 4.12. HAdV-B-driven generation of high-molecular-weight complexes is observable through endogenous RuvBL1.** A549 cells were infected with indicated HAdV serotypes. After 24 hours, cells were cross-linked with 1% formaldehyde, harvested, and lysed with RIPA buffer. Endogenous RuvBL1 was IP'ed from lysate, protein was resolved on SDS gel, transferred to PVDF membrane, blotted with the same RuvBL1 antibody, and visualized by ECL.

### 4.3.6 HAdV infection disrupts the interaction between RuvBL1 and RNA polymerase II

As the HMW complexes observed in Fig. 4.10 and Fig. 4.11 seem to be induced by HAdV infection, it is likely that their presence is desirable for the virus. RuvBL1 and RuvBL2 binding to RPII is known to be important for expression of ISGs[90], and RuvBL2 in its own right is heavily involved in licensing of RPII at promoters[303]. As such, the possibility existed that the virus was sequestering RuvBL1 into these HMW complexes in order to make it non-functional. I therefore sought to determine whether HAdV infection has any effect on the binding affinity of RuvBL1 to RPII or RuvBL2 (Fig. 4.13).

HAdV-C2 and B7 infections greatly reduced the level of interaction between RuvBL1 and RPII. HAdV-B14 did not have as much of an effect here, but the reduction in binding affinity was still noticeable. The interaction between RuvBL1 and RuvBL2 was also affected, noticeably improving in cells infected with HAdV-C2 and B7. The effect of HAdV-B14 here was minimal. These results demonstrate that different HAdV species have differing levels of influence on the interaction between the RuvBLs, and between RuvBL1 and RPII.

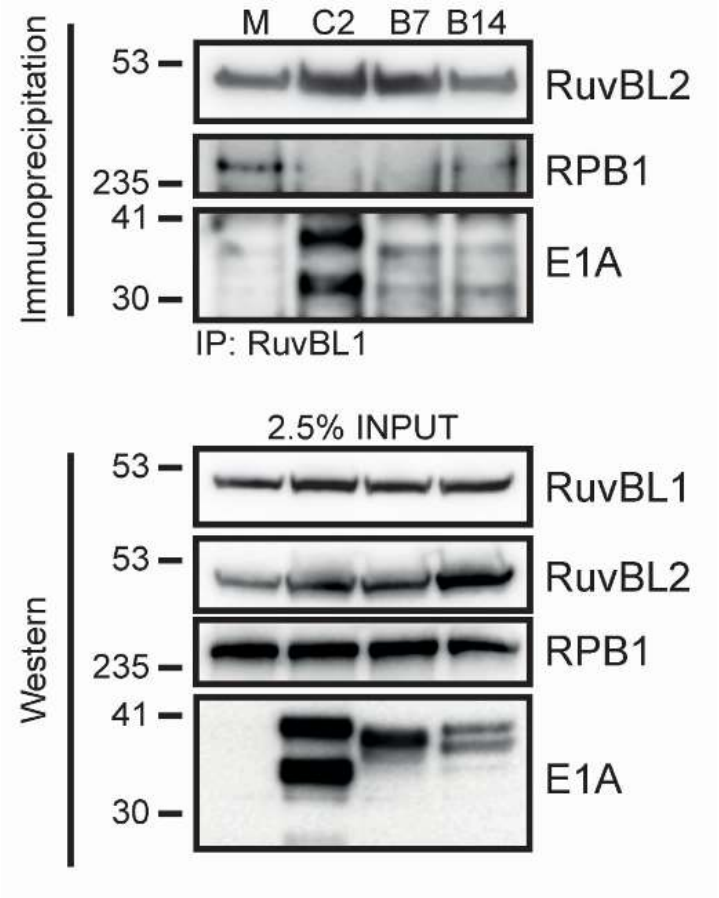


**Figure 4.13. HAdV infection disrupts RuvBL1/RNA Pol II interaction.** A549 cells were infected with indicated viral strains for 24 hours, lysed, and indicated proteins were immunoprecipitated. Precipitates were then resolved on SDS gel, transferred to the PVDF membrane, and blotted with the indicated antibodies. RPB1: RNA Polymerase II.

### 4.3.7 STAT2-RuvBL1 interaction is disrupted in HAdV-B7 and B14-infected cells

Another key component for ISG activation is STAT2, a critical element of the IFN-stimulated gene factor 3 (ISGF3) complex[304,305], that has also been shown to interact with RuvBL1/2 in the process of ISG expression[90]. Therefore, my next goal was to determine whether RuvBL1/STAT2 interaction was affected by HAdV infection, as this would represent a possible viral method of ISG suppression.

I immunoprecipitated RuvBL1 from variously infected A549 cells and blotted for STAT2 to investigate their level of interaction under these conditions, and saw a loss of binding in HAdV-B-infected cells, but not in mock- or HAdV-C-infected cells (Fig. 4.14). This suggests a level of impairment of STAT2 function during HAdV-B infection that is more efficient than that performed by HAdV-C.

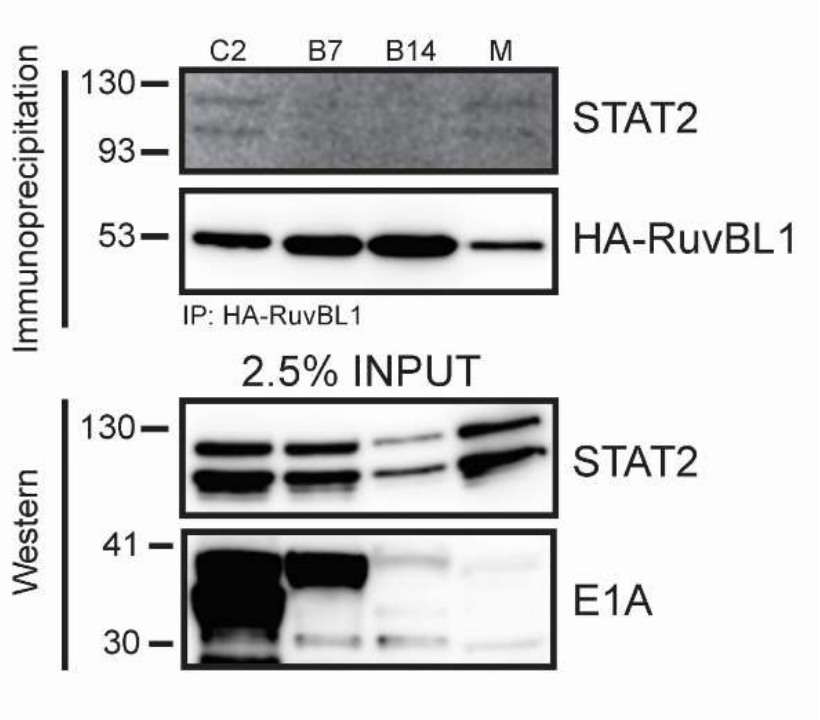


**Figure 4.14. HAdV-B7 and B14 disrupt STAT2/RuvBL1 interaction.** A549 cells were transfected with HA-tagged RuvBL1 expression vector and infected with the indicated HAdV strains 24 hours later. Sixteen hours after infection, IFN α-2A was applied. After 8 more hours, cells were harvested and lysed, and HA-tagged RuvBL1 was precipitated *via* 12CA5 anti-HA antibody. Samples were resolved on SDS gel, transferred to PVDF membrane, and blotted with the indicated antibodies.

### 4.3.8 Recruitment of STAT2 and RPII to ISG promoters is impaired in HAdV-infected cells

After IFN treatment, STAT2 and RPII are recruited to ISG promoters, which quickly leads to ISG expression[306]. Having previously observed reduced levels of STAT2/RuvBL1 interaction (Fig. 4.14) and RuvBL1/RPII interaction (Fig. 4.13) in HAdV-B-infected cells, I wanted to determine whether this was accompanied by a loss of STAT2 and RPII recruitment to ISG promoters during these infections as well. To do so, I performed ChIP on IFN-treated A549 cells, 24 hours after infection with species B or C HAdVs (Fig. 4.15). I examined promoter occupancy of STAT2 and RPII at three ISG promoters to form a representative sample – *IFI6*, *IFIT1*, and *OAS2*.

At each measured promoter, I saw a significant reduction in STAT2 and RPII recruitment in all infected cells, compared to mock infection. However, while some recruitment was still observed in HAdV-C infection, both HAdV-B species resulted in recruitment levels comparable to background (IgG negative control). A repeat of this experiment in IMR-90 (primary) cells (Fig. 4.16) showed similar results: Once again, STAT2 recruitment was reduced to almost nothing by species B, and while RNA polymerase II recruitment was not affected as strongly, it was still lower at all promoters measured in HAdV-B infection than HAdV-C. We also examined recruitment of RuvBL1 to these promoters (Fig. 4.17), and while this was reduced overall by all three viruses compared to mock infection, no significant differences were observed between HAdV-C2, B7, or B14.

The reduced recruitment of STAT2 to ISGs could still be explained away by an overall reduction in protein levels, perhaps through ubiquitination and subsequent proteasome-mediated degradation, as has been previously-reported for STAT2[307,308]. To see whether this was the case, I looked to determine levels of ubiquitination on STAT2 in cells infected with species B or C

HAdVs. I transfected HT-1080 cells with an HA-tagged ubiquitin expression vector and infected them with HAdV types C2, B7, and B14 (Fig. 4.18). I immunoprecipitated STAT2, detecting levels of ubiquitination with an anti-HA antibody, and observed that contrary to expectations, not only is STAT2 ubiquitination not increased in species B HAdVs, it is actually reduced, compared to species C2. As would be expected, this is accompanied by higher total levels of STAT2 in cells infected with species B HAdVs, compared to species C.

It has also been reported, more recently, that host proteins GCN5 and BRD2 are required for eviction of H2A.Z from nucleosomes, increasing levels of ISG expression[309]. Therefore, I investigated whether H2A.Z, histone H3 lysine 4 trimethyl (H3K4Me3 – a histone modification that co-localizes with H2A.Z on promoters[310]), and total histone H3 were differentially present on ISG promoters (Fig. 4.19). No significant differences in histone density were found between any of the observed ISG promoters and the promoter for *ACTB* (a common housekeeping gene). That said, there was an overall increase in H2A.Z density observed in all HAdV infections, which may be the result of E4orf3-driven heterochromatinization, as previously reported[155,160]. Knockdown of H2A.Z or GCN5 *via* siRNA did not have a noticeable effect on ISG suppression in infected cells (Fig. 4.20).

In totality, these results show that HAdV-B is highly efficient at inhibiting STAT2 and RNA polymerase II recruitment to cellular ISG promoters, and that this is largely unaffected by reduction of H2A.Z or GCN5 levels. Interestingly, these species B HAdVs appear to protect cellular STAT2 from ubiquitination and subsequent proteasomal degradation, despite its role in ISG expression.

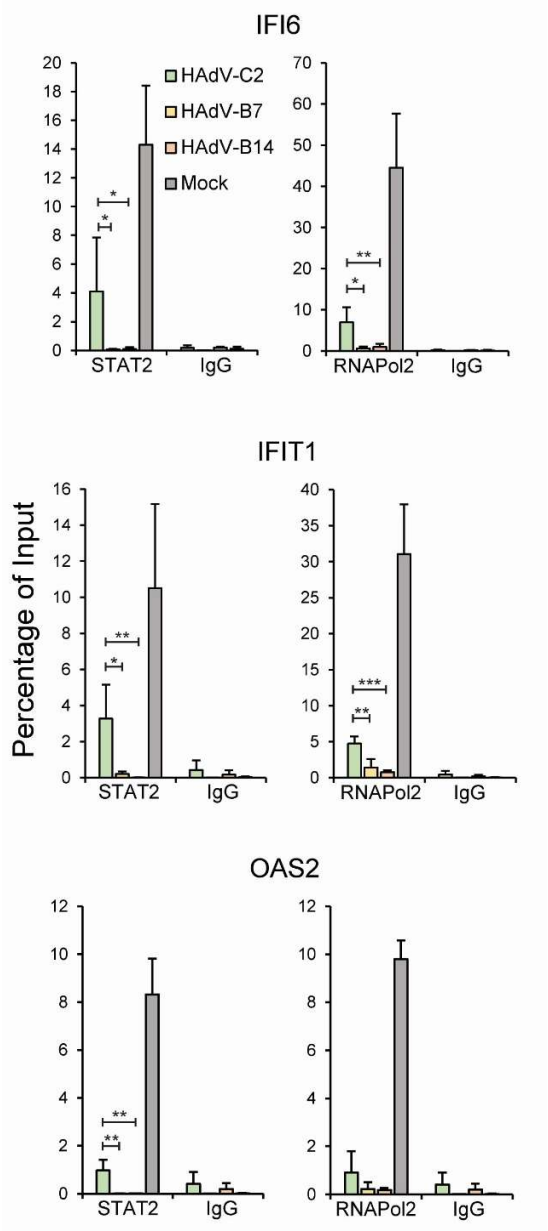


**Figure 4.15. Recruitment of STAT2 and RNA polymerase II to ISG promoters is dramatically reduced in HAdV-B7 and HAdV-B14 compared to HAdV-C2.** A549 cells were treated with IFN α-2A 20 hours after infection with the indicated HAdVs, and 4 hours later (24 hours after infection), cells were cross-linked, harvested, and indicated proteins were immunoprecipitated. Cross-linking was reversed, DNA was isolated, and relative levels were analyzed *via* qPCR. Statistical analysis was performed *via* unpaired student's *t*-test. One asterisk signifies a *P*-value of <0.05, two represent <0.01, and three indicate <0.001; $n = 2$.

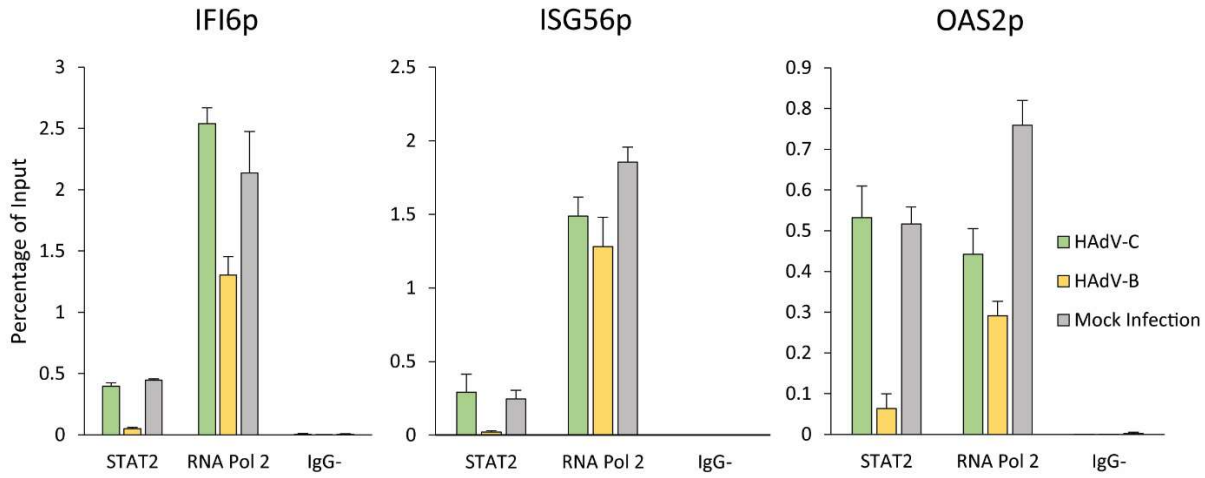


**Figure 4.16. Previously-observed STAT2 and RNA Pol 2 recruitment patterns are maintained in primary cells.** IMR90 cells were plated and allowed to grow to confluency before infection with indicated HAdV strains at MOI 10. Cells were IFN-treated 20h post-infection and cross-linked and harvested four hours later. Cells were lysed, nuclei isolated and lysed in turn, and chromatin was sheared *via* sonication. IPs were performed using indicated antibodies before cross-linking was reversed, DNA extracted, and qPCR reads taken.

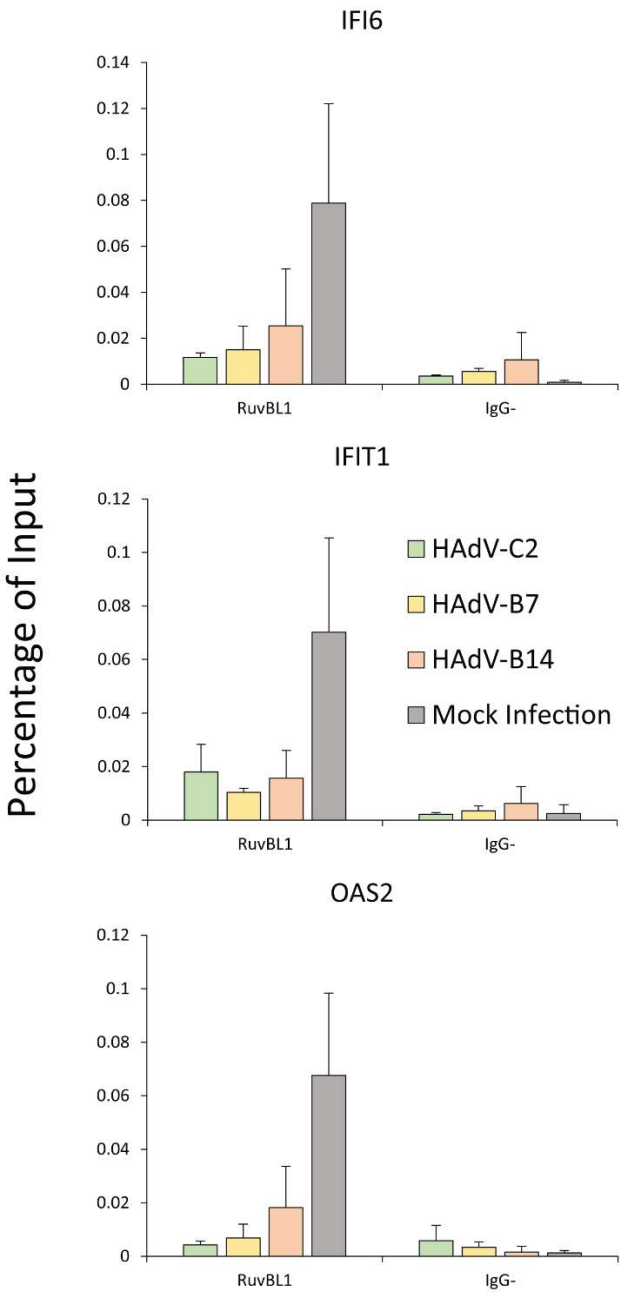


**Figure 4.17. Recruitment of RuvBL1 to ISG promoters in IFN-treated cells is universally reduced during HAdV-infection.** A549 cells were infected with indicated HAdV strains for 24 hours, treated with IFN, and harvested eight hours later. Cells were cross-linked and lysed, and RuvBL1 was immunoprecipitated. Cross-linking was reverse, DNA isolated, and relative ISG promoter levels analyzed *via* qPCR. Results based on biological duplicate samples.

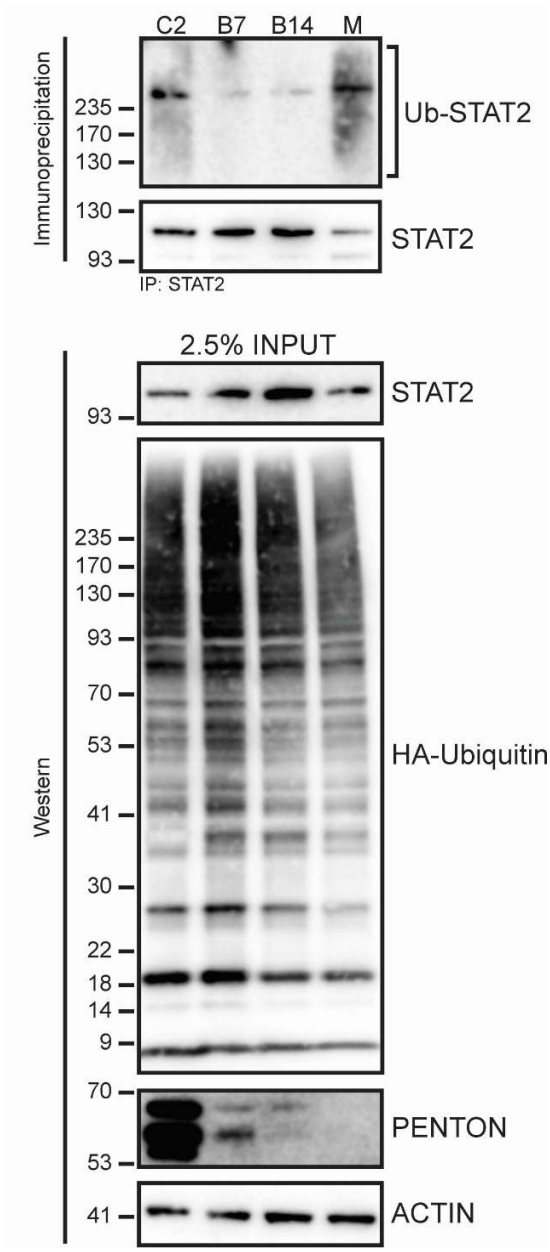


**Figure 4.18. Ubiquitination of STAT2 is reduced in HAdV-B7 and B14-infected cells.** HT1080 cells were transfected with the HA-ubiquitin expression vector and subsequently infected with the indicated viruses for 24 hours at MOI 10. Cells were lysed and immunoprecipitations were carried out for STAT2 in RIPA buffer as described. Immunoprecipitates were then resolved on a 4%–12% gradient SDS gel and blotted for the indicated proteins. PENTON was used to indicate infection, note that higher levels of PENTON in C2 do not reflect higher protein expression in this virus, but rather the sensitivity of the anti-PENTON antibody for C2, for which it was raised, is much higher than for B7 and B14.

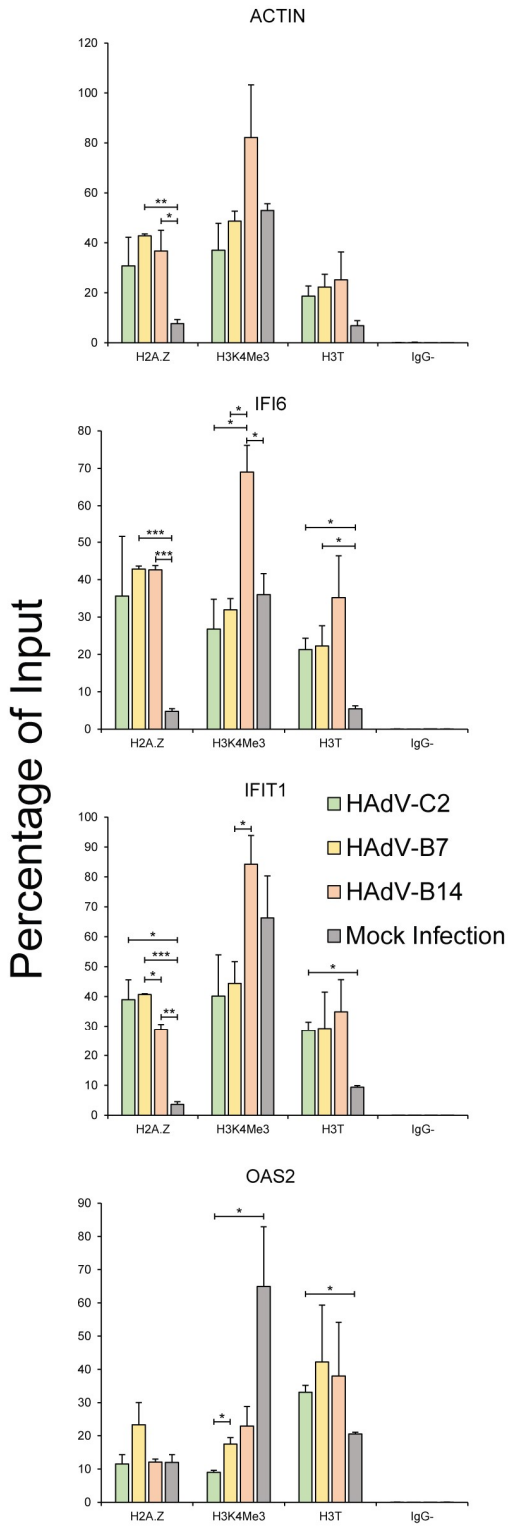


**Figure 4.19. HAdV alters histone recruitment to ISG promoters as part of universal histone alteration.** A549 cells were treated with interferon α-2a at a concentration of 1 unit/mL 20 hours before infection with indicated HAdV stocks. 24 hours after infection, cells were cross-linked and harvested, and indicated proteins were immunoprecipitated. Cross-linking was reversed, DNA isolated, and relative levels analyzed *via* qPCR. Bars represent biological duplicates. Statistical significance determined by student's T-test and indicated where present. * represents $p<0.05$, ** $p<0.01$, and *** $p<0.001$.

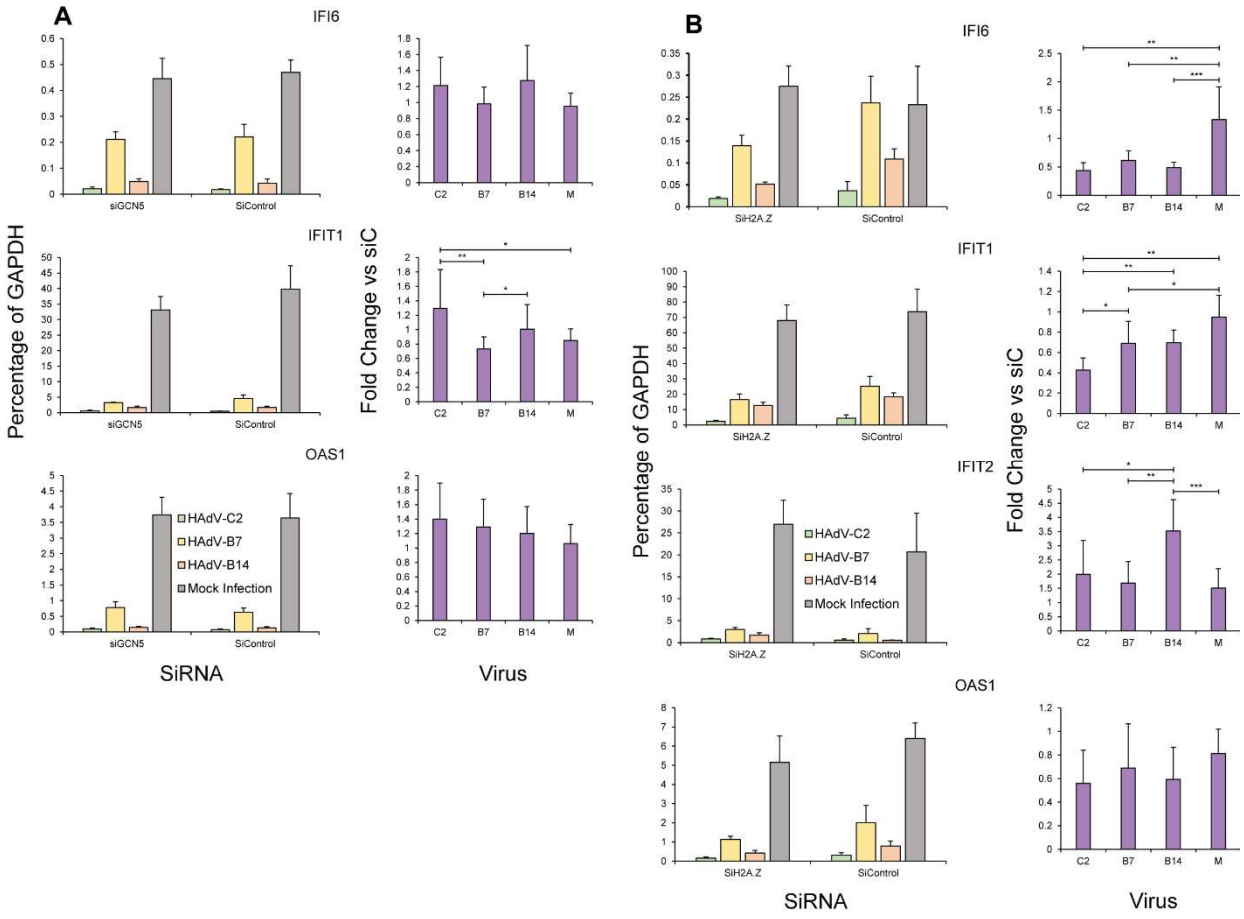


**Figure 4.20. HAdV ISG suppression is mostly unaffected by knockdown of GCN5 or H2A.Z.** A549 cells were treated with siRNA to knock down GCN5 (A) or H2A.Z (B) for 72 and 24 hours respectively. Cells were then infected with indicated HAdV strains and treated with IFN 16 hours later. After eight more hours, RNA was extracted, cDNA generated, and gene expression measured *via* qPCR. Results are presented as percentage of GAPDH (left column) and fold change versus cells treated with control siRNA (right column). Each column based on the results of biological triplicate samples. Statistical significance determined by student's T-test and noted where present. * represents p-value<0.05, ** p<0.01, *** p<0.001.

### 4.3.9 RuvBL1/RuvBL2 knockdown has little effect on ISG suppression by HAdV-B7 and B14

Previous work from the Pelka lab revealed that knocking down levels of RuvBL1 *via* siRNA decreased HAdV-C5's ability to properly suppress ISG activation[11]. To determine whether this was also true in species B, the same experiment was performed in cells infected with HAdVs C2, B7, and B14 (Fig. 4.21A). The reduction of RuvBL1 did not have any significant effect on ISG expression in cells infected with either type of species B, but as previously seen, it had a significant effect in species C-infected cells. Knockdown of RuvBL2 had similar effects to the knockdown of RuvBL1, if slightly less pronounced for some ISGs. Specifically, HAdV-B7, but not HAdV-B14, lost the ability to suppress *IFI6* in the absence of RuvBL2, while both species B viruses were less able to suppress *OAS1*. *IFIT1* and *IFIT2* results were both consistent with those observed in the absence of RuvBL1. This suggests that RuvBL1 and 2 provide a major route for ISG suppression by HAdV-C2, but not for HAdV-B7 or B14.

Additionally, three more E1A-binding proteins have recently been shown to be involved in HAdV-C ISG suppression, these being FoxK1&2 (FoxK collectively) and DCAF7[82]. I wanted to expand on this by investigating their role in species B ISG expression, so I measured ISG expression levels in species B-infected cells siRNA knocked down for each of these three proteins (Fig. 4.21B and C). Knockdown of DCAF7 had mostly minimal effects on suppression of each observed ISG, though suppression of *IFIT1* and *IFIT2* in HAdV-B7 did seem to be somewhat affected. Results were mostly similar for FoxK1 and 2, though in this case, suppression of a few ISGs (*IFIT1*, *IFIT2*, and *OAS1*) seemed to be reduced exclusively for HAdV-B14. An immunoprecipitation to investigate binding affinities of these three proteins for each variant of E1A (Fig. 4.21D) showed no detectible binding to FoxK and minimal binding to DCAF7 by either species B E1A. Substantial binding was observed for species C E1A, as expected.

In total, these results show that the presences of RuvBL1 and 2 are significantly less important for species B ISG suppression than that of species C. However, we see also that E1A-binding proteins FoxK1, FoxK2, and DCAF7, which are less important for species C ISG suppression, seem to have more of a role here for species B. Specifically, B7 seems to rely more heavily on DCAF7, while B14 relies more heavily on the FoxKs.

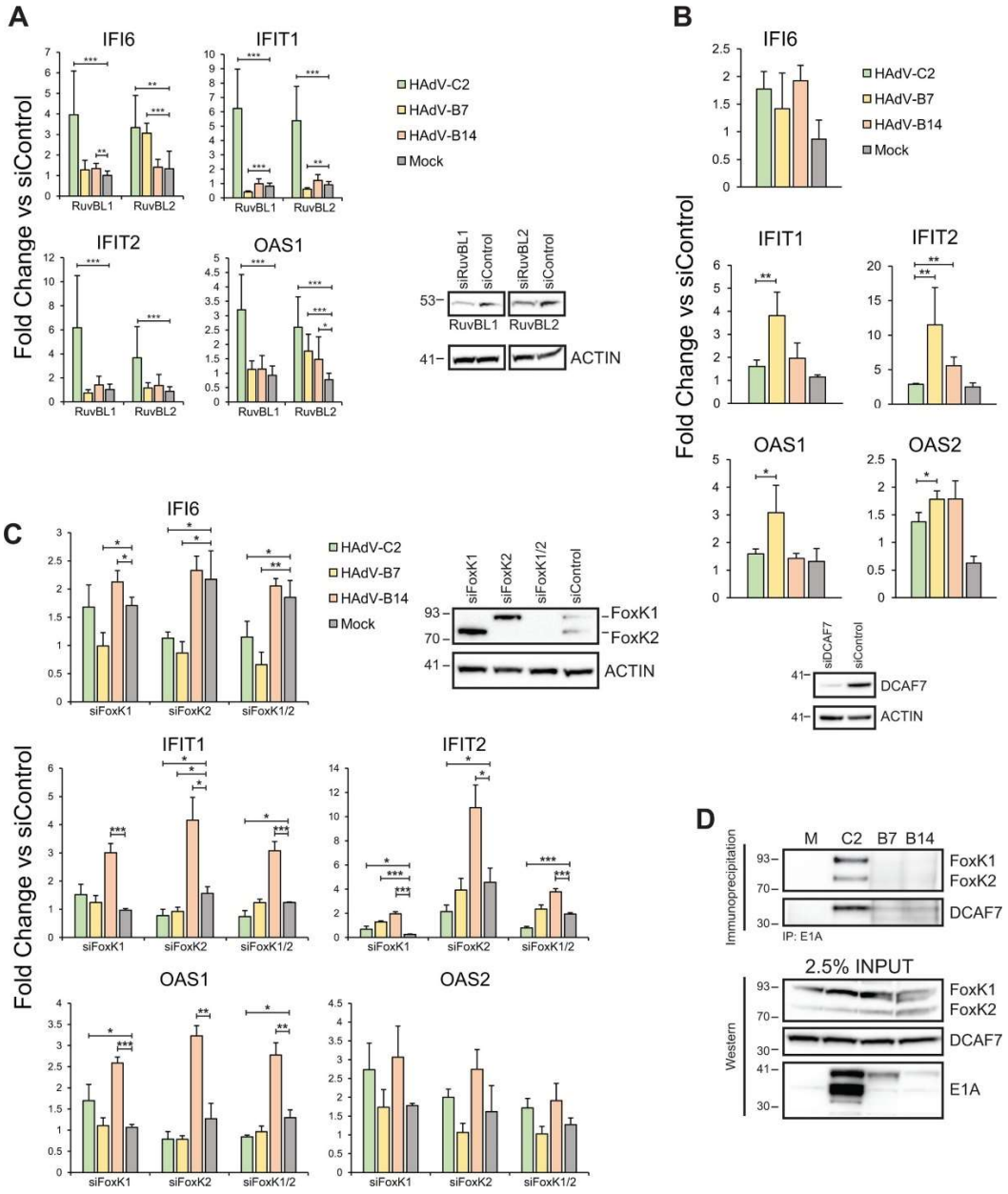


**Figure 4.21. Viral ISG suppression relies on the presence of different, species-specific host proteins.** A549 cells were treated with siRNA to knock down RuvBL1 or RuvBL2 (A), DCAF7 (B), and FoxK1/FoxK2 (C), as indicated, for 72 hours. Cells were then infected with indicated HAdV strains and treated with IFN 16 hours later. After 8 more hours, RNA was extracted, cDNA generated, and gene expression measured *via* qPCR. Results are presented as fold change versus cells treated with control siRNA. (D) Species C HAdV E1A interacts more strongly with FoxK and DCAF7 than species B. A549 cells were infected with indicated viral strains for 24 hours, lysed, and indicated proteins were immunoprecipitated. These were then resolved on SDS gel, transferred to the PVDF membrane, and blotted with indicated antibodies. M: mock infected, C2: HAdV-C2, B7: HAdV-B7, B14: HAdV-B14. Statistical analysis was performed by unpaired student's *t*-test. One asterisk represents a *P*-value of <0.05, two represent <0.01, and three represent <0.001; $n = 3$.

### 4.3.10 RuvBL1 and RuvBL2 are cytoplasmically retained in species B-infected cells

The reduction in localization of STAT2 and RNA polymerase II to ISG promoters observed in Fig. 4.15 and Fig. 4.16 may be the result of RuvBL1 and 2 being sequestered into non-functional or differently-functional high molecular weight complexes, like those observed in Fig. 4.12 and Fig. 4.13. This sequestration would likely result in an alteration to the subcellular localization of RuvBL1 and 2, as observed in the cases of other host proteins such as FUBP1[311], Ku70[312], and Nek9[313]. To compare subcellular localization of RuvBL1 and RuvBL2 in different infection scenarios, I performed immunofluorescent analysis on HT-1080 cells transfected with an HA-tagged RuvBL1 expression vector and infected with species B and C HAdVs, using antibodies for HA (RuvBL1) and E1A (Fig. 4.22). Uninfected cells treated with IFN saw RuvBL1 and 2 mostly nucleocytoplasmic, with some nuclear enrichment in the case of RuvBL2. When the infecting virus was HAdV-C2, both RuvBLs were predominantly nuclear, with almost no cytoplasmic protein to be seen. In the cases of both species B HAdV-infected cells, the localization was decidedly nucleocytoplasmic. When E1A was transfected alone (Fig. 4.23), rather than as part of an infection, this pattern was observed again, implying that E1A alone is sufficient to alter RuvBL1 sub-cellular localization, at least in the case of HAdV-C2. These results suggest that RuvBL1 is retained in the cytoplasm more readily in species B infections than in species C, making it less available for promoter recruitment and ISG activation. I also looked at the subcellular localization of STAT1 and STAT2 (Fig. 4.24), observing no significant differences between HAdV species. Finally, I examined the effect of HAdVs on the interaction between STAT1/2 and RNA polymerase II (Fig. 4.25). Interaction was majorly reduced in all cases, but there was no significant difference between species B and C here.

These results show that RuvBL1 and 2, which undergo major subcellular relocalizations during HAdV-C infection, or even simple transfection with HAdV-C E1A, are minimally affected in their location by HAdV-B. No notable differences are present in the subcellular localization of STAT1 or STAT2.

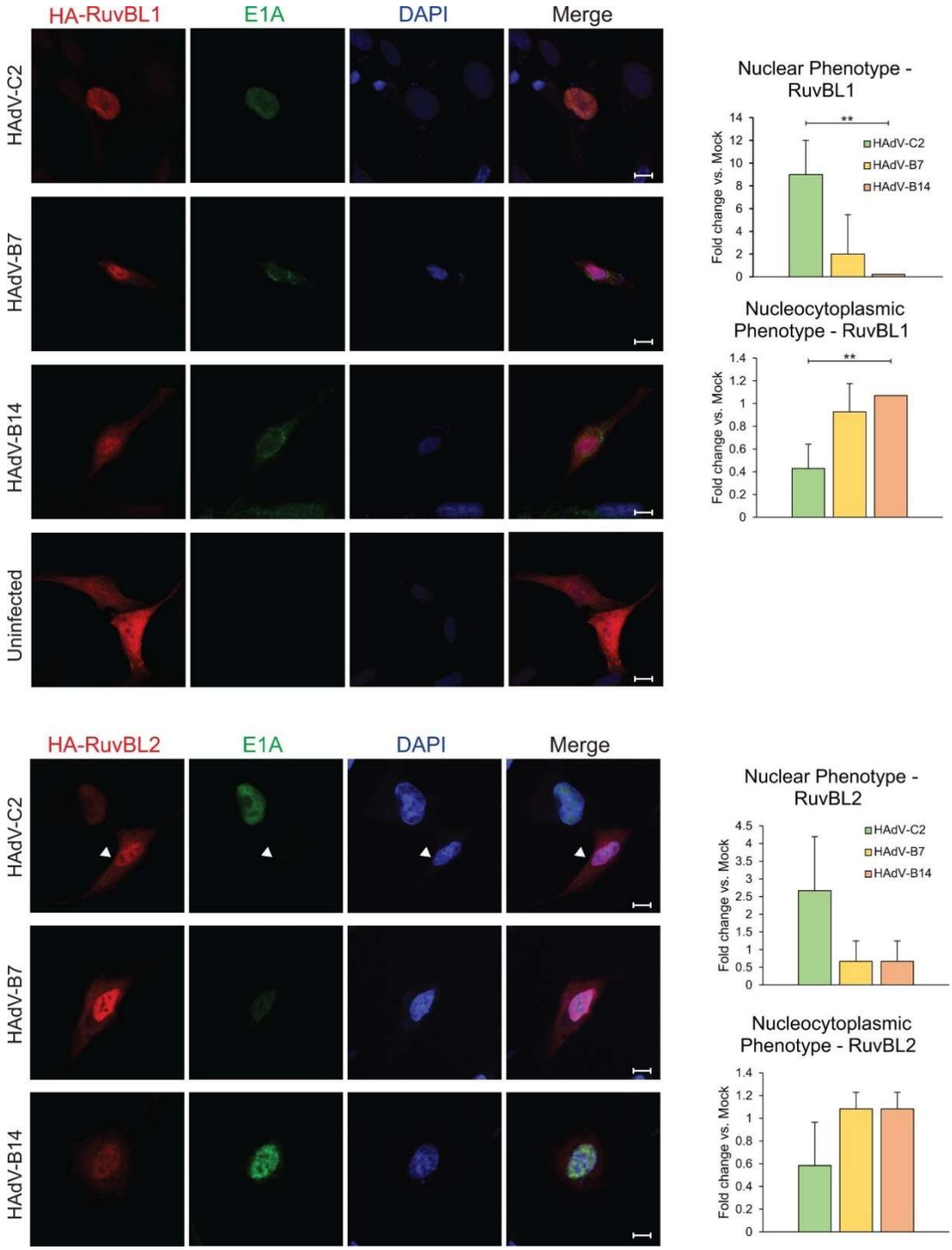


**Figure 4.22. RuvBL1 and RuvBL2 are unable to completely localize to the nucleus in cells infected with HAdV-B7 and HAdV-B14.** HT-1080 cells were seeded onto chamber slides and infected with indicated viral strains. After 16 hours, IFN was applied and cells were fixed and permeabilized 8 hours later. Antibodies were then applied as indicated and cells were imaged on a Zeiss LSM700 laser confocal microscope. Carats show uninfected cells as internal controls; scale bar represents 5 μm. Bar charts show the relative frequency of the observed phenotypes with two asterisks representing a *P*-value of <0.01; $n = 5$ random fields of view.

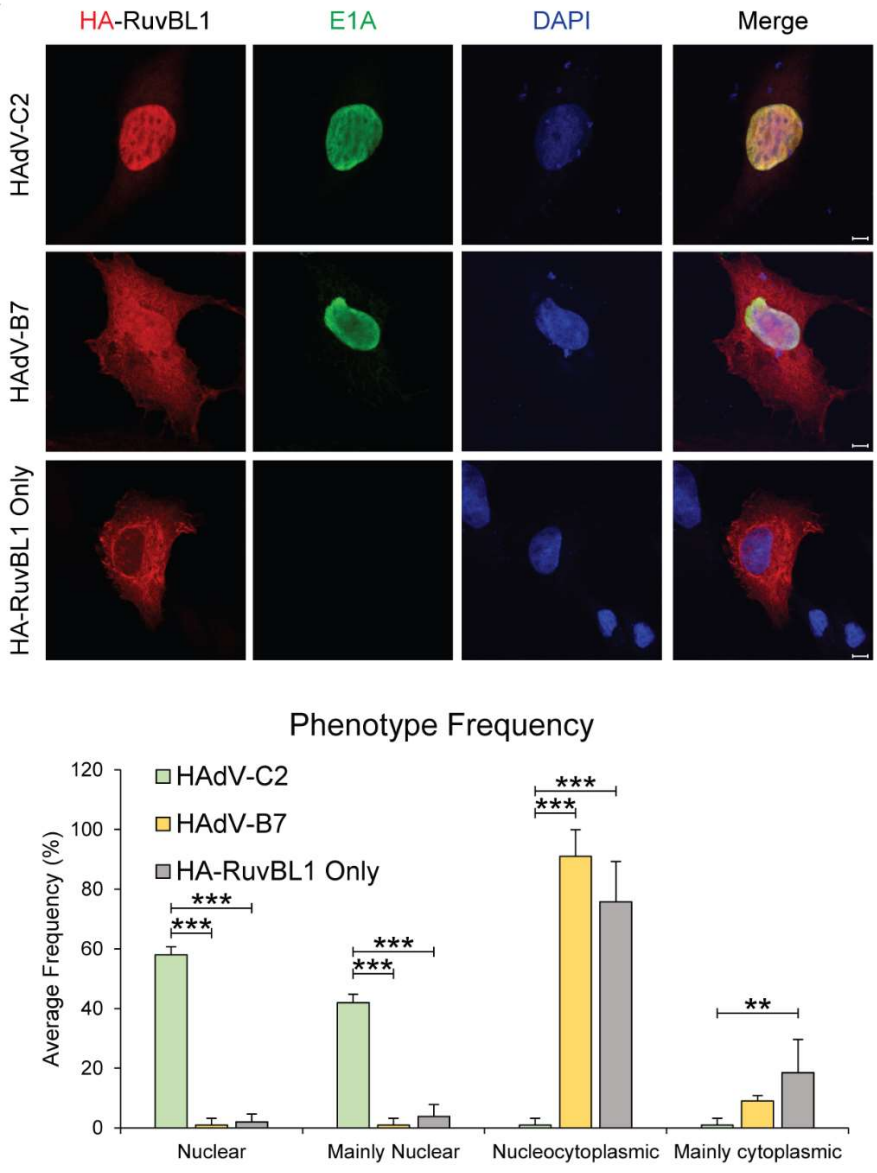


**Figure 4.23. Subcellular localization of RuvBL1 is affected by transfected E1A.** HT-1080 cells were transfected with expression vectors for HA-RuvBL1 and E1A from indicated HAdV strains. Cells were fixed and IF-stained for HA- and E1A and imaged *via* confocal microscopy. Scale bars represent a distance of 5 μm. Graph represents relative frequencies of indicated phenotypes based on random samples of 20 cells from five fields of view each. Statistical significance was determined *via* student's T-test. ** indicates $p<0.01$, *** $p<0.001$.

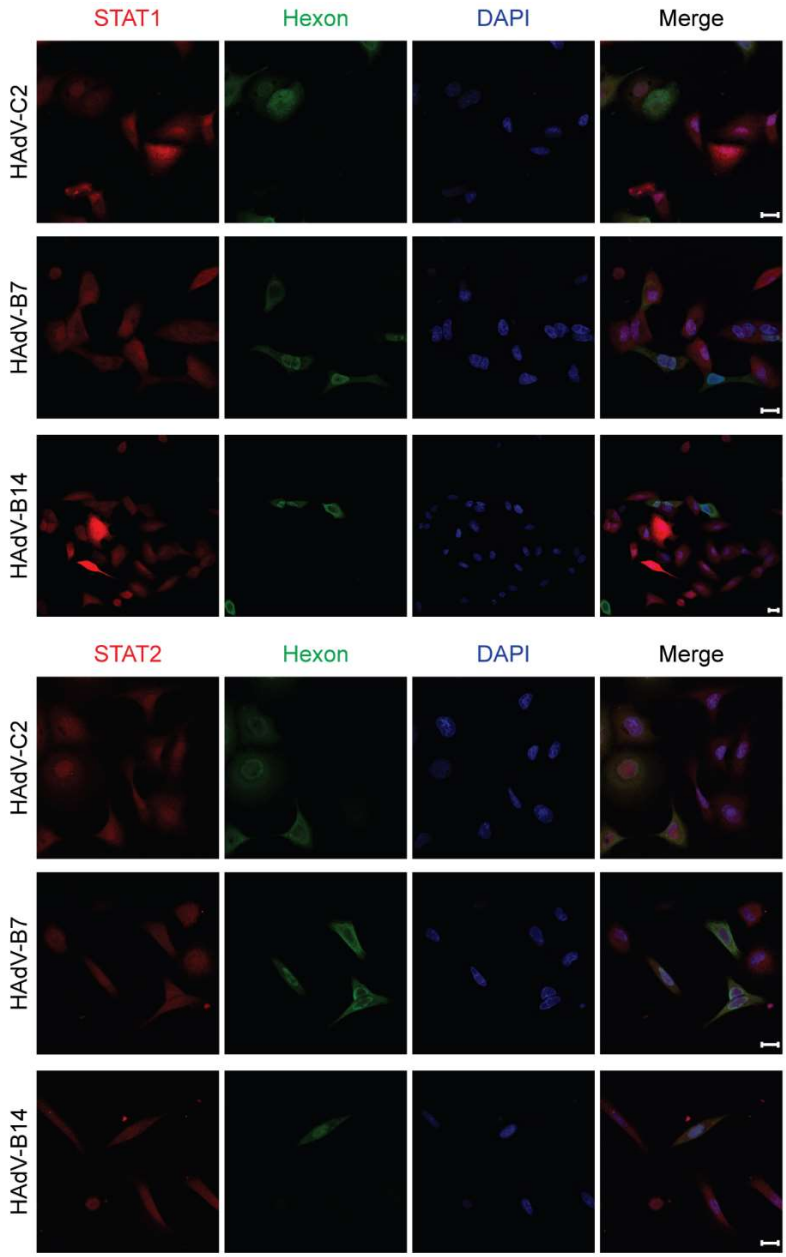


**Figure 4.24. Subcellular localization of STAT1 and STAT2 is mostly unaffected by infection with HAdV strains.** After 16 hours, IFN was applied, and cells were fixed and permeabilized 8 hours after that. Antibodies were then applied as indicated, and cells were fluorescently visualized. All scale bars represent a distance of 10 μm.

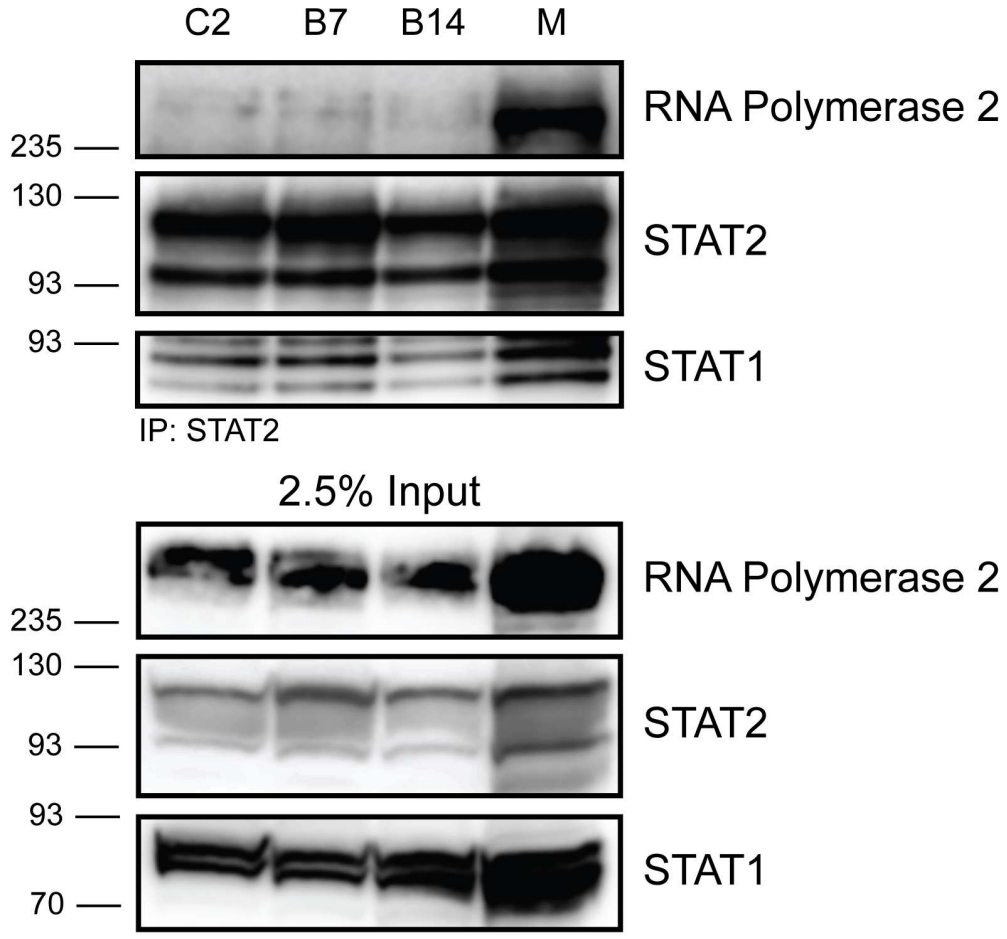


**Figure 4.25. HAdV infection decreases STAT2-RNA polymerase II interaction.** A549 cells were treated with IFN and infected with indicated viral strains 16 hours later. Cells were harvested and lysed 72 hours after infection. Cell lysate was precipitated for STAT2, resolved on SDS gel, transferred to PVDF membrane, and blotted as indicated.

### 4.3.11 E1A is not responsible for the presence of high molecular weight RuvBL1 Complexes

In addition to all else, the causative agent of the HMW RuvBL1 phenotype remained to be determined. As such, I investigated whether the presence of E1A alone is solely responsible. I transfected cells with species B or C E1A, as well as HA-tagged RuvBL1, and performed a cross-linked IP to maintain protein complexes, precipitating out HA-RuvBL1 (Fig. 4.26). Interestingly, I did observe HMW RuvBL1, but it was only present in detectible quantities when no E1A was present. Any difference in the amount of HMW RuvBL1 between the two E1A variants appears negligible, though there may actually be slightly more in the species C column than in species B.

These results show that despite the previously-observed differences in sequence (Fig. 4.9) and RuvBL1 binding efficiency (Fig.4.10), E1A itself is not responsible for the HMW RuvBL1 phenotype. When present on its own, E1A, regardless of species variant, seems to actively reduce levels of HMW RuvBL1, rather than increase it. This implies that a separate viral protein may be responsible for the sequestration of RuvBL1 in the host cell.

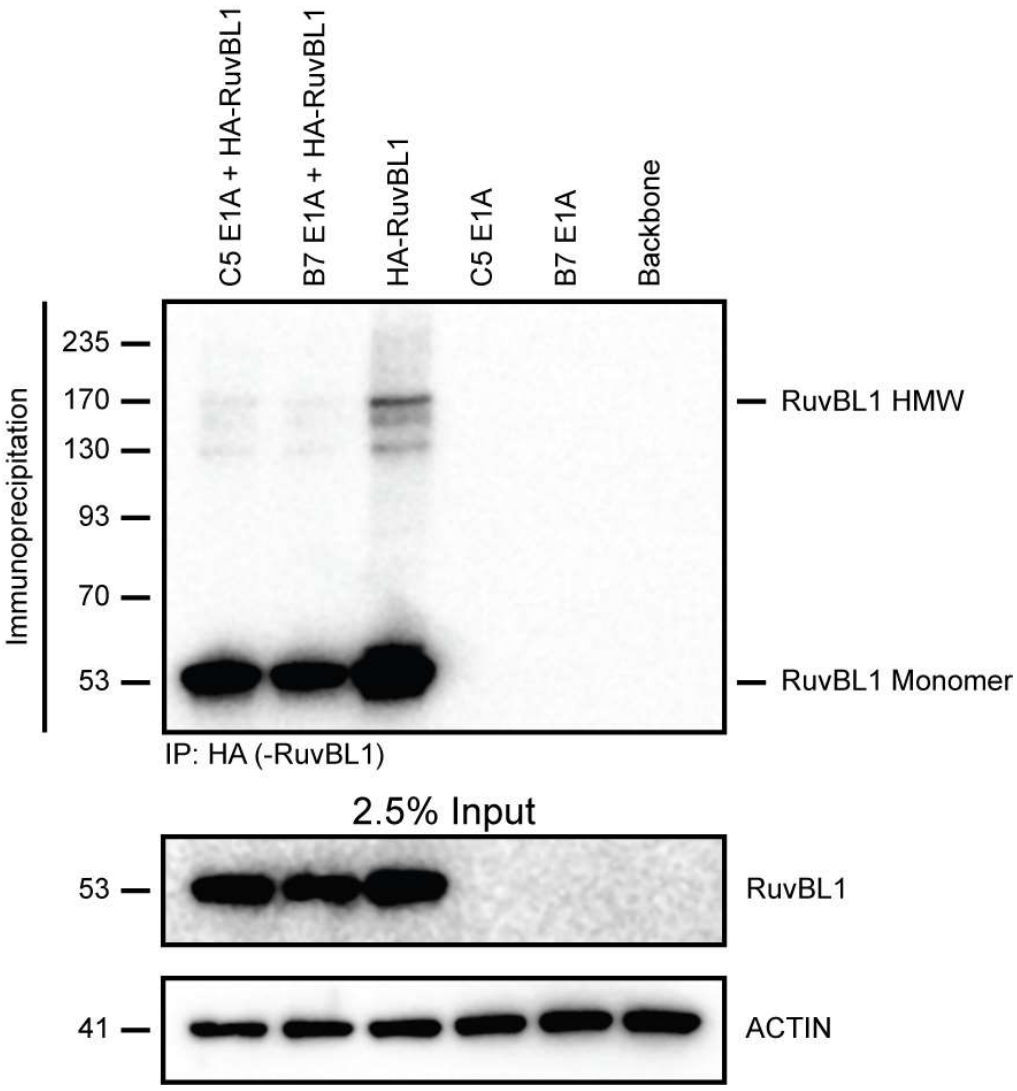


**Figure 4.26. HMW RuvBL1 complex formation is unaffected by E1A isoform.** HT-1080 cells were transfected with E1A variants and HA-tagged RuvBL1 as indicated for 16 hours, cross-linked with formaldehyde, lysed with RIPA buffer, immunoprecipitated for HA, and resolved by SDS-PAGE. Membranes were blotted for HA using a differently sourced HA antibody and imaged by ECL. Where only one, or no plasmids were transfected, an equivalent mass of empty backbone was used to ensure equal transfection levels in all cases.

### 4.3.12 Proteomic comparison of HAdV-B and HAdV-C

Finally, I wanted to compare the broad-range effects of infection by species B HAdV on the host cell. As such, I infected A549 cells with HAdV-C2, B7, and B14, treated them with IFN, and analyzed their proteome *via* shotgun 2D-LC-MS/MS. I analyzed the results by two metrics: proteins upregulated or downregulated at least two-fold in each infected cell line as compared to an uninfected control, and proteins similarly up- or downregulated in HAdV-B7 and B14, as compared to C2 (Fig. 4.27). Overall, I saw hundreds of proteins differentially expressed between the three different HAdV types (Fig. 4.27B), with significant overlap between those upregulated in HAdVs B7 and B14 (21% commonly upregulated and 14% commonly downregulated versus C2, compared to 11% and 16% universally up- and downregulated respectively – Fig. 4.27C). Surprisingly, HAdV types C2 and B7 showed a higher degree of similarity to one another when all three were compared to uninfected than B7 showed to B14: ~20% and ~18% up- and downregulated respectively between C2 and B7, as opposed to ~6% and ~4% between B7 and B14.

I also examined up- and downregulation of biological processes by each strain through gene ontology analysis of previously-mentioned sorted clusters of up- and downregulated proteins, presented in tables 4.1 and 4.2. HAdV-B7 was particularly efficient at upregulating processes involved in host cell RNA metabolism, while HAdV-B14 upregulated energy and biomolecule synthesis pathways. I observed sizable downregulation of innate defence pathways such as MDA5, T-cell-mediated cytotoxicity, type I IFN response, and negative regulation of viral genome replication by HAdV-B7. HAdV-B14, meanwhile, was found to suppress ISG15-protein conjugation, NF-κB signaling, and pyroptosis. Both species B HAdVs, in comparison to

C2, were shown to be better at suppressing protein dephosphorylation pathways, ubiquitination-mediated protein catabolic processes, and cellular metabolic compound salvage pathways.

On the whole, these results suggest that despite their shared species typing and IFN resistance, HAdVs B7 and B14 are just as different from one another in terms of mechanism of action as they are from HAdV-C2, possibly more so. Gene ontology results suggest that HAdV-B7 strongly downregulates a host of innate immune pathways, while B14 instead focuses on IFN-regulated pathways to inhibit immune-driven cell death while upregulating energy-producing metabolic processes. Clusters of up- and downregulated proteins are presented in Fig. 4.28 through Fig. 4.31.

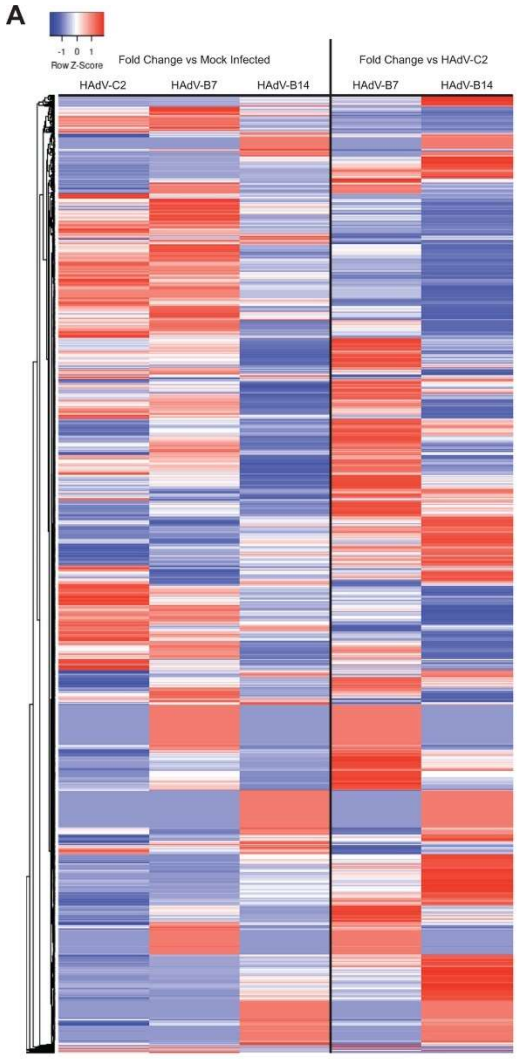


B

| | Viral Strain | Upregulated | Downregulated |
|---|---|---|---|
| Vs Mock Infected | HAdV-C2 | 383 | 474 |
| | HAdV-B7 | 550 | 338 |
| | HAdV-B14 | 442 | 397 |
| Vs HAdV-C2 | HAdV-B7 | 413 | 124 |
| | HAdV-B14 | 561 | 446 |

C

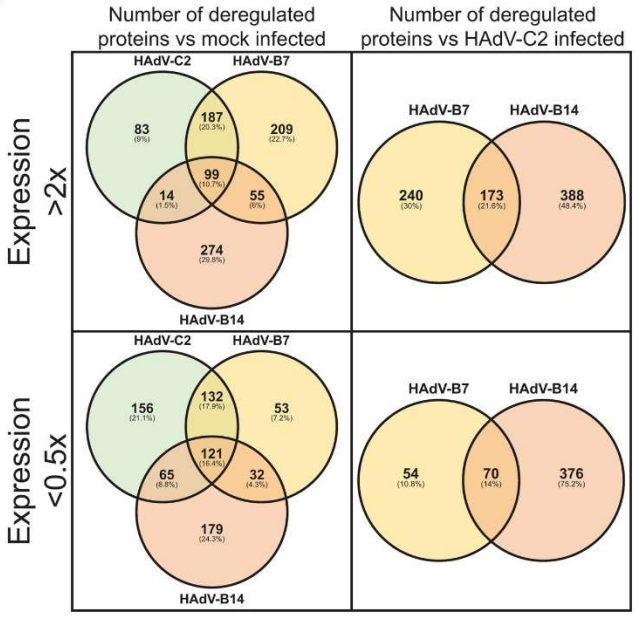


D

| | Fold Change from Mock Infection | | | Fold Change from HAdV-C2 | |
|---|---|---|---|---|---|
| Protein Name | HAdV-C2 | HAdV-B7 | HAdV-B14 | HAdV-B7 | HAdV-B14 |
| IFIT1 | 0.078 | 0.089 | 0.133 | 1.143 | 1.714 |
| IFIT2 | 0.143 | 0.071 | 0.143 | 0.500 | 1.000 |
| IFIT3 | 0.154 | 0.154 | 0.212 | 1.000 | 1.375 |
| OAS1 | 0.028 | 0.083 | 0.028 | 3.000 | 1.000 |
| OAS3 | 0.278 | 0.222 | 0.222 | 0.800 | 0.800 |
| STAT1 | 0.332 | 0.412 | 0.363 | 1.240 | 1.093 |
| STAT2 | 0.143 | 0.143 | 0.143 | 1.000 | 1.000 |
| IFIH1 | 0.056 | 0.056 | 0.167 | 1.000 | 3.000 |
| DDX58 | 0.033 | 0.033 | 0.033 | 1.000 | 1.000 |
| TRIM21 | 0.308 | 0.385 | 0.231 | 1.250 | 0.750 |

**Figure 4.27. Proteomic analysis of HAdV-B and C infections.** A549 cells were infected with HAdV-C2, HAdV-B7, HAdV-B14, or a mock infection as indicated, IFN-treated, and harvested. Protein was extracted and analyzed *via* 2D-LC-MS. (A) Results were broadly visualized *via* heat mapper software. Red indicates upregulation and blue represents downregulation. (B) Numbers of proteins up- and downregulated in HAdV-B and C as compared to uninfected control and HadV-B as compared to HAdV-C. (C) Venn diagrams showing overlap of proteins up- and downregulated in each condition. (D) Selection of notable ISGs and their levels of up- and downregulation.

| *Upregulated Biological Processes* | *Fold Enrichment in Indicated Strain* | | |
|---|---|---|---|
| ***HAdV-B7*** | ***C2*** | ***B7*** | ***B14*** |
| ***mRNA 5'-splice site recognition (GO:0000395)*** | NC | 14.75 | NC |
| ***mRNA 3'-splice site recognition (GO:0000389)*** | NC | 14.75 | NC |
| ***miRNA-mediated gene silencing by inhibition of translation (GO:0035278)*** | NC | 7.37 | NC |
| ***mRNA 3'-end processing (GO:0031124)*** | 4.82 | 6.51 | NC |
| ***rRNA transcription (GO:0009303)*** | NC | 6.45 | NC |
| ***multivesicular body organization (GO:0036257)*** | NC | 6.03 | NC |
| ***HAdV-B14*** | ***C2*** | ***B7*** | ***B14*** |
| ***positive regulation of mitochondrial RNA catabolic process (GO:0000962)*** | NC | NC | 26.17 |
| ***acetyl-CoA biosynthetic process (GO:0006085)*** | NC | NC | 13.08 |
| ***viral mRNA export from host cell nucleus (GO:0046784)*** | NC | NC | 13.08 |
| ***glutathione transport (GO:0034635)*** | NC | NC | 11.63 |
| ***tricarboxylic acid cycle (GO:0006099)*** | NC | NC | 10.31 |
| ***proton motive force-driven ATP synthesis (GO:0015986)*** | NC | NC | 8.6 |
| ***ribonucleoside triphosphate biosynthetic process (GO:0009201)*** | NC | NC | 6.6 |
| ***ATP metabolic process (GO:0046034)*** | NC | NC | 5.99 |
| ***nucleoside triphosphate metabolic process (GO:0009141)*** | NC | NC | 5.2 |
| ***HAdV-B7 and HAdV-B14*** | ***C2*** | ***B7*** | ***B14*** |
| ***transcription elongation-coupled chromatin remodeling (GO:0140673)*** | NC | 14.75 | 17.44 |
| ***regulation of RNA export from nucleus (GO:0046831)*** | NC | 11.06 | 13.08 |
| ***mRNA cis splicing, via spliceosome (GO:0045292)*** | NC | 9.22 | 10.9 |
| ***regulation of nucleobase-containing compound transport (GO:0032239)*** | NC | 8.85 | 10.47 |
| ***negative regulation of DNA-templated transcription, elongation (GO:0032785)*** | NC | 7.04 | 8.33 |

**Table 4.2. Notable biological processes upregulated in HAdV-B7 and HAdV-B14.** Biological process gene ontologies were generated from genes upregulated in HAdV species compared to uninfected control. Processes uniquely enriched more than five times in indicated strains were isolated, and pathways of interest are presented here. NC is short for no change. P-values associated with presented numbers are all less than 0.01.

| *Downregulated Biological Processes* | *Fold Enrichment in Indicated Strain* | | |
|---|---|---|---|
| ***HAdV-B7*** | ***C2*** | ***B7*** | ***B14*** |
| ***MDA-5 signaling pathway (GO:0039530)*** | NC | 22.29 | NC |
| ***response to type I interferon (GO:0034340)*** | 4.82 | 6.05 | 4.67 |
| ***negative regulation of viral genome replication (GO:0045071)*** | 4.64 | 5.84 | 4.5 |
| ***positive regulation of T cell mediated cytotoxicity (GO:0001916)*** | NC | 5.2 | NC |
| ***HAdV-B14*** | ***C2*** | ***B7*** | ***B14*** |
| ***ISG15-protein conjugation (GO:0032020)*** | NC | NC | 15.27 |
| ***somatic diversification of immune receptors via somatic mutation (GO:0002566)*** | NC | NC | 8.81 |
| ***negative regulation of NIK/NF-kappaB signaling (GO:1901223)*** | NC | NC | 5.73 |
| ***pyroptosis (GO:0070269)*** | NC | NC | 5.17 |
| ***HAdV-B7 and HAdV-B14*** | ***C2*** | ***B7*** | ***B14*** |
| ***negative regulation of protein dephosphorylation (GO:0035308)*** | 4.74 | 6.5 | 6.44 |
| ***ubiquitin-dependent protein catabolic process via the multivesicular body sorting pathway (GO:0043162)*** | 4.69 | 5.62 | 5.57 |
| ***cellular metabolic compound salvage (GO:0043094)*** | NC | 5.57 | 7.16 |

**Table 4.3. Notable biological processes downregulated in HAdV-B7 and HAdV-B14.** Biological process gene ontologies were generated from genes downregulated in HAdV species compared to uninfected control. Processes uniquely enriched more than five times in indicated strains were isolated, and pathways of interest are presented here. NC is short for no change. P-values associated with presented numbers are all less than 0.01.

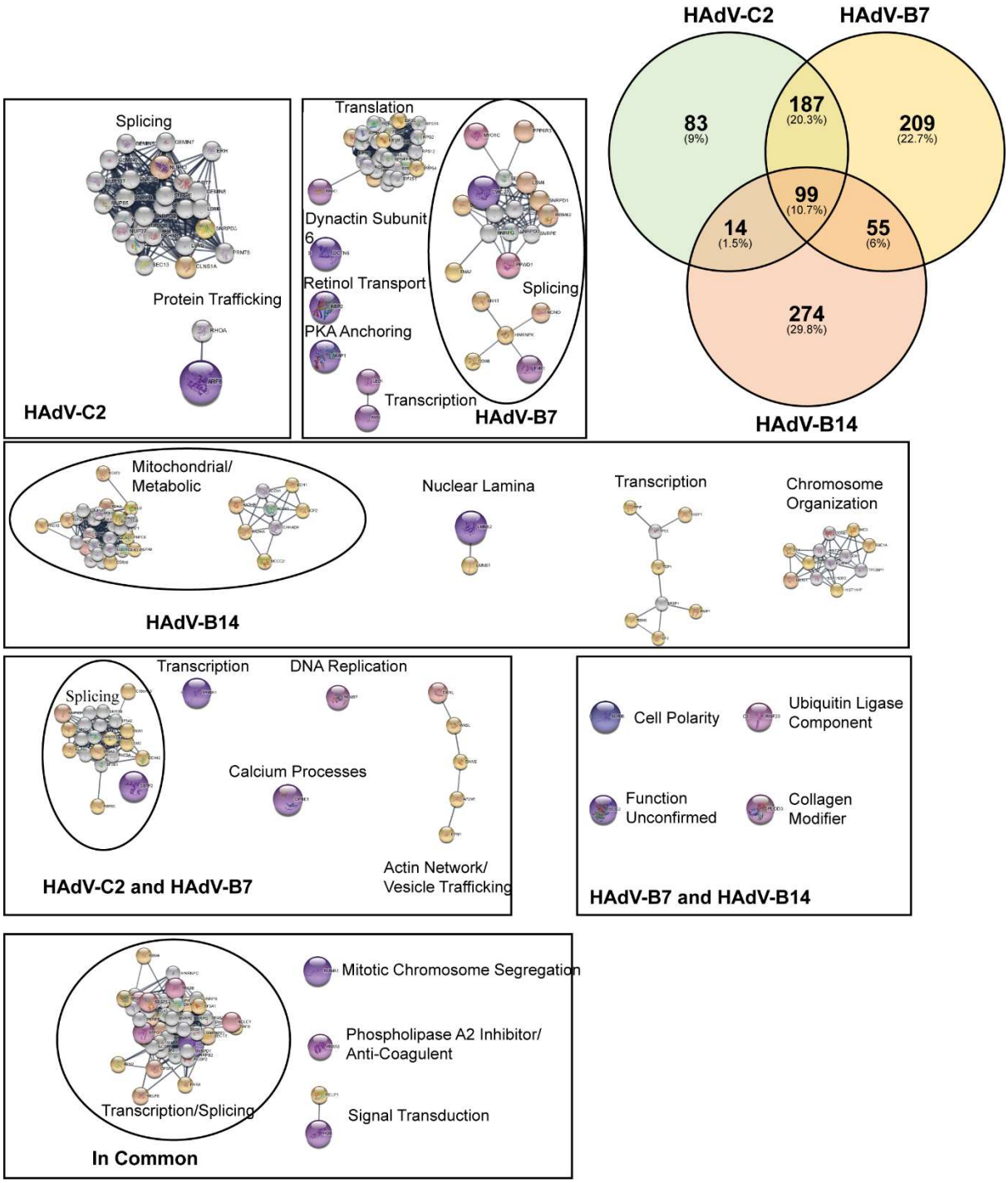


**Figure 4.28. Notable clusters of proteins upregulated in HAdV-infected compared to uninfected cells.** A549 cells were infected with HAdV-C2, HAdV-B7, HAdV-B14, or a mock infection, IFN-treated, and harvested. Protein was extracted and analyzed *via* 2D-LC-MS. Protein levels in each infected cell group were compared to those in uninfected cells, and notable proteins (fold change >2) were isolated and clustered in cytoscape. Circle size is proportional to magnitude of fold change, and grey circles were randomly added by Cytoscape to allow for broader clusters.

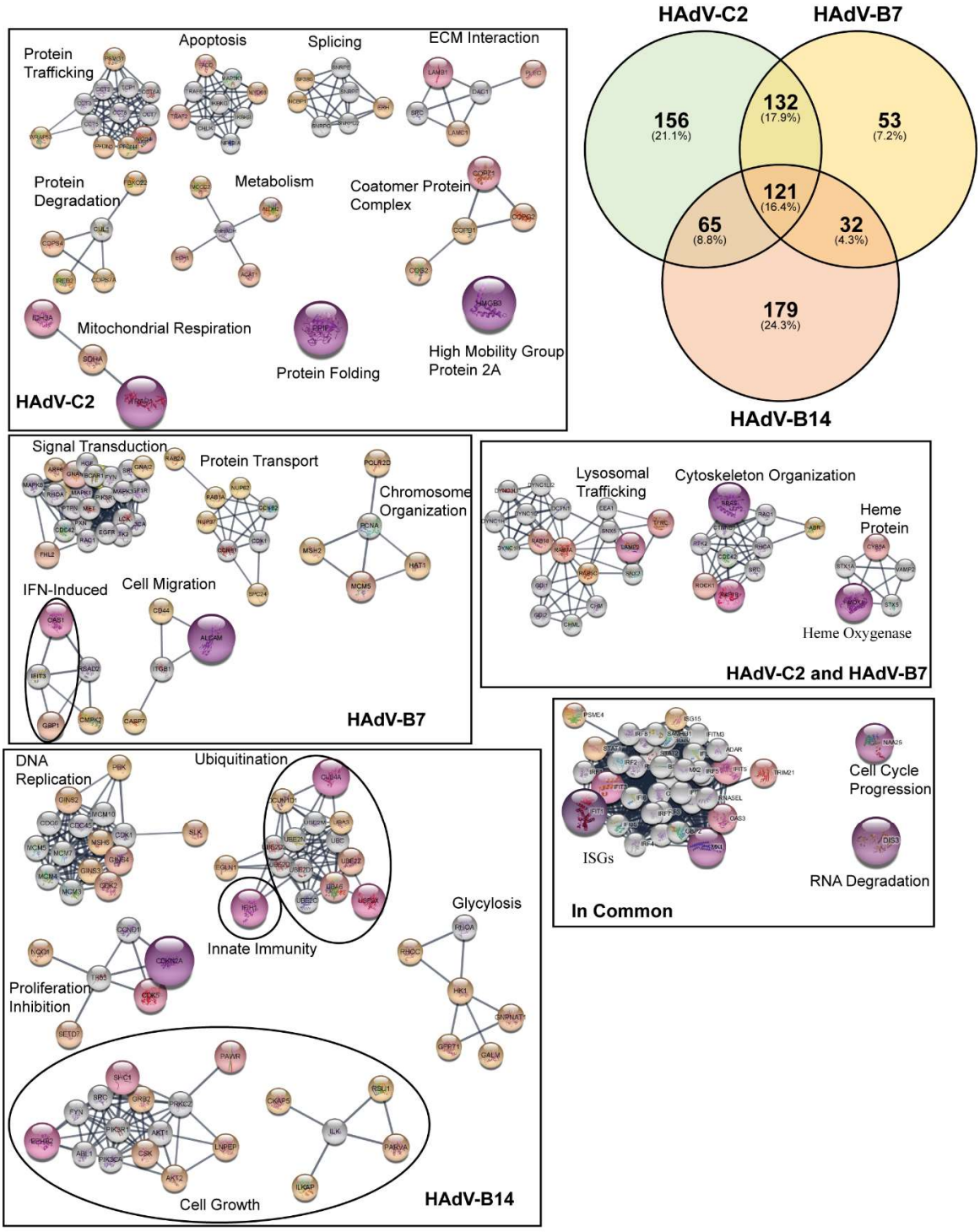


**Figure 4.29. Notable clusters of proteins downregulated in HAdV-infected compared to uninfected cells.** A549 cells were infected with HAdV-C2, HAdV-B7, HAdV-B14, or a mock infection, IFN-treated, and harvested. Protein was extracted and analyzed *via* 2D-LC-MS. Protein levels in each infected cell group were compared to those in uninfected cells, and notable proteins (fold change >2) were isolated and clustered in cytoscape. Circle size is proportional to magnitude of fold change, and grey circles were randomly added by Cytoscape to allow for broader clusters.

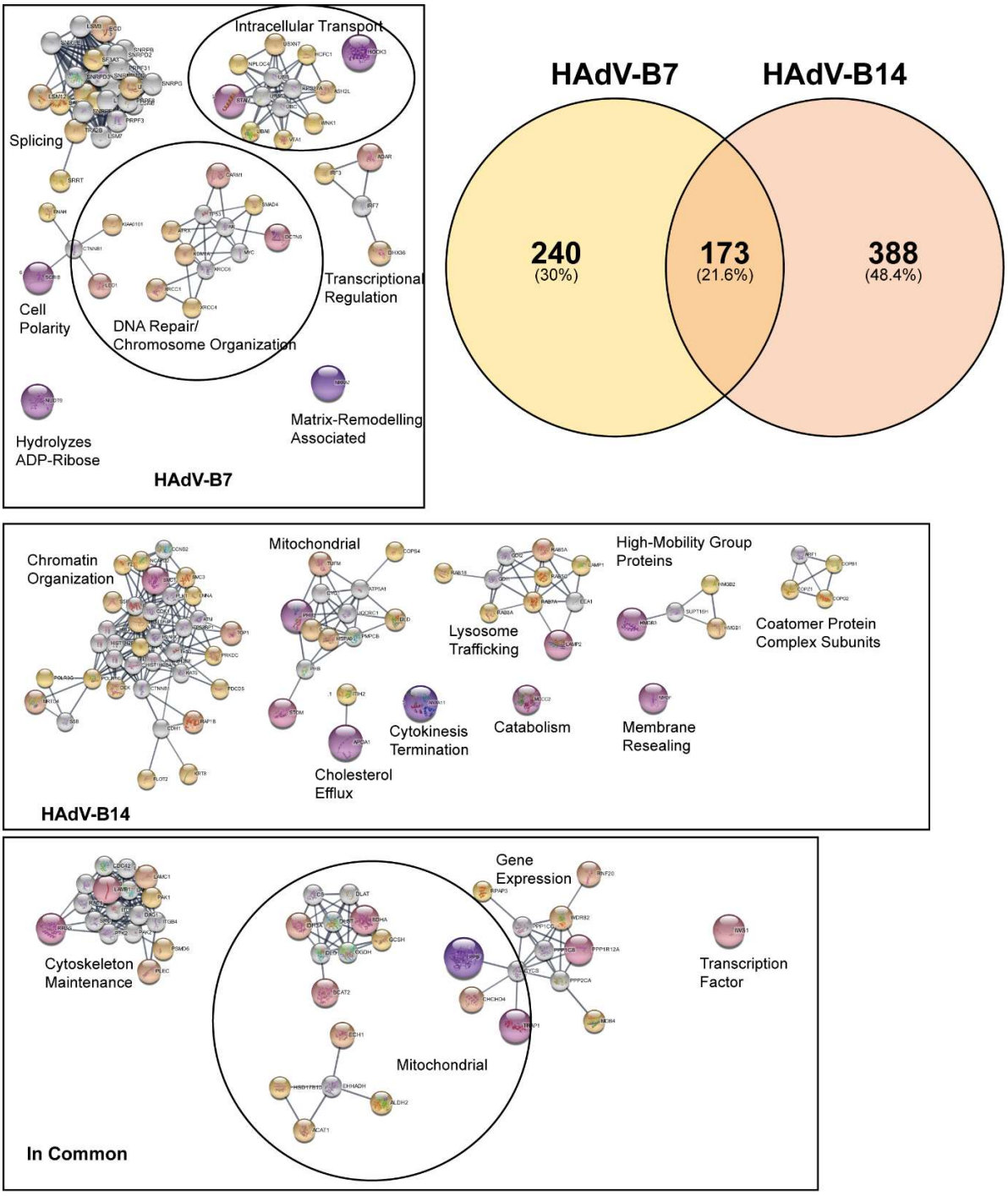


**Figure 4.30. Notable clusters of proteins upregulated in HAdV-B-infected compared to HAdV-C-infected cells.** A549 cells were infected with HAdV-C2, HAdV-B7, HAdV-B14, or a mock infection, IFN-treated, and harvested. Protein was extracted and analyzed *via* 2D-LC-MS. Protein levels in each HAdV-B-infected cell group were compared to those in HAdV-C-infected cells, and notable proteins (fold change >2) were isolated and clustered in cytoscape. Circle size is proportional to magnitude of fold change, and grey circles were randomly added by Cytoscape to allow for broader clusters.

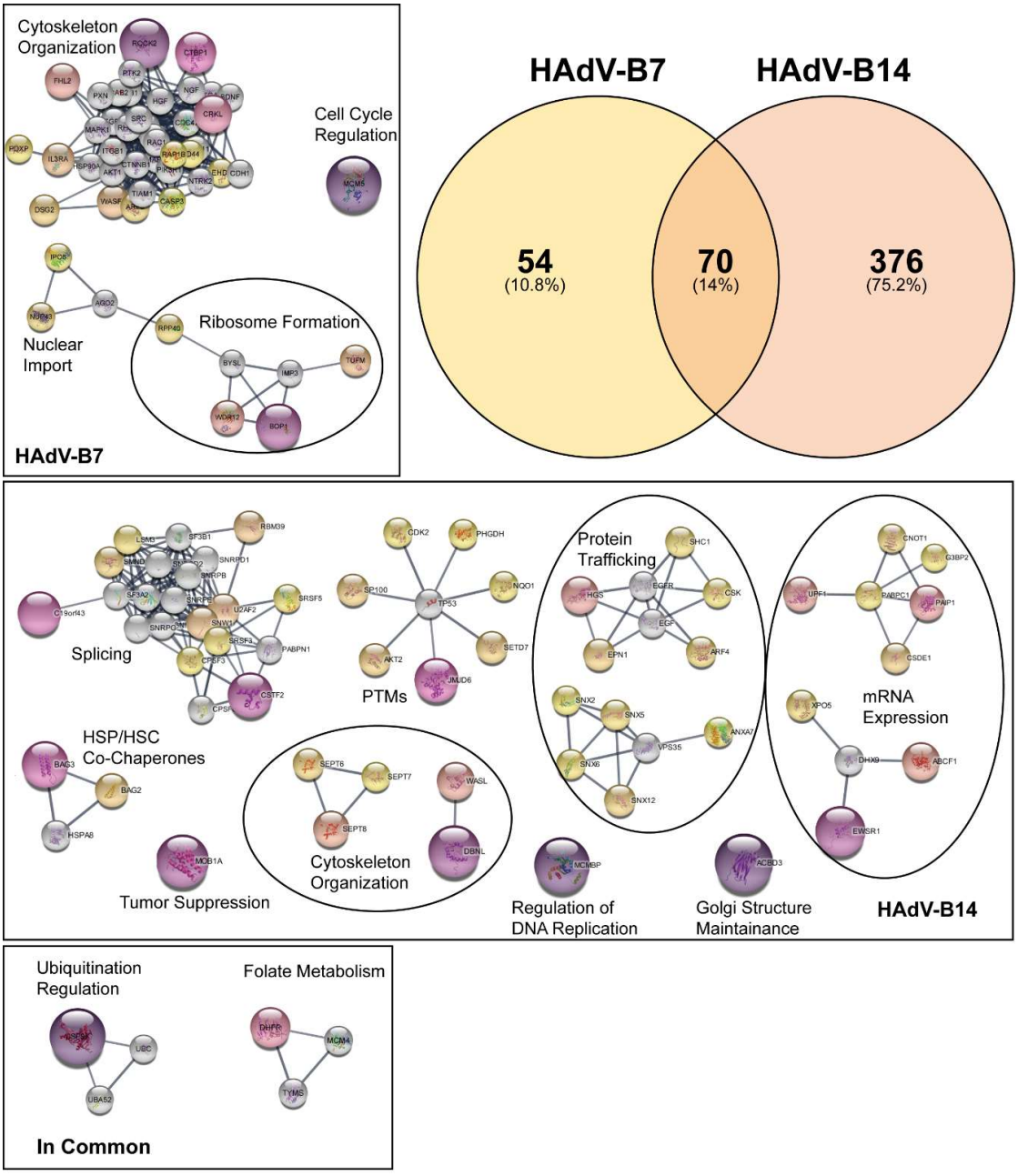


**Figure 4.31. Notable clusters of proteins downregulated in HAdV-B-infected compared to HAdV-C-infected cells.** A549 cells were infected with HAdV-C2, HAdV-B7, HAdV-B14, or a mock infection, IFN-treated, and harvested. Protein was extracted and analyzed *via* 2D-LC-MS. Protein levels in each HAdV-B-infected cell group were compared to those in HAdV-C-infected cells, and notable proteins (fold change >2) were isolated and clustered in cytoscape. Circle size is proportional to magnitude of fold change, and grey circles were randomly added by Cytoscape to allow for broader clusters.

## 5. Discussion

In these studies, I investigated HAdV from two angles, both related to its first-expressed protein: E1A. In the first, I examined how the splicing patterns and subcellular localization of E1A change depending on whether it is provided in *trans* or *cis*; and in the second, I followed up on a previous observation regarding a difference in the binding strength of E1A to RuvBL1 between HAdVs B and C. HAdV B's E1A-RuvBL1 interaction was weaker than that of HAdV-C, and as this interaction has been shown to be partially responsible for repression of host cell ISG expression[11], I sought to compare the effect of IFN stimulation on each of these two species.

### 5.1 Effects of in *trans* expression of E1A on the HAdV infection pathway compared to in *cis*.

Overall, the first study revealed a major difference in terms of E1A processing between wild type HAdV (type C5) and an E1A-null mutant (*dl*312) grown in a cell line providing E1A in *trans* (HEK-293). I observed a notable lack of the smallest three E1A isoforms (217R, 171R, and 55R; translated from the 11S, 10S, and 9S mRNA splice isoforms respectively) by means of direct observation of mRNA splice isoform levels by reverse transcriptase agarose gel electrophoresis (Fig. 3.1A), quantification of mRNA splice isoforms *via* qPCR (Fig. 3.4), and observation of protein isoform levels *via* western blot (Fig. 3.1B and Fig. 3.3C). It is worth noting that the qualitative results presented in Fig. 3.1A and the quantitative results presented in Fig. 3.4 seem to disagree on the levels of 12S and 13S E1A mRNA, and the reason for this is not completely clear. A possibility exists that this is due to issues with PCR efficiency, as the Fig. 3.1A PCR was performed using a global set of primers, while the primers used to generate Fig. 3.4 were unique to each individual isoform of E1A. As such, in Fig. 3.1A, it is possible that the small (later) isoforms were replicated more efficiently, reducing the accumulation of the larger isoforms. This may be further affected by even slight differences in RNA quality between samples.

I theorized that the lack of small E1A isoforms in *dl*312-infected cells may be due to differences in subcellular mRNA localization based on the gene's physical location within the cell. To confirm this, I performed fluorescent microscopy (Fig. 3.2) on cells tagged for HAdV DBP (to show the locations of viral replication centres) and E1A mRNA (*via* in-*situ* hybridization). As anticipated, HAdVs that provided their own E1A generated two distinct types of E1A mRNA clusters: one that co-localized to sites of viral replication (indicated by carats), and one that did not. These clusters in HAdV infections that did not provide their own E1A (*dl*312) only fell into one of these categories: their location was not related to the viral replication centres. The distribution of splicing factors within the nucleus is already known to be variable based on a multitude of factors, such as the cell's metabolic state, position in the cell cycle, differentiation state, and stress level, and each of these variations affects the identity and outcome of splicing targets[314]. My results suggest that during HAdV infection, splicing factor composition within viral replication centres is distinct from that found in the rest of the nucleoplasm, and that only these splicing conditions are capable of properly producing the smallest three E1A isoforms. The change to production of these isoforms is likely governed by the same mechanisms that drive the shift from early to late transcript expression of the viral genome[47], but it remains unclear why this change does not affect E1A mRNA that originates from the cellular genome. One possibility is that the sequestration and resultant titration of SR splicing factors that governs the shift in E1A splicing is not nucleus wide, but instead localized to viral replication centres. Another possibility is that viral splicing modulators such as E4orf4[169] and L4-33K[212] remain localized to these replication centres and play some role in regulating E1A splicing. More likely, the answer is some combination of the two. Other factors that may have some impact here include the specificity of the U1 snRNP, that when altered from its original site (downstream from E1A 12S 5' splice site), induces the

appearance of 10S and 11S E1A mRNA far earlier than normal in infection[48], and the level of E1A pre-mRNA itself, which is simply higher when provided in *cis* than when provided only in *trans* (Fig. 3.4). The question of which – or more likely which combination – of these factors is responsible for the observed difference between splicing of E1A from the viral genome and splicing of E1A provided by the host cell will need to be the subject of further research.

Given the relative lack of knowledge regarding the functions of these late E1A isoforms within the literature, I investigated the effects of their observed deficiency by several metrics: I directly measured viral growth *via* plaquing assay (Fig. 3.3A), observed the overall efficiency of the infection by imaging for differences in CPE (Fig. 3.3B), and measured the expression levels of VA-RNAs, the other early viral genes, and a selection of late viral genes (Fig. 3.5, Fig. 3.6, and Fig. 3.7 respectively) *via* qPCR. By all metrics measured, strictly in *trans* provision of E1A resulted in a worse overall performance compared to wild type. Viral growth was slowed, being reduced by nearly 100 times at 24 hours post infection, and never quite catching up, ending up roughly two-fold lower. This was in stark contrast to a previous report that showed roughly equal growth between wild type and *dl*312 HAdVs in 293 cells[285]. I cannot be sure of the source of this discrepancy, but as the previous report did not include standard deviation or indeed any statistics at all, the possibility exists that it was a one-time observation. In addition to lower overall growth, we observed a delay in onset of CPE, and across the board lower viral gene expression, with the exception of E1B. This implies one of two things: either the expression of E1B is only affected by the early (large) E1A isoforms, or the E1B gene already present in 293 cells expresses at a high enough level to mask any changes to E1B expressed from the viral genome. DBP, while repressed in terms of mRNA, seemed about equal between the two in protein levels (Fig. 3.3C), though interestingly the DBP from *dl*312 expressed both at its normal size and as a collection of lower

molecular weight species. I remain unsure of the identities of these small DBP species, but they have been observed before, late in infection[315]. The most likely possibilities are that they are either cleavage products of proteases, possibly conditionally expressed viral proteases, or that they result from alternative translational initiation or splicing. A previous study identified two smaller DBP species as the result of low-level treatment of DBP with chymotrypsin[316], though the species observed there (44 kDa and 26 kDa) were different than those observed here (roughly 63 kDa and 48 kDa). It is worth noting that I saw 9S E1A mRNA overtake the others as the dominant species at the 24 hour timepoint (Fig. 3.1A and Fig. 3.4), much earlier than previously reported in normal lung fibroblasts[43,46].

Levels of E1A, overall, were higher in wild type-infected cells, which is to be expected given the increased copy number of the gene. This difference in total amount is likely responsible for the difference in E1A levels over time between the two observable in Fig. 3.1A, wherein wild type and *dl*309 HAdVs both show clearly visible E1A for the whole period of the experiment, whereas E1A levels start elevated in the *dl*312 infection, but are indistinguishable from mock by 72 hours post infection. This difference in the amount of E1A present may explain some of the differences in viral gene expression, but it cannot explain those present at 16 hours post infection, when 12S and 13S mRNA levels are roughly the same between the two viruses (Fig. 3.4). Mutant HAdVs expressing only 10S or 11S E1A do not replicate in HeLa cells, and are transformation-deficient with either E1B or activated Ras[44]. Both of these transcripts (as well as 9S) produce proteins missing residues 27 to 98, discarding a large number of N-terminal binding sites, including those for p300/CBP and pRb[315]. These binding partners are the primary mechanisms by which E1A transforms the host cell[2], and as such it is unsurprising that a HAdV expressing only E1A that does not bind these proteins efficiently would exhibit these deficiencies.

To confirm the relationship between the source of E1A and performance of the virus, I created a pair of cell lines based on 293 cells: one expressing all three of the smaller E1A isoforms and one expressing only the smallest two (Fig. 3.8; 293 9S/10S/11S and 293 9S/10S respectively), in addition to both expressing 12S and 13S mRNAs and their derived proteins. I compared the growth of HAdV *dl*312 in standard 293 cells to each of these manufactured cell lines and found that complementation of all three smaller E1A isoforms rescued the growth phenotype of the virus, increasing the final viral titre by nearly twofold. Complementation of only the 9S and 10S isoforms, however, had no observable effect. Whether this indicates that all three isoforms are necessary for proper viral replication, or just 11S/217R, remains to be seen. Indeed, 11S is notable among E1A isoforms, as it is the only isoform other than the largest that maintains the CR3 region, which contains a binding site for host proteins MED23[55] and p300/CBP[68]. This interaction is indispensable for E1A 289R's role in upregulating expression of both E1A itself and the other early viral genes[54,55], a role which is necessary for proper viral replication. Indeed, it is possible that these small E1A isoforms are produced late as a means of maintaining the transactivation state of other viral genes. It has been shown that E1A 243R, *via* its N-terminus, is able to titrate away the transactivators on which E1A 289R relies to maintain viral gene expression, while not able to use them in this way due to its lack of a CR3 region[58,68]. The 9S and 10S-derived species (55R and 171R) also do not contain residues 27 to 98, meaning they are unlikely to titrate away transactivation partners from E1A 217R. In short, E1A 217R may function as a late-stage replacement for E1A 289R, for when its role as a viral transactivator is still necessary, but its role in host cell transformation becomes less so. It is worth noting that levels of E1A 289R are generally lower than those of E1A 243R, and that they fall off more quickly as well[46]. As such, without E1A 217R to take 289R's place due to improper splicing, viral gene expression may be reduced overall.

Finally, it is worth noting that when I complemented for E1As 55R, 171R, and 217R (Fig. 3.8), while *dl*312 growth in the 9S/10S/11S cell line did eventually overtake and surpass standard 293s, at the 24-hour timepoint, it was observably (though not significantly) lower. Indeed, at the same time, *dl*312 growth in the 9S/10S cell line was significantly lower, and only caught up over the course of the infection. Levels of DBP were universally lower in these complementing cell lines as well, most prominently at 24 hours post-infection, but never quite catching up. This implies that the virus "saves" these isoforms for later for a good reason: that early on they are detrimental to the process of infection, which can be recovered from in cell culture, but which may prove insurmountable to the virus in a real infection scenario, giving the immune system the opportunity to turn the tables and halt the infection entirely. The reduced levels of DBP, at the very least, suggest that these isoforms suppress E2 expression. As E2 proteins are critical to replication of the viral genome, it would make sense not to express these E1A isoforms at scale until viral DNA synthesis is well underway.

Within the field of gene therapy by way of viral vectors, HAdV remains the most commonly used backbone, occupying roughly 50% of all clinical trials[3]. A number of COVID-19 vaccines made use of HAdV vectors to express the spike protein of SARS-CoV-2[227–230], and other diseases that have been treated with HAdV-based vaccines include Ebola virus[234], Zika virus[235], HIV[236], and influenza[237,238]. The specifics of constructing these types of vectors vary depending on the generation of backbone being used (first, second, or helper-dependant[3]), but they all have one thing in common, in that growing up the virus always requires supplementation of the E1 region, which is removed for the dual purpose of making room for the inserted gene and preventing the virus from replicating outside of a specific cell type. The most commonly used cell line for this purpose is 293 cells, which have been a staple of HAdV vector research since they were originally

developed in the 1970s[10]. Based on human embryonic kidney cells, this line has the first 4,344 nucleotides of the HAdV-C5 genome integrated into the pregnancy-specific β-1-glycoprotein 4 (PSG4) gene on chromosome 19[317]. Similar cell lines have since been generated, such as 911[221], PER.C6[318], and SL0003[319], to limit the number of viral nucleotides present outside of the E1 region, thus lowering the chance of a recombination event generating replicating HAdV. My work shows that complementation of the E1 region to E1-deficient HAdVs results in deficiencies in expression of the smallest three isoforms of E1A, which leads to inefficient growth. I showed this specifically in 293 cells, but it is likely true in most E1-complementing cell lines, as while the base cell line, insertion site, and surrounding nucleotides may change, each of these cell lines are functionally the same: the E1 region of the HAdV genome is expressed from the genome of the cell line. Indeed, it would be interesting to perform a similar study on the splicing of the E1B transcription unit (primarily expressed to prevent apoptosis of the cell[4]), which is also expressed in 293 cells, and spliced to produce multiple protein products.

My findings have implications for anyone using 293 cells, whether for research in general or for production of therapeutic viral constructs, proving that E1-deficient HAdV mutants can still be grown with greater efficiency, by supplementing all E1A isoforms in the cell line.

### 5.2 Molecular Mechanisms of Innate Immune Suppression by HAdV Species B

The second study revealed a sizable difference between species B and C HAdV in terms of ISG suppression. This finding began with the observation that the E1A of species B HAdVs had a weaker binding affinity for the host cell ATPase RuvBL1 (Fig. 4.10). This was supported by sequence alignment (Fig. 4.9A) of the E1A genes of three representative HAdVs: C2, B7, and B14, which showed mostly similarity between the three, but revealed two sizable deletions conserved between types B7 and B14, within or near the regions known to be involved with RuvBL1 binding.

RuvBL1 has been previously shown to be involved in the process of ISG expression as part of the IFN response pathway[90], and has been previously found by the Pelka lab to be used by E1A as part of HAdV's ISG suppression strategy (in HAdV-C)[11]. Such a difference would logically imply that species B HAdVs are more susceptible to IFN than their species C counterparts. However, this would contradict clinical evidence that species B HAdV is significantly more dangerous than species C[9,20,31–33].

To investigate this, I performed a direct growth comparison of species B and C HAdVs in cells treated with IFN (Fig. 4.1) and found that species B grew far better than species C – species C's growth was reduced roughly five-fold while type B14's was reduced by only one fifth, and type B7's appeared completely unaffected. This was interesting, given that previous reports had shown species B HAdVs to be sensitive to IFNs β and γ[290–292]. It is worth noting however that in each study that used type I IFN, the only species B representative was HAdV-B3. In the study that did include HAdV-B7, only type II IFN (γ) was used. IFNs serve as a front-line defence against viral invaders[320], and as such, it is in any virus's best interest to target this pathway as shortly following the entry step as possible. This trend has already been observed in HAdV-C, which expresses its VA-RNA (another mechanism of innate immune suppression[184–186,189,190]) within three hours of initial infection[43].

The presence of interferon did not have any effect on the development of cytopathic effect (Fig. 4.2), nor on viral gene or protein expression (Fig. 4.3 and Fig. 4.4), or on viral entry into the host cell (Fig. 4.5), suggesting host-intrinsic inhibition that does not affect viral gene regulation. HAdV-B14 only was shown to exhibit a distinctive large plaque phenotype when subjected to a plaquing assay with IFN present in its overlay media (Fig. 4.6), with further experimentation (not shown) revealing this to be a result of premature apoptosis of the infected cells in response to IFN.

While this observation was interesting, it was not ultimately related to the growth differences between the species, and so was not pursued. That said, it remains a topic warranting further research. The resistance of these species to IFN treatment, and the presence of this large plaque phenotype may have clinical implications, as IFN has a history of use in treating viral infection[243].

RT-qPCR revealed that the expression of a representative suite of ISGs in infected cells varied widely depending on the infecting agent (Fig. 4.7). While they were mostly expressed at a level similar to, and sometimes exceeding, that seen in uninfected cells during HAdV-C2 infection, HAdVs B7 and B14 universally reduced the presence of these genes, by anywhere from two- to eight-fold. This pattern was observed not only in transformed cells (A549s), but also in primary lung fibroblasts (IMR-90s) (Fig. 4.8). There are over 300 ISGs, and the overall effect of their expression is to reduce the suitability of the host cell for viral replication, targeting nearly every stage of the viral life cycle[260]. Given this, it is no wonder that HAdVs better at suppressing them grow better in the presence of IFN.

To investigate the mechanisms behind HAdV-B's ISG suppression, I performed a number of immunoprecipitations. In addition to the initial results regarding E1A's binding affinity to RuvBL1, Fig. 4.10 also shows differences in binding affinity for RuvBL2, a common binding partner of RuvBL1. Interestingly, the pattern for RuvBL2 is near-opposite to that of RuvBL1. Whereas we see a clear hierarchy of E1A binding strength in RuvBL1, with HAdV-C2 at the top, B14 in the middle, and B7 at the bottom, the E1A-RuvBL2 affinity is weakest in HAdV-C2 and roughly equal between both species B representatives. In another IP, where the cells were transfected for HA-tagged RuvBL1 prior to infection and cross-linked with formaldehyde immediately before harvest to maintain any protein complexes in the cell lysate (Fig. 4.11), I observed a conspicuous collection of HMW complexes ranging from 130-170 kDa, which were

most numerous in cells infected with HAdV-B7, then HAdV-B14, and finally HAdV-C5. They did not appear to be present in mock-infected cells, but this is inconclusive as baseline HA-RuvBL1 levels were quite a bit lower in in these cells than any of the others, likely as a result of the CMV promoter in the transfected vector being activated by E1A protein expressed by the infecting HAdVs, when they were present. Nevertheless, when this experiment was repeated precipitating for endogenous RuvBL1 (Fig. 4.12), the overall pattern was observed again, albeit much weaker likely both on account of less RuvBL1 to detect and weaker binding strength of the antibody (affecting both precipitation efficiency and detection strength), but with a noticeable band present in mock-infected cells as well. The identity of this complex is uncertain. RuvBL1 is known to form a dimer with RuvBL2, as well as a hexamer with itself[321], but these structures would be too small and too large respectively to be any of the complexes observed here. RuvBL1 is also known to be a component of a number of chromatin remodeling complexes, such as TIP60[89] and INO80[322], and chaperone complexes such as HSP90[323], but these are also too large to be the observed complex. It has been shown that RuvBL1's ISG-expressing activity is likely performed as part of a yet-unidentified complex[90], which may be the same that we observe here. This seems unlikely however, as increased quantities of this complex would more likely result in enhancement of ISG expression, rather than reduction.

Another pair of immunoprecipitations (Fig. 4.13 and Fig. 4.25) revealed that HAdV infection results in a loss of interaction between RuvBL1 and RPII, and between RPII and STAT2, further linking RuvBL1 to ISG expression, though this was not limited to species B HAdVs, as HAdV-C2 was just as capable of interfering with these interactions. The Fig. 4.13 IP also revealed that HAdVs-C2 and B7 stimulate a stronger interaction between RuvBLs 1 and 2, though surprisingly not HAdV-B14.

Further investigation (Fig. 4.14) revealed that the interaction between STAT2 and RuvBL1 following IFN treatment, weak as it may be, is broken completely during infection with species B HAdV. This interaction appears unaffected compared to mock during HAdV-C infection, but it is important to note that this experiment was carried out *via* immunoprecipitation of HA-tagged RuvBL1 in a similar manner to that used in Fig. 4.11. As was the case there, the CMV promoter on the transfected plasmid was activated by HAdV infection, resulting in elevated RuvBL1 signal in all infected cells. It can be assumed that the appearance of equal STAT2-RuvBL1 interaction in HAdV-C infected cells compared to mock, then, actually represents a weakened, but still present interaction. In contrast, tagged RuvBL1 expression seemed even stronger in the species B-infected cells than in species C, and yet STAT2 interaction was not detectable at all. As such, it can be concluded that species C HAdV weakens the interaction between STAT2 and RuvBL1, while species B HAdV severs it completely. STAT2 is one of three components of the ISGF3 complex (along with STAT1 and IRF9), and is directly recruited to ISG promoters as a result of IFN stimulation[258]. It is known that RuvBL1 has a role here as well, though what that role is remains unclear[90]. That said, the species B-based disruption of this interaction accompanying reduced ISG expression implies the two observations to be related, at the site of the ISG promoters themselves.

To confirm this, I performed a ChIP assay comparing recruitment of STAT2 and RNA polymerase II to the promoter regions of three representative ISGs (IFI6, IFIT1, OAS2) in HAdV species B and C infections (Fig. 4.15). Following the same pattern as observed in STAT2-RuvBL1 interaction, recruitment of STAT2 and RPII to ISG promoters was highest in uninfected cells, reduced in HAdV-C-infected cells, and effectively non-existent in HAdV-B-infected cells. This pattern was also observed in primary lung fibroblasts (Fig. 4.16).

A possible explanation for reduction of STAT2 recruitment could simply be that species B HAdVs bring about an overall reduction in the total amount of STAT2 in the cell, possibly *via* ubiquitin-mediated proteasomal degradation, as has been previously reported[307,308]. I investigated this by precipitating STAT2 out of cells previously transfected with tagged ubiquitin, and then blotting for the ubiquitin tag (Fig. 4.18). This revealed that not only is STAT2 not more heavily ubiquitinated in species B-infected cells, it is actually significantly less so, seemingly against the virus's own best interest. As expected, considering that ubiquitination of STAT2 triggers proteasomal degradation, levels of STAT2 are noticeably higher in species B-infected cells, when it is less heavily ubiquitinated. Another possibility may be related to an earlier study, which revealed that HAdV-C5 is able to sequester STAT1 to viral replication centres[289], likely as another method of ISG suppression. I performed IF to compare intracellular localization of STAT1 and STAT2 in cells infected with HAdVs C2, B7, and B14, finding very little in terms of difference between any of these and uninfected cells (Fig. 4.24). Close examination suggests that there may be more nuclear STATs in infected cells, but there is no observable difference in this regard between species B and C.

Interestingly, recruitment of RuvBL1 to ISG promoter regions (Fig. 4.17) was universally reduced to background in most cases, implying that all investigated HAdV species are removing RuvBL1 from its intended place at the ISG promoters, but only HAdV-B is preventing its interaction with STAT2, implying a fundamental difference in the approach taken by these two species toward ISG suppression.

This was confirmed by further results obtained from immunofluorescent analysis of the subcellular localization of RuvBL1 and 2 in cells infected with species B or C HAdVs (Fig. 4.22). Here, I observed three distinct phenotypes of RuvBL1/2 localization: nuclear, somewhat nuclear,

and nucleocytoplasmic. The nuclear phenotype of both RuvBL1 and 2 was the most commonly observed in HAdV-C-infected cells, whereas the somewhat nuclear and nucleocytoplasmic phenotypes were more common for species B. This implies that while species C is actively recruiting RuvBL1/2 to the nucleus for ISG suppression as previously reported[11], species B is at least not doing so as strongly, reinforcing the theory that these viruses have some alternate mechanism for ISG suppression, and that their use of RuvBL1/2 here only goes as far as keeping them out of the nucleus. This phenotype was observed more strongly when E1A was provided alone by transfection, rather than as part of an infection (Fig. 4.23). Here, the nuclear RuvBL1/2 phenotype was near-exclusive to species C E1A, and the nucleocytoplasmic phenotype was present in nearly all species B E1A-transfected and untransfected cells. STAT1/2 localization was not visibly affected by HAdV (Fig. 4.24).

RNAi-based knockdowns (Fig. 4.21) corroborated the differences between species B and C further. Knockdown of RuvBL1 and RuvBL2 (Fig. 4.21A) had a significant effect on HAdV-C ISG suppression, reducing its effectiveness by up to sixfold. This was in line with previous observations[11], but the effect on HAdV-B was different. ISG levels were nearly unaffected by the presence or absence of RuvBL1 in either species, with a few limited exceptions in the form of IFI6 and OAS1, which were not as strongly repressed by HAdV-B in the absence of RuvBL2, only. IFIT1 and IFIT2 however saw no such difference at all. It can be concluded, then, that species B HAdV prevents ISG expression in a RuvBL1/2-independent manner. The question remains then, by what means do these HAdVs prevent ISG expression?

E1A's role in innate immune suppression is not a new discovery, and a 2017 paper showed that species C E1A represses IFN-independent ISG expression in a manner dependent on the presence of three specific interaction partners, each binding in the CR4 region. These proteins are

FoxK1/2, DCAF7, and CtBP[82], and I theorized that these interactions may be more effective at innate immune suppression in species B HAdV than in species C. To test this, I measured levels of ISG expression *via* qPCR in IFN-treated cells infected with species B or C HAdVs in the presence or absence of DCAF7, FoxK1, and FoxK2 (Fig. 4.21B and Fig. 4.21C). This revealed what appears to be a species-specific dependence on a single binding partner for each species B type measured. The absence of DCAF7 (4.21B) had little to no effect on HAdV-C ISG suppression, nor on that of HAdV-B14, but its effect on HAdV-B7, while not as pronounced as that of RuvBL1/2 on HAdV-C, was significant and observable. ISG level ratios between the presence and absence of DCAF7 varied wildly based on the ISG in question, with IFIT2 expression increasing over tenfold compared to control-treated cells, but with expression of IFI6 barely changing at all. The absence of FoxK1, FoxK2, or both (4.21C) had a similar effect for HAdV-B14. Once again, the effect was the weakest for IFI6 (though a slight significant difference was present this time, with expression in B14-infected cells increasing over mock when only FoxK1 was knocked down), but was undeniable for all others. Knockdown of both FoxK1 and FoxK2 did not have the strongest effect on any ISG. Instead, knockdown of FoxK2 alone seemed to show the strongest effect, topping out with IFIT2, where its reduction (alone) increased expression by roughly tenfold. This is likely a fluke however, as the most common pattern had the effect of all three knockdowns within one another's standard deviations. From this, it can be concluded that these host protein interactions, which seem minor in scale and functionally redundant in species C HAdV, are significantly more important avenues of ISG suppression in species B. It is worth noting, however, that the effects of FoxK knockdown may be indirect results of the protein's role in STAT1/2 activation[324], rather than a direct influence on HAdV-B14.

There is yet more work to be done on the mechanisms by which HAdV-Bs make use of DCAF7 and FoxK1 and 2. This question is complicated, however, by another IP (Fig. 4.21D), precipitating E1A and blotting for FoxK1/2 and DCAF7. This revealed that while HAdV-C E1A binds quite well to all three proteins, as was previously understood, HAdV-B E1A (7 and 14) shows very little apparent binding affinity, if any at all. This makes sense for the FoxK proteins, as species B E1A is missing its binding site for them, but is quite puzzling for DCAF7 whose binding site from peptides 202-227[91] is conserved between the three (observable in Fig. 4.9). Regardless, this lack of binding affinity raises the possibility that these proteins are being made use of by a viral protein other than E1A.

Indeed, another cross-linked IP performed in cells transfected for species B and C E1A (Fig. 4.26), rather than infected, revealed that generation of the previously observed HMW RuvBL1 complex does not appear to be caused by E1A. As a matter of fact, the presence of only E1A seemed to reduce the amount of RuvBL1 in the complex, as the cells transfected with only HA-RuvBL1, without E1A, showed by far the most of these bands out of the three tested. If anything, species B E1A may prevent formation of this complex more efficiently than species C, as the species B lane may contain slightly less HMW RuvBL1 than the species C lane, though this difference is minor enough that it could also be a result of slight variations in transfection efficiency.

To summarize, I observed that HAdV-B was more resistant to the effects of interferon on viral replication than HAdV-C, as what appeared to be a result of its enhanced ability to suppress ISGs. This was the result of its ability to seemingly completely prevent localization of STAT2/ISGF3 to ISG promoters, preventing their transcription. I already knew from previous work that RuvBL1 was used by HAdV-C E1A to suppress ISG activation[11], but I observed here that this

interaction was much weaker in species B. A high molecular weight complex containing RuvBL1 was observed at higher quantities in species B-infected cells than species C, following a hierarchy inverse to the binding strength of E1A to RuvBL1 (i.e. RuvBL1 and E1A bound most strongly with HAdV-C where the HMW complex was least present, and bound most weakly with HAdV-B where the complex was most present). I also saw that HAdV-C infection resulted in near-total localization of RuvBL1 to the nucleus, from its standard nucleocytoplasmic distribution, but that HAdV-B infection did not completely have this effect. Finally, I saw that transfection of E1A alone is not enough to generate the HMW complex, implying it to be the result of another section of the viral genome entirely. Finally, the absence of different host cell proteins affects the ability of different HAdV types to repress ISGs. RuvBL1/2 interferes with HAdV-C2, DCAF7 interferes with HAdV-B7, and FoxK1/2 interferes with HAdV-B14.

Two possible explanations make sense of these observations. In both, it can be assumed that the two HAdV-Bs observed have a fundamentally different method of ISG suppression than that of HAdV-C, the question is exactly what they do with RuvBL1. The first possible explanation is that the HMW RuvBL1 complex observed is the same one theorized to exist by Gnatovskiy et. al.[90] as part of its role in expression of type I ISGs. It may follow that HAdV-Bs prevent ISGF3 assembly/nuclear localization without intentionally touching RuvBL1 at all, resulting in a negative feedback loop overproducing the unknown ISG expression helper complex in the absence of any ISGF3 to help. This would also explain why the E1A-only cross-linked IP showed more of this complex in untransfected cells, rather than less: it would make sense that without any viral interference, IFN stimulation would result in higher levels of complex formation. This explanation is not perfect, however. RuvBL2 was also found to be necessary to the ISG helper complex, and as such is should follow that HAdV-B E1A-RuvBL2 interaction should follow the same pattern as

E1A-RuvBL1 interaction, but it does not. HAdV-B E1A binds more strongly to RuvBL2, but less strongly to RuvBL1 than HAdV-C E1A, which implies, at the very least, that something different is being done with each. It is also worth noting that we were unable to show RuvBL2 as a component of the HMW complex (data not shown), despite its confirmed involvement in ISG expression[90]. In the other explanation, RuvBL1 is still not the primary means by which HAdV-B prevents ISG expression, but the virus still interacts with it, only to sequester it away and prevent it from aiding in ISG expression. In this explanation, the HMW complex is not any naturally occurring host cell assembly, but is instead assembled by the virus as a way of preventing nuclear localization of RuvBL1. This theory is opposed by fewer observations than the first, the only case being the appearance of HMW complex in the non-E1A-transfected lane of Fig. 4.26. It is unclear why this complex appeared in any sizable quantities without the presence of any viral agents to instigate it. That said, all bands observed in this figure were relatively weak, and it is entirely possible that this sequestration complex is a naturally occurring feature of the cell that is only amplified by the virus. Perhaps the complex normally forms transiently, and the virus adds some factor that prevents it from disassembling, for example. It would not be the first time that a HAdV species was shown to interfere with the function of a cellular protein by sequestering it away, as such a strategy of sub-cellular redistribution has previously been observed for Nek9[313,325], Ku70[312], DREF[326], FUBP1[311], and PKA[327].

Regardless of the exact mechanism, it is very interesting to note that E1A does not appear to be involved in any of the phenotypes observed. E1A does not increase appearance of HMW RuvBL1 (Fig. 4.26), and species B E1A does not appear to bind to either of the host proteins whose absence prevents these viruses from suppressing ISGs, meaning that it is likely some other viral protein making use of them (Fig. 4.21). The exact identity of the ISG-suppressing protein in species

B remains to be determined. One possibility is an unclassified ORF exclusive to HAdV-B7 (observable as a region of localized total non-homology in the E3 alignment section of Fig. 4.9B), which predictive software has calculated to produce a transmembrane protein. That said, this can only work as an explanation for HAdV-B7, as this ORF is not present in the genome of HAdV-B14. Indeed, the whole of the E3 region is suspect, it being almost entirely dedicated to immune suppression in all HAdV types[4]. The role of the E3 region, as well as the E4 region in HAdV-B ISG suppression are prime targets for further study.

### 5.3 Proteomic Comparison of Cells Infected with HAdVs C2, B7, and B14

One key takeaway from this research was the level of difference even between two HAdVs of the same species (B7 and B14). Though similar in terms of overall IFN resistance, they consistently expressed phenotypes just as different from one another as from the HAdV-C2 to which they were being compared. Their overall growth yields were orders of magnitude apart (Fig. 4.1), their CPE phenotypes were clearly distinct (HAdV-B14-infected cells floated off in much smaller clumps than HAdV-B7 – Fig. 4.2A), and as discussed earlier, despite their commonalities in IFN resistance, it was ultimately knockdown of two different proteins that interfered with this resistance (Fig. 4.21). The level of distinction between the two is best illustrated in the final set of figures presented here (Fig. 4.27 through Fig. 4.31 and tables 4.2 and 4.3), an overall proteomic analysis of cells infected with HAdVs C2, B7, and B14, and treated with IFN.

While this study did not turn up useful results in the way of IFN resistance, it did reveal that HAdV-B7 and HAdV-B14 were at least as different from each other as they each were from HAdV-C2. In Fig. 4.27C, we see that the number of proteins significantly up- or downregulated in exclusively in HAdV-B14 always greatly exceeds those in common with one or both of the other species. This is not true for HAdV-B7, sending the message that HAdVs C2 and B7 may have more in common

with one another than HAdVs B7 and B14. Gene ontologies revealed that the two activate and deactivate many host cell pathways completely independently of one another. For example, table 4.2 predicts that HAdV-B14, and HAdV-B14 alone, is particularly good at activating a variety of energy-producing metabolic pathways, likely to support its own replication. This would explain the overall higher levels of growth observed in Fig. 4.1. Meanwhile, HAdV-B7 appears to be uniquely efficient at downregulating a number of innate immunity pathways, such as MDA5[328] and type I IFN response (table 4.3). The overall picture presents both as efficient suppressors of ISG activation, with B14 specializing in driving metabolic pathways and inhibiting immune-mediated cell death, and B7 in suppression of even more innate immune pathways and T-cell mediated cell death. Essentially, what I observed suggests that HAdV-B7 achieves its high pathogenicity through specialized evasion of innate immunity, while HAdV-B14 achieves its own through a rapid, prolonged, and highly productive replication cycle. It is worth noting that HAdVs B7 and B14, while members of the same HAdV species, belong to two distinct subgroups within it, these being species B1 and B2 respectively. These subgroups express slightly different cellular tropism, with B1-related illness being almost exclusively respiratory in nature, while B2 species have also been associated with renal and urinary infections[20,21]. The possibility exists that these differences in functionality reflect their differences in cell tropism, with group B2 HAdVs requiring a more general approach to infect a wider range of cell types.

## 6. Conclusions and Future Directions

The work presented here covered two distinct aspects of HAdV research: the first mostly examining the functional impact of small E1A isoforms 9, 10, and 11S-derived E1As on the viral replicative cycle, with potential impact on virus yields. The second part compared IFN resistance of the most commonly studied species (HAdV-C) to the less-researched, but more pathogenic, HAdV-B, and investigated a possible novel mechanism of ISG suppression. What these topics have in common is that they both represent critically understudied aspects of HAdV biology. Despite E1A's widely understood importance to the adenovirus replication cycle for a multitude of reasons[2], the roles of three of its five splicing isoforms remain mostly unknown[4]. Regardless of numerous case studies illustrating the danger posed by certain HAdV species as pathogenic agents[9,20,31–33], the vast majority of research is performed on the model species (HAdV-C). In the wake of the 2020 worldwide SARS-CoV2 outbreak, it is important to remember that we can never be sure from where the next pandemic threat will emerge, and at least a general understanding of what seems like a common nuisance virus now may be invaluable in the years to come. The modification of oncolytic HAdVs to target membrane receptors other than the standard CAR[240,241], for example, creates a scenario wherein a single recombination event (rescue of the deleted genes within the modified virus) may suddenly produce an extremely dangerous variant. Even without any further research, the observed HAdV-B14 large plaque phenotype (Fig. 4.6) is worth noting, as IFN is in some cases administered as anti-viral treatment[243]. This treatment may have to be carefully considered for HAdV-B14 infections, as the apoptosis of infected cells simultaneously may very well result in more harm to the patient than any good the treatment otherwise provides.

My research into E1A splicing revealed that the subcellular location of the E1A gene influences the expression of its splicing variants. E1A-deleted viruses relying on in *trans*

expression from the host cell are unable to produce the smaller, late variants of the protein, leading to reduced viral gene/protein expression across the board and poorer overall titres. This can be corrected for by providing these additional E1A isoforms in *trans*, improving overall viral performance and titre. In addition to E1A, these viruses are also deficient and supplemented in trans for the *E1B* gene, which also has multiple splice isoforms. These results both shed light on the regulation and functions of the small E1A isoforms and provide a helpful option to anyone making use of E1A-deleted adenovirus (research, viral vector production, etc.), allowing for greater yields of said viral stock. Going forward, it would be interesting to investigate whether the relative levels of these proteins are thrown off by in *trans* supplementation as well, and if so, what effect this has on viral fitness and whether it can also be corrected for in the cell line. Additionally, to further research the role of the smaller E1A isoforms, it may prove fruitful to more closely examine their binding partners and promoter recruitment, contrasting them by these metrics to the large isoforms.

Investigating HAdVs B and C in terms of response to type I IFN, I found a large (five-fold) difference between the two in terms of final titre. This seemed to be the result of more efficient prevention of STAT2 and RPII recruitment to ISG promoters and may have involved the sequestration of the AAA+ cellular protein RuvBL1 into high-molecular weight complexes, keeping it in the cytoplasm. The two HAdV-B types investigated (7 and 14) seemed to lose some of this resistance in response to knockdown of different cellular proteins from one another (DCAF7 and FoxK1/2 respectively). This implied a higher-than-expected level of difference between the two strains, which was backed up by proteomic analysis that revealed completely different patterns of protein up- and down-regulation between them. HAdV-B7 appeared to focus on suppression of innate immune pathways, while HAdV-B14 was able to upregulate host metabolism while

inhibiting cell death, for a faster and more productive replicative cycle. These differences may reflect variance in host cell tropism between the two types. Further research is still necessary into the mechanisms of ISG resistance in these HAdV types. Transfection of E1A alone did not induce formation of HMW RuvBL1 complexes, as was observed during infection, and it remains to be determined which viral protein is responsible for this phenotype. By the same token, despite the importance of DCAF7 and FoxK1/2 to HAdVs B7 and B14 for ISG suppression, the E1A of neither type bound to either protein, implying either that E1A uses these proteins indirectly for ISG suppression, or that these strains use another protein altogether for this purpose. If the former is true, then the exact mechanism will need to be deduced, and in the case of the latter, then the responsible viral protein will need to be identified. One experiment revealed that HAdV-B, seemingly against its own best interest, reduces ubiquitination and proteasomal degradation of STAT2, which will also warrant further analysis.

Overall, my research represents a set of pioneering investigations into a familiar virus. The first reveals a function for three long-understudied E1A isoforms and presents a method of improving E1-deficient viral construct yields, and the second uncovers a fundamental difference between the mechanisms of ISG suppression used by HAdV species B and C, and more broadly reveals a surprising level of difference between HAdVs B7 and B14. There remains much to be studied on the mechanisms by which these E1A isoforms contribute to late HAdV replication, the exact means by which HAdVs B7 and B14 go about ISG suppression, and the functions of the remainder of the E1 genomic region to this, as well as E3 and E4.

## 7. References


1. Lion, T. & Wold, W. S. M. Adenoviruses. in *Fields Virology: DNA Viruses* (eds. Howley, P. M. & Knipe, D. M.) vol. 2 158–226 (Wolters Kluwer, Philadelphia, 2022).
2. King, C. R., Zhang, A., Tessier, T. M., Gameiro, S. F. & Mymryk, J. S. Hacking the Cell: Network Intrusion and Exploitation by Adenovirus E1A. *mBio* **9**, e00390-18 (2018).
3. Bulcha, J. T., Wang, Y., Ma, H., Tai, P. W. L. & Gao, G. Viral vector platforms within the gene therapy landscape. *Sig Transduct Target Ther* **6**, 53 (2021).
4. Hearing, P. Adenoviridae: The Viruses and Their Replication. in *Fields Virology: DNA Viruses* (eds. Howley, P. M. & Knipe, D. M.) vol. 2 122–157 (Wolters Kluwer, Philadelphia, 2022).
5. Avvakumov, N., Kajon, A. E., Hoeben, R. C. & Mymryk, J. S. Comprehensive sequence analysis of the E1A proteins of human and simian adenoviruses. *Virology* **329**, 477–492 (2004).
6. Gray, G. C. & Chorazy, M. L. Human Adenovirus 14a: A New Epidemic Threat. *J INFECT DIS* **199**, 1413–1415 (2009).
7. Sammons, J. S. *et al.* Outbreak of Adenovirus in a Neonatal Intensive Care Unit. *Ophthalmology* **126**, 137–143 (2019).
8. Lewis, P. F. *et al.* A Community-Based Outbreak of Severe Respiratory Illness Caused by Human Adenovirus Serotype 14. *J INFECT DIS* **199**, 1427–1434 (2009).
9. Cui, X. *et al.* Human Adenovirus Type 7 Infection Associated with Severe and Fatal Acute Lower Respiratory Illness and Nosocomial Transmission. *J Clin Microbiol* **53**, 746–749 (2015).
10. Graham, F. L., Smiley, J., Russell, W. C. & Nairn, R. Characteristics of a human cell line transformed by DNA from human adenovirus type 5. *J Gen Virol* **36**, 59–74 (1977).
11. Olanubi, O., Frost, J. R., Radko, S. & Pelka, P. Suppression of Type I Interferon Signaling by E1A via RuvBL1/Pontin. *J Virol* **91**, e02484-16 (2017).

12. Rowe, W. P., Huebner, R. J., Gilmore, L. K., Parrott, R. H. & Ward, T. G. Isolation of a Cytopathogenic Agent from Human Adenoids Undergoing Spontaneous Degeneration in Tissue Culture. *Experimental Biology and Medicine* **84**, 570–573 (1953).
13. Current ICTV Taxonomy Release | ICTV. https://ictv.global/taxonomy.
14. Peter M. Howley, David M. Knipe, Jeffrey L. Cohen, & Blossom A. Damania. *Fields Virology: DNA Viruses*. vol. Seventh edition (Wolters Kluwer Health, Philadelphia, 2022).
15. Genus: Testadenovirus | ICTV. https://ictv.global/report/chapter/adenoviridae/adenoviridae/testadenovirus.
16. Benkő, M. *et al.* ICTV Virus Taxonomy Profile: Adenoviridae 2022: This article is part of the ICTV Virus Taxonomy Profiles collection. *Journal of General Virology* **103**, (2022).
17. Genus: Mastadenovirus | ICTV. https://ictv.global/report/chapter/adenoviridae/adenoviridae/mastadenovirus.
18. Dhingra, A. *et al.* Molecular Evolution of Human Adenovirus (HAdV) Species C. *Sci Rep* **9**, 1039 (2019).
19. Seto, D., Chodosh, J., Brister, J. R., Jones, M. S., & Members of the Adenovirus Research Community. Using the Whole-Genome Sequence To Characterize and Name Human Adenoviruses. *J Virol* **85**, 5701–5702 (2011).
20. Kajon, A. E. *et al.* Molecular Epidemiology and Brief History of Emerging Adenovirus 14–Associated Respiratory Disease in the United States. *J INFECT DIS* **202**, 93–103 (2010).
21. Sakurai, F., Kawabata, K. & Mizuguchi, H. Adenovirus vectors composed of subgroup B adenoviruses. *Curr Gene Ther* **7**, 229–238 (2007).
22. Heim, A. Management of Adenovirus Infections (Adenoviridae). in *Encyclopedia of Virology* 197–205 (Elsevier, 2021). doi:10.1016/B978-0-12-814515-9.00149-1.
23. Ghebremedhin, B. Human adenovirus: Viral pathogen with increasing importance. *Eur J Microbiol Immunol (Bp)* **4**, 26–33 (2014).

24. Crenshaw, B. J., Jones, L. B., Bell, C. R., Kumar, S. & Matthews, Q. L. Perspective on Adenoviruses: Epidemiology, Pathogenicity, and Gene Therapy. *Biomedicines* **7**, 61 (2019).
25. MacNeil, K. M. *et al.* Adenoviruses in medicine: innocuous pathogen, predator, or partner. *Trends Mol Med* **29**, 4–19 (2023).
26. Rozwadowski, F. *et al.* Notes from the Field: Fatalities Associated with Human Adenovirus Type 7 at a Substance Abuse Rehabilitation Facility - New Jersey, 2017. *MMWR Morb Mortal Wkly Rep* **67**, 371–372 (2018).
27. Brown, J. R., Shah, D. & Breuer, J. Viral gastrointestinal infections and norovirus genotypes in a paediatric UK hospital, 2014-2015. *J Clin Virol* **84**, 1–6 (2016).
28. Wan, G.-H. *et al.* Surveillance of airborne adenovirus and Mycoplasma pneumoniae in a hospital pediatric department. *PLoS One* **7**, e33974 (2012).
29. Kandel, R. *et al.* Outbreak of Adenovirus Type 4 Infection in a Long-Term Care Facility for the Elderly. *Infection Control & Hospital Epidemiology* **31**, 755–757 (2010).
30. Kajon, A. E. *et al.* Major Articles-Molecular Epidemiology of Adenovirus Type 4 Infections in US Military Recruits in the Postvaccination Era (1997–2003). *The Journal of Infectious Diseases* **196**, 67–75 (2007).
31. Park, J. Y. *et al.* Clinical Features and Courses of Adenovirus Pneumonia in Healthy Young Adults during an Outbreak among Korean Military Personnel. *PLOS ONE* **12**, e0170592 (2017).
32. Payne, S. B., Grilli, E. A., Smith, A. J. & Hoskins, T. W. Investigation of an outbreak of adenovirus type 3 infection in a boys' boarding school. *Epidemiology & Infection* **93**, 277–283 (1984).
33. Bautista-Gogel, J. *et al.* Outbreak of Respiratory Illness Associated With Human Adenovirus Type 7 Among Persons Attending Officer Candidates School, Quantico, Virginia, 2017. *The Journal of Infectious Diseases* **221**, 697–700 (2020).
34. Van Der Veen, J. & Kok, G. Isolation and typing of adenoviruses recovered from military recruits with acute respiratory disease in The Netherlands. *Am J Hyg* **65**, 119–129 (1957).

35. Hang, J. *et al.* Human Adenovirus Type 55 Distribution, Regional Persistence, and Genetic Variability. *Emerg. Infect. Dis.* **26**, 1497–1505 (2020).
36. HAN Archive - 00462 | Health Alert Network (HAN). https://emergency.cdc.gov/han/2022/han00462.asp (2022).
37. Martin, N. A. *et al.* Adeno-Associated Virus 2 and Human Adenovirus F41 in Wastewater during Outbreak of Severe Acute Hepatitis in Children, Ireland. *Emerg. Infect. Dis.* **29**, 751–760 (2023).
38. Rabaan, A. A. *et al.* Suspected Adenovirus Causing an Emerging HEPATITIS among Children below 10 Years: A Review. *Pathogens* **11**, 712 (2022).
39. Ostapchuk, P. & Hearing, P. Control of adenovirus packaging. *Journal of Cellular Biochemistry* **96**, 25–35 (2005).
40. Westergren Jakobsson, A. *et al.* The Human Adenovirus 2 Transcriptome: an Amazing Complexity of Alternatively Spliced mRNAs. *J Virol* **95**, e01869-20 (2021).
41. Chow, L. T., Gelinas, R. E., Broker, T. R. & Roberts, R. J. An amazing sequence arrangement at the 5’ ends of adenovirus 2 messenger RNA. *Cell* **12**, 1–8 (1977).
42. Berget, S. M., Moore, C. & Sharp, P. A. Spliced segments at the 5’ terminus of adenovirus 2 late mRNA. *Proc Natl Acad Sci U S A* **74**, 3171–3175 (1977).
43. Crisostomo, L., Soriano, A. M., Mendez, M., Graves, D. & Pelka, P. Temporal dynamics of adenovirus 5 gene expression in normal human cells. *PLoS ONE* **14**, e0211192 (2019).
44. Stephens, C. & Harlow, E. Differential splicing yields novel adenovirus 5 E1A mRNAs that encode 30 kd and 35 kd proteins. *EMBO J* **6**, 2027–2035 (1987).
45. Svensson, C., Pettersson, U. & Akusjärvi, G. Splicing of adenovirus 2 early region 1A mRNAs is non-sequential. *Journal of Molecular Biology* **165**, 475–495 (1983).
46. Radko, S., Jung, R., Olanubi, O. & Pelka, P. Effects of Adenovirus Type 5 E1A Isoforms on Viral Replication in Arrested Human Cells. *PLoS ONE* **10**, e0140124 (2015).

47. Himmelspach, M., Cavaloc, Y., Chebli, K., Stévenin, J. & Gattoni, R. Titration of serine/arginine (SR) splicing factors during adenoviral infection modulates E1A pre-mRNA alternative splicing. *RNA* **1**, 794–806 (1995).

48. Yuo, C. Y. & Weiner, A. M. A U1 small nuclear ribonucleoprotein particle with altered specificity induces alternative splicing of an adenovirus E1A mRNA precursor. *Mol Cell Biol* **9**, 3429–3437 (1989).

49. Nakajima, T., Masuda-Murata, M., Hara, E. & Oda, K. Induction of Cell Cycle Progression by Adenovirus ElA Gene 13S- and 12S-mRNA Products in Quiescent Rat Cells. *Molecular and Cellular Biology* **7**, 3846–3852 (1987).

50. Stabel, S., Argos, P. & Philipson, L. The release of growth arrest by microinjection of adenovirus E1A DNA. *The EMBO Journal* **4**, 2329–2336 (1985).

51. Köhler, M., Görlich, D., Hartmann, E. & Franke, J. Adenoviral E1A Protein Nuclear Import Is Preferentially Mediated by Importin α3 in Vitro. *Virology* **289**, 186–191 (2001).

52. Cohen, M. J., King, C. R., Dikeakos, J. D. & Mymryk, J. S. Functional analysis of the C-terminal region of human adenovirus E1A reveals a misidentified nuclear localization signal. *Virology* **468–470**, 238–243 (2014).

53. Marshall, K. S. *et al.* Identification and characterization of multiple conserved nuclear localization signals within adenovirus E1A. *Virology* **454–455**, 206–214 (2014).

54. Montell, C., Fisher, E. F., Caruthers, M. H. & Berk, A. J. Resolving the functions of overlapping viral genes by site-specific mutagenesis at a mRNA splice site. *Nature* **295**, 380–384 (1982).

55. Stevens, J. L. *et al.* Transcription Control by E1A and MAP Kinase Pathway via Sur2 Mediator Subunit. *Science* **296**, 755–758 (2002).

56. Wang, G. *et al.* Mediator requirement for both recruitment and postrecruitment steps in transcription initiation. *Mol Cell* **17**, 683–694 (2005).

57. Cantin, G. T., Stevens, J. L. & Berk, A. J. Activation domain–mediator interactions promote transcription preinitiation complex assembly on promoter DNA. *Proceedings of the National Academy of Sciences* **100**, 12003–12008 (2003).

58. Hsu, E., Pennella, M. A., Zemke, N. R., Eng, C. & Berk, A. J. Adenovirus E1A Activation Domain Regulates H3 Acetylation Affecting Varied Steps in Transcription at Different Viral Promoters. *J Virol* **92**, e00805-18 (2018).

59. Ström, A. C., Ohlsson, P. & Akusjärvi, G. AR1 is an integral part of the adenovirus type 2 E1A-CR3 transactivation domain. *J Virol* **72**, 5978–5983 (1998).

60. Liu, F. & Green, M. R. A specific member of the ATF transcription factor family can mediate transcription activation by the adenovirus E1a protein. *Cell* **61**, 1217–1224 (1990).

61. Liu, F. & Green, M. R. Promoter targeting by adenovirus E1a through interaction with different cellular DNA-binding domains. *Nature* **368**, 520–525 (1994).

62. Maguire, K. *et al.* Interactions between adenovirus E1A and members of the AP-1 family of cellular transcription factors. *Oncogene* **6**, 1417–1422 (1991).

63. Weintraub, S. J. & Dean, D. C. Interaction of a common factor with ATF, Sp1, or TATAA promoter elements is required for these sequences to mediate transactivation by the adenoviral oncogene E1a. *Molecular and Cellular Biology* **12**, 512 (1992).

64. Ferrari, R. *et al.* Epigenetic Reprogramming by Adenovirus e1a. *Science (New York, N.Y.)* **321**, 1086 (2008).

65. Miller, D. L., Myers, C. L., Rickards, B., Coller, H. A. & Flint, S. J. Adenovirus type 5 exerts genome-wide control over cellular programs governing proliferation, quiescence, and survival. *Genome Biology* **8**, R58 (2007).

66. Zhao, H., Granberg, F., Elfineh, L., Pettersson, U. & Svensson, C. Strategic Attack on Host Cell Gene Expression during Adenovirus Infection. *Journal of Virology* **77**, 11006 (2003).

67. Granberg, F., Svensson, C., Pettersson, U. & Zhao, H. Modulation of host cell gene expression during onset of the late phase of an adenovirus infection is focused on growth inhibition and cell architecture. *Virology* **343**, 236–245 (2005).

68. Pelka, P. *et al.* Transcriptional control by adenovirus E1A conserved region 3 via p300/CBP. *Nucleic Acids Research* **37**, 1095–1106 (2009).

69. Dyson, N., Guida, P., McCall, C. & Harlow, E. Adenovirus E1A makes two distinct contacts with the retinoblastoma protein. *J Virol* **66**, 4606–4611 (1992).

70. Vousden, K. H. & Jat, P. S. Functional similarity between HPV16E7, SV40 large T and adenovirus E1a proteins. *Oncogene* **4**, 153–158 (1989).

71. Bagchi, S., Raychaudhuri, P. & Nevins, J. R. Adenovirus E1A proteins can dissociate heteromeric complexes involving the E2F transcription factor: A novel mechanism for E1A *trans*-activation. *Cell* **62**, 659–669 (1990).

72. Kent, L. N. & Leone, G. The broken cycle: E2F dysfunction in cancer. *Nat Rev Cancer* **19**, 326–338 (2019).

73. Chan, H. M., Krstic-Demonacos, M., Smith, L., Demonacos, C. & Thangue, N. B. L. Acetylation control of the retinoblastoma tumour-suppressor protein. *Nat Cell Biol* **3**, 667–674 (2001).

74. Pelka, P. *et al.* Adenovirus E1A Directly Targets the E2F/DP-1 Complex. *J Virol* **85**, 8841–8851 (2011).

75. Ghosh, M. K. & Harter, M. L. A Viral Mechanism for Remodeling Chromatin Structure in G0 Cells. *Molecular Cell* **12**, 255–260 (2003).

76. Rea, S. *et al.* Regulation of chromatin structure by site-specific histone H3 methyltransferases. *Nature* **406**, 593–599 (2000).

77. Sha, J., Ghosh, M. K., Zhang, K. & Harter, M. L. E1A Interacts with Two Opposing Transcriptional Pathways To Induce Quiescent Cells into S Phase. *J Virol* **84**, 4050–4059 (2010).

78. Chinnadurai, G. Modulation of oncogenic transformation by the human adenovirus E1A C-terminal region. *Curr Top Microbiol Immunol* **273**, 139–161 (2004).

79. Subramanian, T., Zhao, L.-J. & Chinnadurai, G. Interaction of CtBP with adenovirus E1A suppresses immortalization of primary epithelial cells and enhances virus replication during productive infection. *Virology* **443**, 313–320 (2013).

80. Cohen, M. J. *et al.* Dissection of the C-Terminal Region of E1A Redefines the Roles of CtBP and Other Cellular Targets in Oncogenic Transformation. *Journal of Virology* **87**, 10348 (2013).

81. Komorek, J. *et al.* Adenovirus type 5 E1A and E6 proteins of low-risk cutaneous beta-human papillomaviruses suppress cell transformation through interaction with FOXK1/K2 transcription factors. *J Virol* **84**, 2719–2731 (2010).

82. Zemke, N. R. & Berk, A. J. The Adenovirus E1A C-terminus Suppresses a Delayed Antiviral Response and Modulates RAS Signaling. *Cell Host Microbe* **22**, 789-800.e5 (2017).

83. Reich, N., Pine, R., Levy, D. & J E Darnell, J. Transcription of interferon-stimulated genes is induced by adenovirus particles but is suppressed by E1A gene products. *Journal of Virology* **62**, 114 (1988).

84. Gutch, M. J. & Reich, N. C. Repression of the interferon signal transduction pathway by the adenovirus E1A oncogene. *Proceedings of the National Academy of Sciences of the United States of America* **88**, 7913 (1991).

85. Kalvakolanu, D. V., Bandyopadhyay, S. K., Harter, M. L. & Sen, G. C. Inhibition of interferon-inducible gene expression by adenovirus E1A proteins: block in transcriptional complex formation. *Proceedings of the National Academy of Sciences of the United States of America* **88**, 7459 (1991).

86. Routes, J. M., Li, H., Bayley, S. T., Ryan, S. & Klemm, D. J. Inhibition of IFN-stimulated gene expression and IFN induction of cytolytic resistance to natural killer cell lysis correlate with E1A-p300 binding. *J Immunol* **156**, 1055–1061 (1996).

87. Look, D. C. *et al.* Direct suppression of Stat1 function during adenoviral infection. *Immunity* **9**, 871–880 (1998).

88. Shen, X., Mizuguchi, G., Hamiche, A. & Wu, C. A chromatin remodelling complex involved in transcription and DNA processing. *Nature* **406**, 541–544 (2000).

89. Ikura, T. *et al.* Involvement of the TIP60 Histone Acetylase Complex in DNA Repair and Apoptosis. *Cell* **102**, 463–473 (2000).

90. Gnatovskiy, L., Mita, P. & Levy, D. E. The human RVB complex is required for efficient transcription of type I interferon-stimulated genes. *Mol Cell Biol* **33**, 3817–3825 (2013).

91. Zemke, N. R. *et al.* Adenovirus E1A binding to DCAF10 targets proteasomal degradation of RUVBL1/2 AAA+ ATPases required for quaternary assembly of multiprotein machines, innate immunity, and responses to metabolic stress. *Journal of Virology* **97**, e00993-23 (2023).

92. Fonseca, G. J. *et al.* Adenovirus evasion of interferon-mediated innate immunity by direct antagonism of a cellular histone posttranslational modification. *Cell Host Microbe* **11**, 597–606 (2012).

93. Xiao, T. *et al.* Histone H2B ubiquitylation is associated with elongating RNA polymerase II. *Mol Cell Biol* **25**, 637–651 (2005).

94. Moniaux, N. *et al.* The Human RNA Polymerase II-Associated Factor 1 (hPaf1): A New Regulator of Cell-Cycle Progression. *PLoS ONE* **4**, e7077 (2009).

95. Miller, M. S. *et al.* Characterization of the 55-residue protein encoded by the 9S E1A mRNA of species C adenovirus. *J Virol* **86**, 4222–4233 (2012).

96. Arulsundaram, V. D. *et al.* The adenovirus 55 residue E1A protein is a transcriptional activator and binds the unliganded thyroid hormone receptor. *J Gen Virol* **95**, 142–152 (2014).

97. Aubrey, B. J., Kelly, G. L., Janic, A., Herold, M. J. & Strasser, A. How does p53 induce apoptosis and how does this relate to p53-mediated tumour suppression? *Cell Death Differ* **25**, 104–113 (2018).

98. Lin, J., Chen, J., Elenbaas, B. & Levine, A. J. Several hydrophobic amino acids in the p53 amino-terminal domain are required for transcriptional activation, binding to mdm-2 and the adenovirus 5 E1B 55-kD protein. *Genes Dev.* **8**, 1235–1246 (1994).

99. Iwakuma, T. & Lozano, G. MDM2, an introduction. *Mol Cancer Res* **1**, 993–1000 (2003).

100. Yew, P. R., Liu, X. & Berk, A. J. Adenovirus E1B oncoprotein tethers a transcriptional repression domain to p53. *Genes Dev.* **8**, 190–202 (1994).

101. Yew, P. R. & Berk, A. J. Inhibition of p53 transactivation required for transformation by adenovirus early 1B protein. *Nature* **357**, 82–85 (1992).

102. Pennella, M. A., Liu, Y., Woo, J. L., Kim, C. A. & Berk, A. J. Adenovirus E1B 55-Kilodalton Protein Is a p53-SUMO1 E3 Ligase That Represses p53 and Stimulates Its Nuclear Export through Interactions with Promyelocytic Leukemia Nuclear Bodies. *J Virol* **84**, 12210–12225 (2010).

103. Endter, C., Kzhyshkowska, J., Stauber, R. & Dobner, T. SUMO-1 modification required for transformation by adenovirus type 5 early region 1B 55-kDa oncoprotein. *Proc. Natl. Acad. Sci. U.S.A.* **98**, 11312–11317 (2001).

104. Wimmer, P. *et al.* SUMO modification of E1B-55K oncoprotein regulates isoform-specific binding to the tumour suppressor protein PML. *Oncogene* **29**, 5511–5522 (2010).

105. Liu, Y., Shevchenko, A., Shevchenko, A. & Berk, A. J. Adenovirus Exploits the Cellular Aggresome Response To Accelerate Inactivation of the MRN Complex. *J Virol* **79**, 14004–14016 (2005).

106. Zantema, A. *et al.* Localization of the E1 B proteins of adenovirus 5 in transformed cells, as revealed by interaction with monoclonal antibodies. *Virology* **142**, 44–58 (1985).

107. Schreiner, S. *et al.* Proteasome-Dependent Degradation of Daxx by the Viral E1B-55K Protein in Human Adenovirus-Infected Cells. *J Virol* **84**, 7029–7038 (2010).

108. Chahal, J. S., Gallagher, C., DeHart, C. J. & Flint, S. J. The Repression Domain of the E1B 55-Kilodalton Protein Participates in Countering Interferon-Induced Inhibition of Adenovirus Replication. *J Virol* **87**, 4432–4444 (2013).

109. Chahal, J. S., Qi, J. & Flint, S. J. The human adenovirus type 5 E1B 55 kDa protein obstructs inhibition of viral replication by type I interferon in normal human cells. *PLoS Pathog* **8**, e1002853 (2012).

110. Querido, E. *et al.* Degradation of p53 by adenovirus E4orf6 and E1B55K proteins occurs via a novel mechanism involving a Cullin-containing complex. *Genes Dev.* **15**, 3104–3117 (2001).

111. Stracker, T. H., Carson, C. T. & Weitzman, M. D. Adenovirus oncoproteins inactivate the Mre11–Rad50–NBS1 DNA repair complex. *Nature* **418**, 348–352 (2002).

112. Carson, C. T. The Mre11 complex is required for ATM activation and the G2/M checkpoint. *The EMBO Journal* **22**, 6610–6620 (2003).

113. Dallaire, F., Blanchette, P., Groitl, P., Dobner, T. & Branton, P. E. Identification of Integrin α3 as a New Substrate of the Adenovirus E4orf6/E1B 55-Kilodalton E3 Ubiquitin Ligase Complex. *J Virol* **83**, 5329–5338 (2009).

114. Gupta, A., Jha, S., Engel, D. A., Ornelles, D. A. & Dutta, A. Tip60 degradation by adenovirus relieves transcriptional repression of viral transcriptional activator EIA. *Oncogene* **32**, 5017–5025 (2013).

115. Schreiner, S. *et al.* SPOC1-Mediated Antiviral Host Cell Response Is Antagonized Early in Human Adenovirus Type 5 Infection. *PLoS Pathog* **9**, e1003775 (2013).

116. Nazeer, R. *et al.* Adenovirus E1B 55-Kilodalton Protein Targets SMARCAL1 for Degradation during Infection and Modulates Cellular DNA Replication. *J Virol* **93**, e00402-19 (2019).

117. Fu, Y. R. *et al.* Comparison of protein expression during wild-type, and E1B-55k-deletion, adenovirus infection using quantitative time-course proteomics. *Journal of General Virology* **98**, 1377–1388 (2017).

118. Babiss, L. E. & Ginsberg, H. S. Adenovirus type 5 early region 1b gene product is required for efficient shutoff of host protein synthesis. *J Virol* **50**, 202–212 (1984).

119. Babiss, L. E., Ginsberg, H. S. & Darnell, J. E. Adenovirus E1B Proteins Are Required for Accumulation of Late Viral mRNA and for Effects on Cellular mRNA Translation and Transport. *Molecular and Cellular Biology* **5**, 2552–2558 (1985).

120. Berk, A. J. Recent lessons in gene expression, cell cycle control, and cell biology from adenovirus. *Oncogene* **24**, 7673–7685 (2005).

121. Cuconati, A. & White, E. Viral homologs of BCL-2: role of apoptosis in the regulation of virus infection. *Genes Dev.* **16**, 2465–2478 (2002).

122. Kindsmüller, K. *et al.* A 49-kilodalton isoform of the adenovirus type 5 early region 1B 55-kilodalton protein is sufficient to support virus replication. *J Virol* **83**, 9045–9056 (2009).

123. Sieber, T. & Dobner, T. Adenovirus type 5 early region 1B 156R protein promotes cell transformation independently of repression of p53-stimulated transcription. *J Virol* **81**, 95–105 (2007).

124. Donovan-Banfield, I., Turnell, A. S., Hiscox, J. A., Leppard, K. N. & Matthews, D. A. Deep splicing plasticity of the human adenovirus type 5 transcriptome drives virus evolution. *Commun Biol* **3**, 124 (2020).

125. Temperley, S. M. & Hay, R. T. Recognition of the adenovirus type 2 origin of DNA replication by the virally encoded DNA polymerase and preterminal proteins. *The EMBO Journal* **11**, 761–768 (1992).

126. Leegwater, P. A., Van Driel, W. & Van Der Vliet, P. C. Recognition site of nuclear factor I, a sequence-specific DNA-binding protein from HeLa cells that stimulates adenovirus DNA replication. *The EMBO Journal* **4**, 1515–1521 (1985).

127. De Vries, E., Van Driel, W., Van Den Heuvel, S. J. & Van Der Vliet, P. C. Contactpoint analysis of the HeLa nuclear factor I recognition site reveals symmetrical binding at one side of the DNA helix. *The EMBO Journal* **6**, 161–168 (1987).

128. Bosher, J., Robinson, E. C. & Hay, R. T. Interactions between the adenovirus type 2 DNA polymerase and the DNA binding domain of nuclear factor I. *New Biol* **2**, 1083–1090 (1990).

129. Hatfield, L. & Hearing, P. The NFIII/OCT-1 binding site stimulates adenovirus DNA replication in vivo and is functionally redundant with adjacent sequences. *J Virol* **67**, 3931–3939 (1993).

130. Hoeben, R. C. & Uil, T. G. Adenovirus DNA Replication. *Cold Spring Harbor Perspectives in Biology* **5**, a013003–a013003 (2013).

131. Van Der Vliet, P. C. & Levine, A. J. DNA-binding Proteins specific for Cells infected by Adenovirus. *Nature New Biology* **246**, 170–174 (1973).

132. Kanellopoulos, P. N., Van Der Zandt, H., Tsernoglou, D., Van Der Vliet, P. C. & Tucker, P. A. Crystallization and Preliminary X-Ray Crystallographic Studies on the Adenovirus ssDNA Binding Protein in Complex with ssDNA. *Journal of Structural Biology* **115**, 113–116 (1995).

133. Van Breukelen, B., Brenkman, A. B., Holthuizen, P. E. & Van Der Vliet, P. C. Adenovirus Type 5 DNA Binding Protein Stimulates Binding of DNA Polymerase to the Replication Origin. *J Virol* **77**, 915–922 (2003).

134. Lichtenstein, D. L., Toth, K., Doronin, K., Tollefson, A. E. & Wold, W. S. M. FUNCTIONS AND MECHANISMS OF ACTION OF THE ADENOVIRUS E3 PROTEINS. *International Reviews of Immunology* **23**, 75–111 (2004).

135. Benedict, C. A. *et al.* Three Adenovirus E3 Proteins Cooperate to Evade Apoptosis by Tumor Necrosis Factor-related Apoptosis-inducing Ligand Receptor-1 and -2. *Journal of Biological Chemistry* **276**, 3270–3278 (2001).

136. Gooding, L. R., Sofola, I. O., Tollefson, A. E., Duerksen-Hughes, P. & Wold, W. S. The adenovirus E3-14.7K protein is a general inhibitor of tumor necrosis factor-mediated cytolysis. 8.

137. Horton, T. M. *et al.* Adenovirus E3 14.7K protein functions in the absence of other adenovirus proteins to protect transfected cells from tumor necrosis factor cytolysis. *J Virol* **65**, 2629–2639 (1991).

138. Wilson-Rawls, J. & Wold, W. S. M. The E3-6.7K Protein of Adenovirus Is an Asn-Linked Integral Membrane Glycoprotein Localized in the Endoplasmic Reticulum. *Virology* **195**, 6–15 (1993).

139. Schneider-Brachert, W. *et al.* Inhibition of TNF receptor 1 internalization by adenovirus 14.7K as a novel immune escape mechanism. *J. Clin. Invest.* **116**, 2901–2913 (2006).

140. Burgert, H. G., Maryanski, J. L. & Kvist, S. 'E3/19K' protein of adenovirus type 2 inhibits lysis of cytolytic T lymphocytes by blocking cell-surface expression of histocompatibility class I antigens. *Proceedings of the National Academy of Sciences* **84**, 1356–1360 (1987).

141. McSharry, B. P. *et al.* Adenovirus E3/19K Promotes Evasion of NK Cell Recognition by Intracellular Sequestration of the NKG2D Ligands Major Histocompatibility Complex Class I Chain-Related Proteins A and B. *J Virol* **82**, 4585–4594 (2008).

142. Carlin, C. R., Tollefson, A. E., Brady, H. A., Hoffman, B. L. & Wold, W. S. M. Epidermal growth factor receptor is down-regulated by a 10,400 MW protein encoded by the E3 region of adenovirus. *Cell* **57**, 135–144 (1989).

143. Elsing, A. & Burgert, H.-G. The adenovirus E3/10.4K-14.5K proteins down-modulate the apoptosis receptor Fas/Apo-1 by inducing its internalization. *Proceedings of the National Academy of Sciences* **95**, 10072–10077 (1998).

144. Hilgendorf, A. *et al.* Two Distinct Transport Motifs in the Adenovirus E3/10.4-14.5 Proteins Act in Concert to Down-modulate Apoptosis Receptors and the Epidermal Growth Factor Receptor. *Journal of Biological Chemistry* **278**, 51872–51884 (2003).

145. Delgado-Lopez, F. & Horwitz, M. S. Adenovirus RIDαβ Complex Inhibits Lipopolysaccharide Signaling without Altering TLR4 Cell Surface Expression. *J Virol* **80**, 6378–6386 (2006).

146. Georgi, F. & Greber, U. F. The Adenovirus Death Protein – a small membrane protein controls cell lysis and disease. *FEBS Lett* **594**, 1861–1878 (2020).

147. Hawkins, L. K. & Wold, W. S. M. A 12,500 MW protein is coded by region E3 of adenovirus. *Virology* **188**, 486–494 (1992).

148. O'Shea, C. *et al.* Adenoviral proteins mimic nutrient/growth signals to activate the mTOR pathway for viral replication. *EMBO J* **24**, 1211–1221 (2005).

149. Saxton, R. A. & Sabatini, D. M. mTOR Signaling in Growth, Metabolism, and Disease. *Cell* **168**, 960–976 (2017).

150. Thai, M. *et al.* Adenovirus E4ORF1-Induced MYC Activation Promotes Host Cell Anabolic Glucose Metabolism and Virus Replication. *Cell Metabolism* **19**, 694–701 (2014).

151. Carvalho, T. *et al.* Targeting of adenovirus E1A and E4-ORF3 proteins to nuclear matrix-associated PML bodies. *The Journal of cell biology* **131**, 45–56 (1995).

152. Doucas, V. *et al.* Adenovirus replication is coupled with the dynamic properties of the PML nuclear structure. *Genes Dev.* **10**, 196–207 (1996).

153. Ou, H. D. *et al.* A structural basis for the assembly and functions of a viral polymer that inactivates multiple tumor suppressors. *Cell* **151**, 304–319 (2012).

154. Scherer, M. & Stamminger, T. Emerging Role of PML Nuclear Bodies in Innate Immune Signaling. *J Virol* **90**, 5850–5854 (2016).

155. Soria, C., Estermann, F. E., Espantman, K. C. & O'Shea, C. C. Heterochromatin silencing of p53 target genes by a small viral protein. *Nature* **466**, 1076–1081 (2010).

156. Sohn, S.-Y. & Hearing, P. The adenovirus E4-ORF3 protein functions as a SUMO E3 ligase for TIF-1γ sumoylation and poly-SUMO chain elongation. *Proc. Natl. Acad. Sci. U.S.A.* **113**, 6725–6730 (2016).

157. Sohn, S.-Y. & Hearing, P. Adenovirus Regulates Sumoylation of Mre11-Rad50-Nbs1 Components through a Paralog-Specific Mechanism. *J Virol* **86**, 9656–9665 (2012).

158. Sohn, S.-Y., Bridges, R. G. & Hearing, P. Proteomic Analysis of Ubiquitin-Like Posttranslational Modifications Induced by the Adenovirus E4-ORF3 Protein. *J Virol* **89**, 1744–1755 (2015).

159. Stracker, T. H. *et al.* Serotype-Specific Reorganization of the Mre11 Complex by Adenoviral E4orf3 Proteins. *J Virol* **79**, 6664–6673 (2005).

160. Soriano, A. M. *et al.* Adenovirus 5 E1A Interacts with E4orf3 To Regulate Viral Chromatin Organization. *J Virol* **93**, e00157-19 (2019).

161. Kleinberger, T. & Shenk, T. Adenovirus E4orf4 protein binds to protein phosphatase 2A, and the complex down regulates E1A-enhanced junB transcription. *J Virol* **67**, 7556–7560 (1993).

162. Ben-Israel, H., Sharf, R., Rechavi, G. & Kleinberger, T. Adenovirus E4orf4 Protein Downregulates *MYC* Expression through Interaction with the PP2A-B55 Subunit. *J Virol* **82**, 9381–9388 (2008).

163. Bondesson, M., Ohman, K., Manervik, M., Fan, S. & Akusjärvi, G. Adenovirus E4 open reading frame 4 protein autoregulates E4 transcription by inhibiting E1A transactivation of the E4 promoter. *J Virol* **70**, 3844–3851 (1996).

164. Estmer Nilsson, C. The adenovirus E4-ORF4 splicing enhancer protein interacts with a subset of phosphorylated SR proteins. *The EMBO Journal* **20**, 864–871 (2001).

165. Kanopka, A. *et al.* Regulation of adenovirus alternative RNA splicing by dephosphorylation of SR proteins. *Nature* **393**, 185–187 (1998).

166. Müller, U., Kleinberger, T. & Shenk, T. Adenovirus E4orf4 protein reduces phosphorylation of c-Fos and E1A proteins while simultaneously reducing the level of AP-1. *J Virol* **66**, 5867–5878 (1992).

167. Li, S. *et al.* The Adenovirus E4orf4 Protein Induces G $_2$ /M Arrest and Cell Death by Blocking Protein Phosphatase 2A Activity Regulated by the B55 Subunit. *J Virol* **83**, 8340–8352 (2009).

168. Shtrichman, R., Sharf, R. & Kleinberger, T. Adenovirus E4orf4 protein interacts with both Bα and B′ subunits of protein phosphatase 2A, but E4orf4-induced apoptosis is mediated only by the interaction with Bα. *Oncogene* **19**, 3757–3765 (2000).

169. Brestovitsky, A., Sharf, R., Mittelman, K. & Kleinberger, T. The adenovirus E4orf4 protein targets PP2A to the ACF chromatin-remodeling factor and induces cell death through regulation of SNF2h-containing complexes. *Nucleic Acids Res* **39**, 6414–6427 (2011).

170. Zhang, Z. *et al.* Genetic Analysis of B55α/Cdc55 Protein Phosphatase 2A Subunits: Association with the Adenovirus E4orf4 Protein. *J Virol* **85**, 286–295 (2011).

171. Brestovitsky, A., Nebenzahl-Sharon, K., Kechker, P., Sharf, R. & Kleinberger, T. The Adenovirus E4orf4 Protein Provides a Novel Mechanism for Inhibition of the DNA Damage Response. *PLoS Pathog* **12**, e1005420 (2016).

172. Marcellus, R. C. *et al.* The Early Region 4 orf4 Protein of Human Adenovirus Type 5 Induces p53-Independent Cell Death by Apoptosis. *J Virol* **72**, 7144–7153 (1998).

173. Dobner, T., Horikoshi, N., Rubenwolf, S. & Shenk, T. Blockage by Adenovirus E4orf6 of Transcriptional Activation by the p53 Tumor Suppressor. *Science* **272**, 1470–1473 (1996).

174. Higashino, F., Pipas, J. M. & Shenk, T. Adenovirus E4orf6 oncoprotein modulates the function of the p53-related protein, p73. *Proc. Natl. Acad. Sci. U.S.A.* **95**, 15683–15687 (1998).

175. Steegenga, W. T., Shvarts, A., Riteco, N., Bos, J. L. & Jochemsen, A. G. Distinct Regulation of p53 and p73 Activity by Adenovirus E1A, E1B, and E4orf6 Proteins. *Molecular and Cellular Biology* **19**, 3885–3894 (1999).

176. Flinterman, M. *et al.* E1A Activates Transcription of p73 and Noxa to Induce Apoptosis. *Journal of Biological Chemistry* **280**, 5945–5959 (2005).

177. Huang, M. M. & Hearing, P. The adenovirus early region 4 open reading frame 6/7 protein regulates the DNA binding activity of the cellular transcription factor, E2F, through a direct complex. *Genes Dev.* **3**, 1699–1710 (1989).

178. O'Connor, R. J. & Hearing, P. The E4-6/7 Protein Functionally Compensates for the Loss of E1A Expression in Adenovirus Infection. *J Virol* **74**, 5819–5824 (2000).

179. Schaley, J., O'Connor, R. J., Taylor, L. J., Bar-Sagi, D. & Hearing, P. Induction of the Cellular E2F-1 Promoter by the Adenovirus E4-6/7 Protein. *J Virol* **74**, 2084–2093 (2000).

180. Ip, W.-H., Bertzbach, L. D., Speiseder, T. & Dobner, T. The adenoviral E4orf3/4 is a regulatory polypeptide with cell transforming properties in vitro. *Tumour Virus Research* **15**, 200254 (2023).

181. Dix, I. & Leppard, K. N. Expression of adenovirus type 5 E4 Orf2 protein during lytic infection. *Journal of General Virology* **76**, 1051–1055 (1995).

182. Ma, Y. & Mathews, M. B. Structure, function, and evolution of adenovirus-associated RNA: a phylogenetic approach. *J Virol* **70**, 5083–5099 (1996).

183. Mathews, M. B. & Shenk, T. Adenovirus virus-associated RNA and translation control. *J Virol* **65**, 5657–5662 (1991).

184. Kondo, S., Yoshida, K., Suzuki, M., Saito, I. & Kanegae, Y. Adenovirus-Encoding Virus-Associated RNAs Suppress HDGF Gene Expression to Support Efficient Viral Replication. *PLOS ONE* **9**, e108627 (2014).

185. Vachon, V. K. & Conn, G. L. Adenovirus VA RNA: An essential pro-viral non-coding RNA. *Virus Research* **212**, 39–52 (2016).

186. Kitajewski, J. *et al.* Adenovirus VAI RNA antagonizes the antiviral action of interferon by preventing activation of the interferon-induced eIF-2α kinase. *Cell* **45**, 195–200 (1986).

187. Minamitani, T., Iwakiri, D. & Takada, K. Adenovirus Virus-Associated RNAs Induce Type I Interferon Expression through a RIG-I-Mediated Pathway. *Journal of Virology* **85**, 4035–4040 (2011).

188. Desai, S. Y. *et al.* Activation of Interferon-inducible 2′ −5′ Oligoadenylate Synthetase by Adenoviral VAI RNA (∗). *Journal of Biological Chemistry* **270**, 3454–3461 (1995).

189. Andersson, M. G. *et al.* Suppression of RNA Interference by Adenovirus Virus-Associated RNA. *Journal of Virology* **79**, 9556–9565 (2005).

190. Xu, N., Segerman, B., Zhou, X. & Akusjärvi, G. Adenovirus Virus-Associated RNAII-Derived Small RNAs Are Efficiently Incorporated into the RNA-Induced Silencing Complex and Associate with Polyribosomes. *Journal of Virology* **81**, 10540–10549 (2007).

191. San Martín, C. Latest Insights on Adenovirus Structure and Assembly. *Viruses* **4**, 847–877 (2012).

192. Bergelson, J. M. *et al.* Isolation of a common receptor for Coxsackie B viruses and adenoviruses 2 and 5. *Science* **275**, 1320–1323 (1997).

193. Wickham, T. J., Mathias, P., Cheresh, D. A. & Nemerow, G. R. Integrins alpha v beta 3 and alpha v beta 5 promote adenovirus internalization but not virus attachment. *Cell* **73**, 309–319 (1993).

194. Liu, H. *et al.* Atomic structure of human adenovirus by cryo-EM reveals interactions among protein networks. *Science* **329**, 1038–1043 (2010).

195. Martín-González, N. *et al.* Adenovirus major core protein condenses DNA in clusters and bundles, modulating genome release and capsid internal pressure. *Nucleic Acids Research* **47**, 9231–9242 (2019).

196. Karen, K. A. & Hearing, P. Adenovirus core protein VII protects the viral genome from a DNA damage response at early times after infection. *J Virol* **85**, 4135–4142 (2011).

197. Reddy, V. S. & Nemerow, G. R. Structures and organization of adenovirus cement proteins provide insights into the role of capsid maturation in virus entry and infection. *Proc. Natl. Acad. Sci. U.S.A.* **111**, 11715–11720 (2014).

198. Matthews, D. A. & Russell, W. C. Adenovirus core protein V is delivered by the invading virus to the nucleus of the infected cell and later in infection is associated with nucleoli. *J Gen Virol* **79 ( Pt 7)**, 1671–1675 (1998).

199. Anderson, C. W., Young, M. E. & Flint, S. J. Characterization of the adenovirus 2 virion protein, Mu. *Virology* **172**, 506–512 (1989).

200. Chatterjee, P. K., Vayda, M. E. & Flint, S. J. Interactions among the three adenovirus core proteins. *J Virol* **55**, 379–386 (1985).

201. Lee, T. W. R. *et al.* Precursor of human adenovirus core polypeptide Mu targets the nucleolus and modulates the expression of E2 proteins. *J Gen Virol* **85**, 185–196 (2004).

202. Christensen, J. B. *et al.* Presence of the adenovirus IVa2 protein at a single vertex of the mature virion. *J Virol* **82**, 9086–9093 (2008).

203. Brown, M. T., McGrath, W. J., Toledo, D. L. & Mangel, W. F. Different modes of inhibition of human adenovirus proteinase, probably a cysteine proteinase, by bovine pancreatic trypsin inhibitor. *FEBS Lett* **388**, 233–237 (1996).

204. Mangel, W. F., McGrath, W. J., Toledo, D. L. & Anderson, C. W. Viral DNA and a viral peptide can act as cofactors of adenovirus virion proteinase activity. *Nature* **361**, 274–275 (1993).

205. Graziano, V. *et al.* Regulation of a viral proteinase by a peptide and DNA in one-dimensional space: II. adenovirus proteinase is activated in an unusual one-dimensional biochemical reaction. *J Biol Chem* **288**, 2068–2080 (2013).

206. Mangel, W. F., McGrath, W. J., Xiong, K., Graziano, V. & Blainey, P. C. Molecular sled is an eleven-amino acid vehicle facilitating biochemical interactions via sliding components along DNA. *Nat Commun* **7**, 10202 (2016).

207. Greber, U. F., Webster, P., Weber, J. & Helenius, A. The role of the adenovirus protease on virus entry into cells. *EMBO J* **15**, 1766–1777 (1996).

208. Weber, J. M. Adenovirus Endopeptidase and Its Role in Virus Infection. in *The Molecular Repertoire of Adenoviruses I: Virion Structure and Infection* (eds. Doerfler, W. & Böhm, P.) 227–235 (Springer, Berlin, Heidelberg, 1995). doi:10.1007/978-3-642-79496-4_12.

209. Mangel, W. F. & San Martín, C. Structure, function and dynamics in adenovirus maturation. *Viruses* **6**, 4536–4570 (2014).

210. Pérez-Berná, A. J. *et al.* Processing of the L1 52/55k Protein by the Adenovirus Protease: a New Substrate and New Insights into Virion Maturation. *J Virol* **88**, 1513–1524 (2014).

211. Wu, K., Orozco, D. & Hearing, P. The adenovirus L4-22K protein is multifunctional and is an integral component of crucial aspects of infection. *J Virol* **86**, 10474–10483 (2012).

212. Törmänen, H., Backström, E., Carlsson, A. & Akusjärvi, G. L4-33K, an adenovirus-encoded alternative RNA splicing factor. *J Biol Chem* **281**, 36510–36517 (2006).

213. Lee, C. S. *et al.* Adenovirus-mediated gene delivery: Potential applications for gene and cell-based therapies in the new era of personalized medicine. *Genes & Diseases* **4**, 43–63 (2017).

214. Gorziglia, M. I. *et al.* Elimination of both E1 and E2 from adenovirus vectors further improves prospects for in vivo human gene therapy. *J Virol* **70**, 4173–4178 (1996).

215. Engelhardt, J. F., Ye, X., Doranz, B. & Wilson, J. M. Ablation of E2A in recombinant adenoviruses improves transgene persistence and decreases inflammatory response in mouse liver. *Proc Natl Acad Sci U S A* **91**, 6196–6200 (1994).

216. Amalfitano, A. *et al.* Production and characterization of improved adenovirus vectors with the E1, E2b, and E3 genes deleted. *J Virol* **72**, 926–933 (1998).

217. Osada, T. *et al.* Optimization of vaccine responses with an E1, E2b and E3-deleted Ad5 vector circumvents pre-existing anti-vector immunity. *Cancer Gene Ther* **16**, 673–682 (2009).

218. Gao, G. P., Yang, Y. & Wilson, J. M. Biology of adenovirus vectors with E1 and E4 deletions for liver-directed gene therapy. *J Virol* **70**, 8934–8943 (1996).

219. Alba, R., Bosch, A. & Chillon, M. Gutless adenovirus: last-generation adenovirus for gene therapy. *Gene Ther* **12**, S18–S27 (2005).

220. Hartigan-O'Connor, D., Amalfitano, A. & Chamberlain, J. S. Improved Production of Gutted Adenovirus in Cells Expressing Adenovirus Preterminal Protein and DNA Polymerase. *Journal of Virology* (1999) doi:10.1128/jvi.73.9.7835-7841.1999.

221. Fallaux, F. J. *et al.* Characterization of 911: A New Helper Cell Line for the Titration and Propagation of Early Region 1-Deleted Adenoviral Vectors. *Human Gene Therapy* **7**, 215–222 (1996).

222. Kim, J. S. *et al.* Development of a packaging cell line for propagation of replication-deficient adenovirus vector. *Exp Mol Med* **33**, 145–149 (2001).

223. Zabner, J. *et al.* Adenovirus-mediated gene transfer transiently corrects the chloride transport defect in nasal epithelia of patients with cystic fibrosis. *Cell* **75**, 207–216 (1993).

224. Rosengart, T. K. *et al.* Angiogenesis Gene Therapy. *Circulation* **100**, 468–474 (1999).

225. Crystal, R. G. Adenovirus: The First Effective In Vivo Gene Delivery Vector. *Human Gene Therapy* **25**, 3–11 (2014).

226. Raper, S. E. *et al.* Fatal systemic inflammatory response syndrome in a ornithine transcarbamylase deficient patient following adenoviral gene transfer. *Molecular Genetics and Metabolism* **80**, 148–158 (2003).

227. Voysey, M. *et al.* Safety and efficacy of the ChAdOx1 nCoV-19 vaccine (AZD1222) against SARS-CoV-2: an interim analysis of four randomised controlled trials in Brazil, South Africa, and the UK. *Lancet* **397**, 99–111 (2021).

228. Jones, I. & Roy, P. Sputnik V COVID-19 vaccine candidate appears safe and effective. *Lancet* **397**, 642–643 (2021).

229. Huang, Z. *et al.* Effectiveness of inactivated and Ad5-nCoV COVID-19 vaccines against SARS-CoV-2 Omicron BA. 2 variant infection, severe illness, and death. *BMC Med* **20**, 400 (2022).

230. Bos, R. *et al.* Ad26 vector-based COVID-19 vaccine encoding a prefusion-stabilized SARS-CoV-2 Spike immunogen induces potent humoral and cellular immune responses. *NPJ Vaccines* **5**, 91 (2020).

231. COVID19 Vaccine Tracker. https://covid19.trackvaccines.org/.

232. Mendonça, S. A., Lorincz, R., Boucher, P. & Curiel, D. T. Adenoviral vector vaccine platforms in the SARS-CoV-2 pandemic. *npj Vaccines* **6**, 1–14 (2021).

233. Ledford, H. COVID vaccines and blood clots: five key questions. *Nature* **592**, 495–496 (2021).

234. Stanley, D. A. *et al.* Chimpanzee adenovirus vaccine generates acute and durable protective immunity against ebolavirus challenge. *Nat Med* **20**, 1126–1129 (2014).

235. Salisch, N. C. *et al.* A Double-Blind, Randomized, Placebo-Controlled Phase 1 Study of Ad26.ZIKV.001, an Ad26-Vectored Anti-Zika Virus Vaccine. *Ann Intern Med* **174**, 585–594 (2021).

236. Baden, L. R. *et al.* Safety and immunogenicity of two heterologous HIV vaccine regimens in healthy, HIV-uninfected adults (TRAVERSE): a randomised, parallel-group, placebo-controlled, double-blind, phase 1/2a study. *Lancet HIV* **7**, e688–e698 (2020).

237. Scarsella, L. *et al.* Advances of Recombinant Adenoviral Vectors in Preclinical and Clinical Applications. *Viruses* **16**, 377 (2024).

238. Sakurai, F., Tachibana, M. & Mizuguchi, H. Adenovirus vector-based vaccine for infectious diseases. *Drug Metab Pharmacokinet* **42**, 100432 (2022).

239. Shaw, A. R. & Suzuki, M. Immunology of Adenoviral Vectors in Cancer Therapy. *Molecular Therapy - Methods & Clinical Development* **15**, 418–429 (2019).

240. Lang, F. F. *et al.* Phase I Study of DNX-2401 (Delta-24-RGD) Oncolytic Adenovirus: Replication and Immunotherapeutic Effects in Recurrent Malignant Glioma. *JCO* **36**, 1419–1427 (2018).

241. Kanerva, A. *et al.* Targeting adenovirus to the serotype 3 receptor increases gene transfer efficiency to ovarian cancer cells. *Clin Cancer Res* **8**, 275–280 (2002).

242. Lindenmann, J., Burke, D. C. & Isaacs, A. Studies on the production, mode of action and properties of interferon. *Br J Exp Pathol* **38**, 551–562 (1957).

243. Schreiber, G. The Role of Type I Interferons in the Pathogenesis and Treatment of COVID-19. *Front Immunol* **11**, 595739 (2020).

244. Broquet, A. H., Hirata, Y., McAllister, C. S. & Kagnoff, M. F. RIG-I/MDA5/MAVS are required to signal a protective IFN response in rotavirus-infected intestinal epithelium. *J Immunol* **186**, 1618–1626 (2011).

245. Opitz, B. *et al.* IFNbeta induction by influenza A virus is mediated by RIG-I which is regulated by the viral NS1 protein. *Cell Microbiol* **9**, 930–938 (2007).

246. Delhaye, S. *et al.* Neurons produce type I interferon during viral encephalitis. *Proc Natl Acad Sci U S A* **103**, 7835–7840 (2006).

247. Swiecki, M. & Colonna, M. Type I interferons: diversity of sources, production pathways and effects on immune responses. *Current Opinion in Virology* **1**, 463–475 (2011).

248. Kumagai, Y. *et al.* Alveolar macrophages are the primary interferon-alpha producer in pulmonary infection with RNA viruses. *Immunity* **27**, 240–252 (2007).

249. Fejer, G. *et al.* Key role of splenic myeloid DCs in the IFN-alphabeta response to adenoviruses in vivo. *PLoS Pathog* **4**, e1000208 (2008).

250. Toll-like Receptors, Infection | Learn Science at Scitable. https://www.nature.com/scitable/topicpage/toll-like-receptors-sensors-that-detect-infection-14396559/.

251. Ho, V. *et al.* RIG-I Activation by a Designer Short RNA Ligand Protects Human Immune Cells against Dengue Virus Infection without Causing Cytotoxicity. *J Virol* **93**, e00102-19 (2019).

252. Zhang, Z. *et al.* DDX1, DDX21, and DHX36 helicases form a complex with the adaptor molecule TRIF to sense dsRNA in dendritic cells. *Immunity* **34**, 866–878 (2011).

253. Takaoka, A. *et al.* DAI (DLM-1/ZBP1) is a cytosolic DNA sensor and an activator of innate immune response. *Nature* **448**, 501–505 (2007).

254. Ishikawa, H. & Barber, G. N. STING is an endoplasmic reticulum adaptor that facilitates innate immune signalling. *Nature* **455**, 674–678 (2008).

255. Liu, D. *et al.* IFI16 phase separation via multi-phosphorylation drives innate immune signaling. *Nucleic Acids Res* **51**, 6819–6840 (2023).

256. Levy, D. E. & Darnell, J. E. STATs: transcriptional control and biological impact. *Nat Rev Mol Cell Biol* **3**, 651–662 (2002).

257. Ivashkiv, L. B. & Donlin, L. T. Regulation of type I interferon responses. *Nat Rev Immunol* **14**, 36–49 (2014).

258. Wang, W., Xu, L., Su, J., Peppelenbosch, M. P. & Pan, Q. Transcriptional Regulation of Antiviral Interferon-Stimulated Genes. *Trends in Microbiology* **25**, 573–584 (2017).

259. Au-Yeung, N., Mandhana, R. & Horvath, C. M. Transcriptional regulation by STAT1 and STAT2 in the interferon JAK-STAT pathway. *JAKSTAT* **2**, e23931 (2013).

260. Schoggins, J. W. Interferon-Stimulated Genes: What Do They All Do? *Annual Review of Virology* **6**, 567–584 (2019).

261. Gough, D. J., Messina, N. L., Clarke, C. J. P., Johnstone, R. W. & Levy, D. E. Constitutive type I interferon modulates homeostatic balance through tonic signaling. *Immunity* **36**, 166–174 (2012).

262. Abt, M. C. *et al.* Commensal bacteria calibrate the activation threshold of innate antiviral immunity. *Immunity* **37**, 158–170 (2012).

263. Wang, L. *et al.* 'Tuning' of type I interferon–induced Jak-STAT1 signaling by calcium-dependent kinases in macrophages. *Nat Immunol* **9**, 186–193 (2008).

264. Gilchrist, D. A. *et al.* Regulating the regulators: the pervasive effects of Pol II pausing on stimulus-responsive gene networks. *Genes Dev* **26**, 933–944 (2012).

265. de Weerd, N. A. & Nguyen, T. The interferons and their receptors--distribution and regulation. *Immunol Cell Biol* **90**, 483–491 (2012).

266. Gracias, D. T. *et al.* The microRNA miR-155 controls CD8+ T cell responses by regulating interferon signaling. *Nat Immunol* **14**, 593–602 (2013).

267. Yoshimura, A., Naka, T. & Kubo, M. SOCS proteins, cytokine signalling and immune regulation. *Nat Rev Immunol* **7**, 454–465 (2007).

268. Schoggins, J. W. *et al.* A diverse range of gene products are effectors of the type I interferon antiviral response. *Nature* **472**, 481–485 (2011).

269. Shaw, A. E. *et al.* Fundamental properties of the mammalian innate immune system revealed by multispecies comparison of type I interferon responses. *PLOS Biology* **15**, e2004086 (2017).

270. Pichlmair, A. *et al.* IFIT1 is an antiviral protein that recognizes 5′-triphosphate RNA. *Nat Immunol* **12**, 624–630 (2011).

271. Daffis, S. *et al.* 2′-O methylation of the viral mRNA cap evades host restriction by IFIT family members. *Nature* **468**, 452–456 (2010).

272. Hui, D. J., Bhasker, C. R., Merrick, W. C. & Sen, G. C. Viral Stress-inducible Protein p56 Inhibits Translation by Blocking the Interaction of eIF3 with the Ternary Complex eIF2·GTP·Met-tRNAi*. *Journal of Biological Chemistry* **278**, 39477–39482 (2003).

273. Vladimer, G. I., Górna, M. W. & Superti-Furga, G. IFITs: Emerging Roles as Key Anti-Viral Proteins. *Front. Immunol.* **5**, (2014).

274. Richardson, R. B. *et al.* A CRISPR screen identifies IFI6 as an ER-resident interferon effector that blocks flavivirus replication. *Nat Microbiol* **3**, 1214–1223 (2018).

275. Kristiansen, H., Gad, H. H., Eskildsen-Larsen, S., Despres, P. & Hartmann, R. The oligoadenylate synthetase family: an ancient protein family with multiple antiviral activities. *J Interferon Cytokine Res* **31**, 41–47 (2011).

276. Chakrabarti, A., Jha, B. K. & Silverman, R. H. New Insights into the Role of RNase L in Innate Immunity. *J Interferon Cytokine Res* **31**, 49–57 (2011).

277. Malathi, K., Dong, B., Gale, M. & Silverman, R. H. Small self-RNA generated by RNase L amplifies antiviral innate immunity. *Nature* **448**, 816–819 (2007).

278. Rasmussen, S. B. *et al.* Herpes simplex virus infection is sensed by both Toll-like receptors and retinoic acid-inducible gene- like receptors, which synergize to induce type I interferon production. *J Gen Virol* **90**, 74–78 (2009).

279. Tellier, M., Maudlin, I. & Murphy, S. Transcription and splicing: A two-way street. *Wiley Interdiscip Rev RNA* **11**, e1593 (2020).

280. Pelka, P., Ablack, J. N. G., Fonseca, G. J., Yousef, A. F. & Mymryk, J. S. Intrinsic Structural Disorder in Adenovirus E1A: a Viral Molecular Hub Linking Multiple Diverse Processes. *J Virol* **82**, 7252–7263 (2008).

281. Graves, D., Akkerman, N., Bachus, S. & Pelka, P. Differential Splicing of Human Adenovirus 5 E1A RNA Expressed in cis versus in trans. *J Virol* **95**, e02081-20 (2021).

282. Harlow, E., Franza, B. R. & Schley, C. Monoclonal antibodies specific for adenovirus early region 1A proteins: extensive heterogeneity in early region 1A products. *J Virol* **55**, 533–546 (1985).

283. Reich, N. C., Sarnow, P., Duprey, E. & Levine, A. J. Monoclonal antibodies which recognize native and denatured forms of the adenovirus DNA-binding protein. *Virology* **128**, 480–484 (1983).

284. Truett, G. E. *et al.* Preparation of PCR-Quality Mouse Genomic DNA with Hot Sodium Hydroxide and Tris (HotSHOT). *BioTechniques* **29**, 52–54 (2000).

285. Jones, N. & Shenk, T. Isolation of adenovirus type 5 host range deletion mutants defective for transformation of rat embryo cells. *Cell* **17**, 683–689 (1979).

286. Jones, N. & Shenk, T. An adenovirus type 5 early gene function regulates expression of other early viral genes. *Proceedings of the National Academy of Sciences* **76**, 3665–3669 (1979).

287. Thimmappaya, B., Jones, N. & Shenk, T. A mutation which alters initiation of transcription by RNA polymerase III on the Ad5 chromosome. *Cell* **18**, 947–954 (1979).

288. Fu, Y. *et al.* Human adenovirus type 7 infection causes a more severe disease than type 3. *BMC Infect Dis* **19**, 1–11 (2019).

289. Sohn, S.-Y. & Hearing, P. Adenovirus sequesters phosphorylated STAT1 at viral replication centers and inhibits STAT dephosphorylation. *J Virol* **85**, 7555–7562 (2011).

290. Uchio, E., Inoue, H., Fuchigami, A. & Kadonosono, K. Anti-adenoviral effect of interferon-β and interferon-γ in serotypes that cause acute keratoconjunctivitis. *Clin Exp Ophthalmol* **39**, 358–363 (2011).

291. Langford, M. P., Villarreal, A. L. & Stanton, G. J. Antibody and interferon act synergistically to inhibit enterovirus, adenovirus, and herpes simplex virus infection. *Infect Immun* **41**, 214–218 (1983).

292. Mistchenko, A. S. & Falcoff, R. Recombinant human interferon-gamma inhibits adenovirus multiplication in vitro. *J Gen Virol* **68 ( Pt 3)**, 941–944 (1987).

293. Graves, D., Akkerman, N., Fulham, L., Helwer, R. & Pelka, P. Molecular insights into type I interferon suppression and enhanced pathogenicity by species B human adenoviruses B7 and B14. *mBio* **15**, e01038-24 (2024).

294. Varghese, R., Mikyas, Y., Stewart, P. L. & Ralston, R. Postentry Neutralization of Adenovirus Type 5 by an Antihexon Antibody. *J Virol* **78**, 12320–12332 (2004).

295. Niman, H. L. *et al.* Generation of protein-reactive antibodies by short peptides is an event of high frequency: implications for the structural basis of immune recognition. *Proc. Natl. Acad. Sci. U.S.A.* **80**, 4949–4953 (1983).

296. Bachus, S. *et al.* ARGLU1 enhances promoter-proximal pausing of RNA polymerase II and stimulates DNA damage repair. *Nucleic Acids Research* gkae208 (2024) doi:10.1093/nar/gkae208.

297. Venteicher, A. S., Meng, Z., Mason, P. J., Veenstra, T. D. & Artandi, S. E. Identification of ATPases Pontin and Reptin as Telomerase Components Essential for Holoenzyme Assembly. *Cell* **132**, 945–957 (2008).

298. Babicki, S. *et al.* Heatmapper: web-enabled heat mapping for all. *Nucleic Acids Res* **44**, W147–W153 (2016).

299. Shannon, P. *et al.* Cytoscape: A Software Environment for Integrated Models of Biomolecular Interaction Networks. *Genome Res.* **13**, 2498–2504 (2003).

300. Morris, J. H. *et al.* clusterMaker: a multi-algorithm clustering plugin for Cytoscape. *BMC Bioinformatics* **12**, 436 (2011).

301. Gallant, P. Control of transcription by Pontin and Reptin. *Trends in Cell Biology* **17**, 187–192 (2007).

302. Sanchez, T. A., Habib, I., Leland Booth, J., Evetts, S. M. & Metcalf, J. P. Zinc finger and carboxyl regions of adenovirus E1A 13S CR3 are important for transactivation of the cytomegalovirus major immediate early promoter by adenovirus. *Am J Respir Cell Mol Biol* **23**, 670–677 (2000).

303. Wang, H. *et al.* The transcriptional coactivator RUVBL2 regulates Pol II clustering with diverse transcription factors. *Nat Commun* **13**, 5703 (2022).

304. Leung, S., Qureshi, S. A., Kerr, I. M., Darnell, J. E. & Stark, G. R. Role of STAT2 in the alpha interferon signaling pathway. *Mol Cell Biol* **15**, 1312–1317 (1995).

305. Platanitis, E. *et al.* A molecular switch from STAT2-IRF9 to ISGF3 underlies interferon-induced gene transcription. *Nat Commun* **10**, 2921 (2019).

306. Delgoffe, G. M. & Vignali, D. A. A. STAT heterodimers in immunity: A mixed message or a unique signal? *JAKSTAT* **2**, e23060 (2013).

307. Lee, C.-J. *et al.* FBXW7-mediated stability regulation of signal transducer and activator of transcription 2 in melanoma formation. *Proc Natl Acad Sci U S A* **117**, 584–594 (2020).

308. Lee, C.-J. *et al.* Stat2 stability regulation: an intersection between immunity and carcinogenesis. *Exp Mol Med* **52**, 1526–1536 (2020).

309. Au-Yeung, N. & Horvath, C. M. Histone H2A.Z Suppression of Interferon-Stimulated Transcription and Antiviral Immunity Is Modulated by GCN5 and BRD2. *iScience* **6**, 68–82 (2018).

310. Ku, M. *et al.* H2A.Z landscapes and dual modifications in pluripotent and multipotent stem cells underlie complex genome regulatory functions. *Genome Biol* **13**, R85 (2012).

311. Frost, J. R. *et al.* Adenovirus 5 E1A-Mediated Suppression of p53 via FUBP1. *J Virol* **92**, e00439-18 (2018).

312. Frost, J. R. *et al.* The interaction of adenovirus E1A with the mammalian protein Ku70/XRCC6. *Virology* **500**, 11–21 (2017).

313. Pelka, P. *et al.* Adenovirus E1A proteins direct subcellular redistribution of Nek9, a NimA-related kinase. *J Cell Physiol* **212**, 13–25 (2007).

314. Galganski, L., Urbanek, M. O. & Krzyzosiak, W. J. Nuclear speckles: molecular organization, biological function and role in disease. *Nucleic Acids Research* **45**, 10350 (2017).

315. Costa, R. *et al.* Characterization of Adenovirus 5 E1A Exon 1 Deletion Mutants in the Viral Replicative Cycle. *Viruses* **12**, E213 (2020).

316. Klein, H., Maltzman, W. & Levine, A. J. Structure-function relationships of the adenovirus DNA-binding protein. *Journal of Biological Chemistry* **254**, 11051–11060 (1979).

317. Louis, N., Evelegh, C. & Graham, F. L. Cloning and sequencing of the cellular-viral junctions from the human adenovirus type 5 transformed 293 cell line. *Virology* **233**, 423–429 (1997).

318. Fallaux, F. J. *et al.* New Helper Cells and Matched Early Region 1-Deleted Adenovirus Vectors Prevent Generation of Replication-Competent Adenoviruses. *Human Gene Therapy* **9**, 1909–1917 (1998).

319. Howe, J. A. *et al.* Matching complementing functions of transformed cells with stable expression of selected viral genes for production of E1-deleted adenovirus vectors. *Virology* **345**, 220–230 (2006).

320. Katze, M. G., He, Y. & Gale, M. Viruses and interferon: a fight for supremacy. *Nat Rev Immunol* **2**, 675–687 (2002).

321. Matias, P. M., Gorynia, S., Donner, P. & Carrondo, M. A. Crystal Structure of the Human AAA+ Protein RuvBL1*. *Journal of Biological Chemistry* **281**, 38918–38929 (2006).

322. Jónsson, Z. O., Jha, S., Wohlschlegel, J. A. & Dutta, A. Rvb1p/Rvb2p Recruit Arp5p and Assemble a Functional Ino80 Chromatin Remodeling Complex. *Molecular Cell* **16**, 465–477 (2004).

323. Dauden, M. I., López-Perrote, A. & Llorca, O. RUVBL1–RUVBL2 AAA-ATPase: a versatile scaffold for multiple complexes and functions. *Current Opinion in Structural Biology* **67**, 78–85 (2021).

324. Yang, L. *et al.* Histone deacetylase 3 contributes to the antiviral innate immunity of macrophages by interacting with FOXK1 to regulate STAT1/2 transcription. *Cell Rep* **38**, 110302 (2022).

325. Jung, R., Radko, S. & Pelka, P. The Dual Nature of Nek9 in Adenovirus Replication. *J Virol* **90**, 1931–1943 (2016).

326. Radko, S. *et al.* Adenovirus E1A targets the DREF nuclear factor to regulate virus gene expression, DNA replication, and growth. *J Virol* **88**, 13469–13481 (2014).

327. King, C. R. *et al.* Functional and Structural Mimicry of Cellular Protein Kinase A Anchoring Proteins by a Viral Oncoprotein. *PLoS Pathog* **12**, e1005621 (2016).

328. Dias Junior, A. G., Sampaio, N. G. & Rehwinkel, J. A Balancing Act: MDA5 in Antiviral Immunity and Autoinflammation. *Trends Microbiol* **27**, 75–85 (2019).